SISOW. In this regard, the quantum system described by our model can be written in the density matrix formalism as:

$$\rho_{kk'}(t) = \int_{-\infty}^{\infty}\int_{-\infty}^{\infty} f(k_c)\cdot\rho^{kc,to}{}_{k'k}(t)\cdot dt_o\cdot dk_c = \int_{-\infty}^{\infty}\int_{-\infty}^{\infty} f(k_c)\cdot a^{kc}(k')a^{kc*}(k)e^{i\frac{(Ek-Ek')(t-t_o)}{\hbar}}\cdot dt_o\cdot dk_c \quad (3.9)$$

we have added an integral over all k_c-SISOWs weighted by $f(k_c)$ with respect to the density matrix of a single SISOW (see eq. 2.17). In this regard, this density matrix represents a double incoherent superposition of wavepackets (i.e. a t_o and k_c integrals). Since we know that Bohm trajectories perfectly reproduce the dynamics of a single k_c-SISOW (see section 2.2.3), we can affirm that the result obtained by our Quantum MC simulations can be reproduced by equation 3.9. This shows that our approach, in spite of being based on intuitive physical ideas, is really a particular solution of the Liouville equation.

Moreover, since we known that the Wigner distribution function is directly obtained from the density matrix, we can compute also this function without solving additional equations. Let us first center on the Wigner distribution function of a single SISOW. In this case, since our density matrix is expressed in the k-representation (equation 2.17), and the typical Wigner-Weil transformation is on the x-representation, we have to compute the Wigner distribution function as:

$$f_W(x,k,t) = \int_{-\infty}^{\infty}dr\int_{-\infty}^{\infty}dg\int_{-\infty}^{\infty}dg'\cdot\varphi_g\left(x+\frac{r}{2}\right)\cdot\rho_{gg'}(t)\cdot\varphi_{g'}\left(x-\frac{r}{2}\right) \quad (3.10)$$

The result obtained for a SISOW, introducing equation (2.17) into (3.10) and using once more the delta function (2.18), will be written as:

$$f_W(x,k,t) = \int_{-\infty}^{\infty}dg\cdot|a(g)|^2\int_{-\infty}^{\infty}dr\cdot e^{ikr}\cdot\varphi_g\left(x+\frac{r}{2}\right)\cdot\varphi_g\left(x-\frac{r}{2}\right) = \int_{-\infty}^{\infty}dg\cdot|a(g)|^2\cdot f_w(x,k,t)\Big|_{\varphi_g} \quad (3.11)$$

Showing that the Wigner function of a SISOW can be computed as a simple sum over the Wigner-Weil transformation eigenstates $f_w(x,k,t)\big|_{\varphi_g}$ that constitute the SISOW. Now, identically to equation (3.9), the Wigner distribution function of the whole quantum system can be written as:

$$f_W(x,k,t) = \int_{-\infty}^{\infty}dk_c\cdot f(k_c)\int_{-\infty}^{\infty}dg\cdot|a^{kc}(g)|^2\cdot f_w(x,k,t)\Big|_{\varphi_g} \quad (3.12)$$

This results explicitly manifest, once more, that we are really solving the Liouville equation with a particular boundary condition for the QW (just as Frensley did [Frensley 1990]). However, it is evident that our approach contains more microscopic information than the others (i.e. *one is really*

tempted to write that we know the exact position and velocities of all electrons at any time). In this regard, we realize that when an integral over t_o is done, we 'loose' the dynamic information that the system contains. This is the procedure we follow to compute the macroscopic steady-state results such us the charge density (2.20) or the current density (2.21). Let us point out, that even the Wigner distribution function (3.12) or the density matrix (2.19) are computed in this way.

3.5.- Possible ways to introduce scattering mechanisms within our quantum Monte Carlo simulation.

First of all, let us to point out that, if we were able to deal with all interactions in a simple Hamiltonian, all the information would be contained in the 'coherent' transport and no scattering model would be needed. Obviously, that is not the case for electronic transport model of RTD. On the other hand, regarding the huge complexity of dealing with scattering, in order to include it in real devices, some level of approximation is always required.

Let us discuss how scattering is introduced in the classical MC. The Fermi Golden rule (a particular case of the first-order time dependent perturbation theory) is used to know which is the probability that a 'free' electron will change its momentum from p to p' due to a particular scattering mechanism (see eq. 3.3). For the calculation of the matrix elements $|M_i|$, plane waves are assumed. In spite of this quite confusing mixture of classical and quantum pictures, the obtained scattering rates work very well for classical MC simulations (always having some adjustable phenomenological parameters).

On the other hand, in the Wigner formalism related with RTD, we basically can distinguish between two possibilities for introducing scattering: the simple relaxation time approximation operator $C_{o|\tau}$, and the Boltzmann collision operator $C_{o|B}$. In the former case, according to Jensen [Jensen 1993], the scattering term takes the following form:

$$C_\tau \cdot f_w(x,k,t) = \frac{1}{\tau}\left\{\frac{n(x)}{n_o(x)} f_w^0(x,k,t) - f(x,k,t)\right\} \qquad (3.13)$$

where τ is the momentum relaxation time and n(x) the electron density ($n_o(x)$ and $f^o_W(x,k,t)$ are the equilibrium functions in the absence of scattering). On the other hand, the classical Boltzamnn collision operator:

$$C_{olB} \cdot f_w(x,k,t) = \frac{1}{2\pi}\int_{-\infty}^{\infty}\sum_i \left\{S_i(k',k)\cdot f_W(x,k,t) - S_i(k,k')\cdot f_W(x,k,t)\right\} \qquad (3.14)$$

has also been used with the same goal [García 1996]. Let us notice that the $S_i(k',k)$ are, generally, the ones used for the classical MC. To be fair, we have to point out that more rigorous scattering mechanisms are studied within the Wigner framework, but their numerical complexity make its application to real devices quite complicated [Brunetti 1996].

At this point, one realises that there are several possible ways to introduce scattering into our model with the same level of approximation of the ones previously discussed. Let us qualitatively present two possible implementations of scattering.

Position independent scattering between SISOWs

Since each SISOW presents a stationary properties, it seems reasonable to model scattering between them (i.e. at the same level as we model scattering between stationary states). From a practical point of view, as a rough approximation, the scattering rates $S_i(k_c,k_c')$ between SISOWs can be considered to be those used in the classical MC. However, to be consistent, a more rigorous calculation will be preferred. In particular, the matrix elements of the Fermi golden rule M_i (see equation 3.3) can be computed using egenfunctions of the Hamiltonian (rather than plane waves).

Once the scattering rates are computed (at the desired level of rigor), in order to provide a consistent scattering model, we have to assure that the stationary distribution of Bohm particles inside a SISOW is not 'disturbed' by the scattering event. In this regard, when a scattering event take place (and after choosing the final k_c'-SISOW) we have to compute two new parameters: t_B and x_B in order to define the boundary condition of the new Bohm trajectory. Both parameters have to be selected according to the stationary presence probability distribution of the SISOW. In other words, we can use the same algorithms described for the classical/quantum matching (already explained in section 3.2.3) to model how t_B and x_B can be selected.

Let us notice that with this kind of scattering model, we think that our MC simulator will behave quite similar to the one recently developed by Fischetti [Fischetti 1998]. The only difference will be related with the parameter σ_x (the spatial dispersion of the wavepacket, or in Fischetti's word: *the size of the electron*) which, however, has an important influence on the macroscopic results.

Position dependent scattering between Bohm trajectories

First of all, let us remind the discussion about the contribution of the 2D-states to the total current in real RTD (see the limitations of the Landauer-Büttiker approach in section 1.3.1). There, we pointed out the transitions from extended states to quasi-2D states due to scattering. With an identical

example, Frensley claims that if a transition from an extended state to a one-side bound state is considered, then the particle probability presence is not conserved. [Frensley 1990]. In particular, he says that the Pauli master equation violates the continuity equation. In this regard, he said: " *Presumably, inelastic transitions are more localized processes, involving superpositions of eigenstates which describes such localization.*" On the other hand, Fischetti refute Frensley's opinion arguing that the probability-current continuity is violated in any quantum jump or wavefunction collapse [Fischetti 1998]. In particular, let us highlight the following sentence: "*Since the 'orthodox' (Copenhagen)interpretation allows, or even demands, nonlocality, one may claim that the introduction of ad hoc local collision operators is a very high price to pay in exchange for 'realism'* ". The discussion about the locality of scattering goes far beyond the scope of this simple work, but we want to stress that within our approach, local scattering mechanism can also be 'naturally' implemented.

In any case, other authors have explicitly used local transition between electrons to study RTDs [Zimmerman 1987]. In this regard, Let us only point out that position-dependent scattering rates, $S_i(k_c,k_c',x)$, can be directly computed from the matrix elements of the Hamiltonian eigenstates. (This result, although not published yet, it is already developed by our group). Once these position scattering rates would be computed, the whole algorithm to consider the scattering transition between Bohm trajectories would be similar to the one described before

Finally, after discussing two possibilities (among others) for introducing scattering, let us make a brief reflection about the historical development of the classical MC technique. Although, in section 3.1, we have formally presented it as a mathematical solution of the Boltzman transport equation, historically, it was used without clear evidences of that. During the last 60s, the pioneers of the application of the MC method to electronic transport (i.e. Kurosawa, Fawcett, Boardmann, etc.) did not show that their method was a solution of the Boltzmann equation, but they only used intuitive arguments about the motion of electrons inside the semiconductors to define their approach. It was quite later that it was realized that their method was a direct solution of the Boltzmann equation (Curiously, although the demonstration is developed from Chambers equation [Chambers 1952], he did not applied it). In this regard, we think that these approaches for scattering, although quite heuristically explained, perhaps can be deduced more rigorously from a complete kinetic treatment.

References

[Ashcroft 1976] N.W.Ashcroft, N.D.Mermin, ***Solid State Physics***, Philadelphia, Saunders

[Cohen-Tanoudji 1977] C. Cohen-Tanoudji, B.Diu, and F.Laloë, ***Quantum Mechanics*** Wiley, New York

[Chambers 1952]R.Chambers, ***The kinetic formulation of the transport problem***, Proc. Phys. Soc. v:A65, p:458

[Fiig 1991] T.Fiig and A.P.Jauho, ***Self-consistent model for two-dimensional accumulation layer states in resonant tunneling devices***, Appl. Phys. Lett., v:59(18), p:2245

[Fischetti 1997] M.V.Fischetti, ***Theory of electron transport in small semiconductor devices using the Pauli master equation***, J. Appl. Phys., v:83(1), p:270

[Frensley 1990] W.R.Frensley ***Boundary conditions for open quantum systems driven far from equilibrium***, Reviews of Modern Physics, v:62(3), p:745

[Garcia 1998] J.J.Garcia, X.Oriols, F.Martín and J.Suñé, ***Effects of the spacer layers on the Wigner simulation of resonant tunneling diodes*** J. Appl. Phys. v:83, p:8057

[Garcia 1996] J.J.Garcia,X.Oriols, F.Martin and J.Suñé, ***Comparison between the relaxation time approximation and the Boltzamnn collision operator for the simulation of dissipative electron transport in resonant tunneling diodes.*** Solid State Electronics, v:39(12), p:1795

[Gonzalez 1994] T.Gonzalez ***Analisis del ruido electronico en materiales y dispositivos semiconductores unipolares medinate el metodo de Monte Carlo***, thesis presented in the Universidad de Salamanca

[Gonzalez 1996] T.Gonzalez and D.Pardo, ***Physical models of ohmic contact for the MC device simulation***, Solid State Electronics, v:39, p:555

[Gruzinkins 1991] V.Gruzinskis, S.Kersulis and A.Reklaitis, ***An efficient Monte Carlo particle technique for two-dimensional transistor modelling***, Semicond. Sci. and Technol., v:6, p:602

[Jacoboni 1989] C. Jacoboni, and P.Lugli, ***The MC method for semiconductor Device simulation***, Springer, New York.

[Jensen 1993] K.L.Jensen and A.K.Ganguly ***Numerical simulation of filed emission and tunneling: A comparision of the Wigner function and the transmission coefficient approaches*** J.Appl. Phys, v:73(9), p:4409

[Kurosawa 1966] T.Kurosawa, ***Monte Carlo calculation of hot-electron problems***, J. .Phys. Soc. Jpn. v:21 , p:424

[Muga 1993] J.G.Muga , R.Sala and R.F.Snider, ***Comparison of Classical and Quantum Evolution of Phase Space Distribution Functions***, Physics Scripta, v:47, p:732

[Rossi 1998] F.Rossi, A.Di Carlo and P.Lugli, ***Microscopic Theory of Quantum MC-Transport in mesoscopic Systems: A MC approach***, Phys. Rev. Lett., v:80, p:3348

[Zimmermann 1987] J.Zimmermann and W.Yen, ***Etdude de la dynamique des electrons a deux dimensions dans les heterojunctions*** Revue de Physique Applique, v:22, p:1501

Chapter 4

CONCLUSIONS

Every time that you decide to climb a mountain, you know that you will spend a long journey before arriving at the top. Perhaps, in spite of all your effort, you will not arrive. At first, you take a wide pathway where you often meet other people that gently explain their experience to you. As you are approaching to the mountain, the path becomes less clear because few people have stepped on it. Then, you have to start to decide, by yourself, which is the better way to get there. In front of you, you only see a big mountain and lots of different possibilities for going up. Sometimes, not always, you are capable of arriving at the top of the mountain. This is a privileged place, where you see an extraordinary beautiful landscape, and understand lots of things. You can visualise, in a few seconds, the whole path you have followed. You can easily understand where have you lost the correct path and compare your mountain with the nearest ones....

Regarding this thesis, we know that we have not arrived at the top of the mountain yet, but we are in quite privileged situation where we are able to understand the whole path that we have followed to arrive here. We can realise if there is any bypass that would have shorten our travel, and we can sincerely compare our work with those of others.

Main conclusions

The original motivation for the present thesis was the development of a simulation tool in order to study the electronic transport in semiconductor devices where quantum effects are relevant. Previous simulation tools for these devices were mainly based on mathematically robust quantum kinetic formulations (*i.e. Wigner functions, Wigner path, Green Functions...*) that

provide highly complex algorithms with a not always physically transparent meaning. On the other hand, following the intuitive simplicity of the Monte Carlo method for conventional electronic devices, we have been interested in developing a physically simple simulation tool for mesoscopic devices. In particular, following the path opened by Salvino and Buot, we have used Bohm trajectories to simulate the self-consistent I-V characteristic of resonant tunnelling diodes (RTD). We have focused on RTD that have much practical interest and offers a rich phenomenology.

1.- We have shown that the information contained in stationary states (i.e eigenfunctions of the Hamiltonian) do not allow them to correctly describe dynamic situations. This result is quite important for several reasons. Experimental I-V curves of RTD present dynamic bistability showing that the microscopic dynamic information can not be always neglected when macroscopic steady-state situations are considered. Moreover, mainly, most of the simulation tools model steady state situations while these devices are potential candidates for very high frequency applications.

These results are partially explained in [paper C] and are completed in section 2.2.

2.- We have presented an new quantum entity that we call Stationary Incoherent Superposition of Wavepackets (SISOW) that adequately describes a quantum system where a constant flux of particles is considered. A SISOW is composed as an infinite sum of identical time-dependent wavepackets but with different initial time.

2.1.- We have shown that the stationary information contained in our quantum entity is quite similar (although not identical) to stationary states. In particular, the charge (and current) associated to this quantum entity are computed as a sum over the charge (and the current) of each eigenstate that compound the SISOW.

2.2.- We have also shown that the dynamic information contained in a SISOW (for example the velocity distribution) perfectly reproduces our dynamic picture of a constant flux of electrons (i.e. they contain the dynamic information of the time dependent wavepacket.)

The central energy and the spatial (momentum) dispersion basically define each SISOW. In particular all the macroscopic results depend on the choice of spatial dispersion. This dependence has been used to criticise our approach because of its arbitrariness. However, in our

opinion, this parameter, directly related with the 'coherent size' of the electron in the sense described by Fischetti, is an advantage rather than a drawback. In other words, the limits of our approach are, on one side, the classical particles and, on the other side, the stationary states.

Some of these results have been published in [paper H] and are explained in section 2.2.2 and 2.2.3.

3.- We have shown that Bohm trajectories perfectly reproduce the static and dynamic information contained in a SISOW. Here, Bohm trajectories can be taken as mathemathical tools which reproduce standard Schrödinger equation results (i.e. no discussion about the physical reality of Bohm trajectories is needed).

These results, although repeatedly explained in several papers of this thesis, are summarised in chapter 2.

4.- We have built up a Monte Carlo simulator for resonant tunnelling diodes using Bohm trajectories associated to a SISOW. Scattering mechanisms are not yet fully implemented in our simulator. We have obtained self-consistent I-V curves for several devices that are perfectly comparable to other approaches without scattering. Using the results pointed out in conclusion 2.2, we have been able to describe our approach in terms of the density matrix and the Wigner function. This allows a direct comparison of our approach with these formalisms showing that our proposal is a particular solution of the Liouville equation (see section 3.4 or [paper H]).

On important property of our approach is its ability to provide either static or dynamic information of the devices. As we have pointed out in the first conclusion, this fact is of potential fundamental importance for the device we are examining.

The obtained simulated results and the MC methodology are explained in [paper E], [paper F], [paper G] and also in the third chapter.

5.- We have also presented complete proposals to include scattering into our simulator at a level of rigour comparable with other approaches. Let us mention that scattering is usually introduced using quite 'artificial' models in the electronic transport (for example, the Fermi golden rule between plane wave in classical Monte Carlo or the relaxation time approximation in Wigner formalism,...).

Moreover, taking profit of Bohm trajectories, we are also able to easily define 'local scattering' in the sense suggested by others (*Frensley, Zimmerman,...*). This is partially discussed in section 3.5.

This point is partially explained in [paper H] and in section 3.5.

Other conclusions

During this work we also worked on other subjects not directly related with the main goal of the present thesis, but that have also helped us to understand our work.

6.- We have presented a new formulation for one-side bound states that are capable of reproducing the current density and the probability presence of quasi-bound states without the explicit consideration of scattering. This result provides an elegant and simple way to overcome the difficulties of quasi-bound states within the Landauer-Büttiker approach. This is explicitly explained in [paper A].

7.- Several practical implications of the nonintersecting property of Bohm trajectories associated to a single wavepacket in the space-time have been examined. In particular, it has been shown that the position of a Bohm particle and the probability distribution of tunneling times, can all be obtained without actually calculating trajectories. See [paper D] for a complete explanation.

8.- The intuitive interpretation of wave-packets dynamics in potential barriers has been discussed within the framework of Bohm's interpretation. In particular, claims that Bohm's approach leads to counterintuitive results are shown to be subjective. See [paper D] and [paper C] and several parts of the second chapter of this thesis.

Some final thoughts

Finally, although I am quite sure that my thesis advisor will make me erase this paragraph, I want to express my opinion about the whole story. On one side, there is a well-establish interpretation of QM (Copenhagen school) that forces us to admit classically counterintuitive behaviour of particles. On the other side, the common sense of many people who have worked during

decades with electronic transport in conventional devices with a classical electron picture in mind. In this regard, if Bohm trajectories are assumed as physically meaningful (let us notice that is not a necessary condition to build up our simulator), we would have a justification for these people who uses the common picture of electrons as localised entities moving inside the device. In particular, we have shown that a resonant tunnelling diode, in spite of presenting a rich quantum phenomenology (such as resonances, tunnelling,..), can be perfectly understood with deterministic trajectories. Let us rewrite, once more, Bell's opinion about the De Broglie-Bohm approach for Quantum Mechanics referred to the double slit experiment: "*This idea* (electrons as particles moving influenced by a wave solution of the Schrödinger equation), *seems to me so natural and simple, to resolve the wave-particle dilemma in such a clear and ordinary way, that is a great mystery to me that it was so generally ignored*".

LIST OF ACRONYMS:

Acronym	meaning
BB	De Broglie-Bohm
BTE	Boltzmann transport equation
MC	Monte Carlo
QM	Quantum mechanics/Quantum mechanical
QW	Quantum window
RTD	Resonant tunnelling diodes
SISOW	Stationary incoherent superposition of wavepackets.

LIST OF SYMBOLS

Symbol	meaning
ρ	density operator/density matrix
Ψ	solution of the time independent Schrödinger equation
φ_n	solution of the time dependent Schrödinger equation
σ_x	spatial dispersion of an inital gaussian wavepacket.
a(k)	k-component associated to a wavepacket.
C_{ol}	Collision operator
C	total charge density
E_c	central energy of an initial gaussian wavepacket.
E_n	Energy of the n state Ψ_n
f	classical distribution function
F	Electric field
f_B	Bohm distribution fucntion
f_w	Wigner distribution function
J	total current density
k	wavevector
L	Liouville operator
m	particle mass.
p	momentum
Q	quantum potential
R	modulus of the time dependent wavefunction
S	phase of the time dependent wavefunction
t_B	Initial time of a Bohm trajectory
t_o:	minimum uncertainty time
V	classical potential
v	particle velocity
x	position
x_B	Initial position of a Bohm trajectory
x_c	central position of an inital gaussian wavepacket

Papers

Stationary modeling of two-dimensional states in resonant tunneling devices

X. Oriols,[a] J. Suñé, F. Martín, and X. Aymerich
Departament de Física, Universitat Autònoma de Barcelona, 08193 Bellaterra, Spain

(Received 17 October 1994; accepted for publication 9 April 1995)

One-side bound states are very important in vertical resonant tunneling devices which contain either lightly doped spacers or a small band-gap pseudomorphic layer adjacent to the barriers. By a proper choice of the boundary conditions, these states are modeled by stationary wave functions which contain the relevant information of the quasi-two-dimensional system under steady-state conditions. In particular, the wave functions allow the calculation of their contributions to the self-consistent charge density and the electrical current. In qualitative agreement with experimental results, it is demonstrated that the main resonant features of the current–voltage characteristic of these devices are due to resonant tunneling from an emitter two-dimensional electron gas. Finally, the proposed model is compared with a previous picture of other authors. © *1995 American Institute of Physics.*

Although the principles of operation of double-barrier resonant tunneling diodes (DBRTDs) are qualitatively well understood,[1] this is still a very active area of research. In particular, to improve the peak-to-valley current ratio, which is a key figure of merit,[2] lightly doped spacer layers[3–5] or pseudomorphic layers of small band-gap materials[6–8] have been placed adjacent to the barriers. However, these layers have more far-reaching consequences for they cause the formation of a quasi-two-dimensional (2D) electron system in the emitter. Thus the design of state-of-the-art devices requires the accurate modeling of resonant tunneling from quasi-2D states. In structures with spacer layers, the potential bulges up, forming a barrier which separates the 3D emitter from the 2D accumulation layer. For this reason, the 3D picture has been applied to these structures by considering an effective three-barrier/two-well system.[5] However, for spacers thicker than about 20 nm, experimental results show that the accumulation quantum well is a separate eigensystem,[4,5] just as in structures with layers of small band-gap materials. In both cases we will make reference to the emitter quantum well (EQW) to distinguish it from the quantum well (QW) intrinsic to DBRTDs. To model these systems, Choi and Wie considered a 3D electron distribution with a threshold energy in the EQW.[7] Recently, a much better approach was used by Burgnies *et al.*,[8] who extended the model of Lassnig and Boxleitner.[9]

For years, an independent particle 3D stationary coherent approach has been assumed to model conventional DBRTDs.[10,11] This stationary picture is an idealization of the actual problem, which is intrinsically dynamic. So, one should ideally consider the kinetic behavior of the system including inelastic interactions (a quantum Monte Carlo simulation[12] or a quantum kinetic treatment based on the Liouville equation,[13] for instance) to describe the steady-state balance reached under dc bias conditions. However, the stationary picture is a convenient approximation because it is simple and intuitive, it captures the main features of tunneling in actual devices, and it can be improved by perturbatively including inelastic interactions via rate equations.[14] It is in this sense that the extension of the stationary approach to structures which contain an emitter quasi-2D system is important. This is done in this communication by proposing a simple model which uses time independent wave functions to describe what is actually a steady-state dynamic situation.

Quasi-2D states are bound in the emitter and extended in the collector (one-side bound states), and should be treated as unstable states with a finite lifetime because electrons can tunnel out to the collector. However, electrons of the emitter can reach these states via inelastic interactions so that a steady-state occupation is reached. As a consequence, the quasi-2D states make a stationary contribution to the electronic charge and electric current. To describe this dynamic balance we propose to use approximate stationary wave functions, and this requires a proper choice of boundary conditions. Since in the collector asymptotic region (i.e., for $x \geq L$, where the potential profile is flat) we want the current to be uniform, the most obvious choice is a transmitted plane wave for $x \geq L$, as in the case of 3D states.[10] Moreover, being bound at the emitter side, we should require $|\psi_i(x)|^2 \to 0$ for $x \to -\infty$ [$\psi_i(x)$ being the envelope wave function of the ith sub-band]. These two boundary conditions are not compatible for eigenstates of the Hamiltonian, which ensure current continuity, but are convenient for an approximate model of unstable states. The method of Vassell *et al.*[10] for the 3D states consists in integrating twice the envelope equation from $x=L$ back to $x \to -\infty$ with initial conditions at $x=L$ to match $\cos[k(x-L)]$ and $\sin[k(x-L)]$. In this way, one obtains two independent functions which are the real and imaginary parts of the wave function, respectively. We propose maintaining the same procedure for the quasi-2D states with the additional condition that the real, $\psi_{i1}(x)$, and the imaginary, $\psi_{i2}(x)$, parts of ψ_i should tend to zero for $x \to -\infty$. Since, as discussed, this is not strictly possible for an eigenstate, these conditions at $x \to -\infty$ are satisfied for two slightly different values of energy, E_{i1} and E_{i2}. So, we propose describing the quasi-2D states by

$$\psi_i(x) = \psi_{i1}(x) + j\psi_{i2}(x), \tag{1}$$

ignoring their time dependence (this is actually a linear com-

[a]Electronic mail:ifel1@cc.uab.es

 0021-8979/95/78(3)/2135/3/$6.00

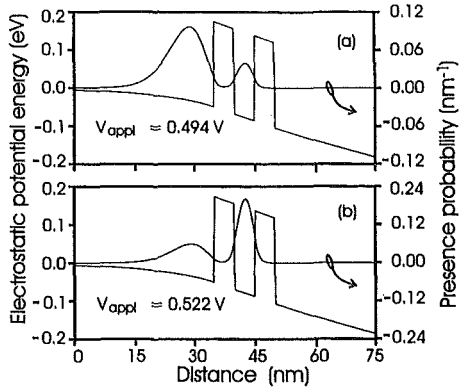

FIG. 1. Self-consistent electrostatic potential (Thomas–Fermi approximation) and ground quasi-bound-state profile in a AsGa/$Ga_{0.67}Al_{0.33}As$ double-barrier structure with lightly doped electrodes ($N_D=2\times10^{16}$ cm^{-3}) at $T=300$ K. (a) $V_{appl}=0.494$ V, i.e., just beneath the main resonant peak of the $I-V$ characteristic (see Fig. 2). (b) $V_{appl}=0.522$ V, i.e., just above the resonance.

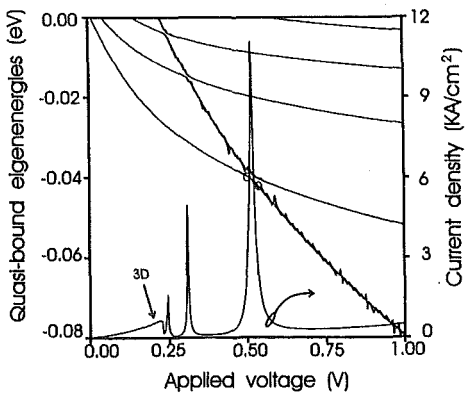

FIG. 2. Simulated current–voltage characteristic and quasi-bound eigenenergies as a function of bias for the same structure of Fig. 1 (the open circles indicate the two particular values of the voltage considered in the previous figure). As for the eigenenergies, both E_{i1} and E_{i2} are shown for each state, but this is only evident in the most vertical regions of these curves, which correspond to states located in the QW. The current peaks perfectly correlate with the anticrossing of two energy levels.

bination of two eigenstates with different eigenenergies) to model the previously presented steady-state situation without explicit consideration of inelastic interactions. For $x\rightarrow-\infty$, the boundary condition is fully accomplished. For $x>L$, $\psi_i(x)$ would only be a plane wave if E_{i1} and E_{i2} were exactly equal. In actual structures, however, the differences between E_{i1} and E_{i2} have been found to be small enough to be practically neglected (even at resonance) provided that the barriers are not extremely thin (a maximum difference of about 0.1% for a typical GaAs/$Ga_{1-x}Al_xAs$ structure with 5 nm barriers and a 5 nm well). So, both the wave-function modulus and the associated probability current are found to be position independent in the collector asymptotic region to within a very good approximation. The tiny difference between E_{i1} and E_{i2} also guarantees that $\psi_i(x)$ is a reasonable approximate solution of the stationary Hamiltonian, and can be shown to be inversely proportional to the lifetime of the state which exponentially decreases with the barrier height and thickness. Hence, for extremely transparent barriers (with no technological interest), the energy difference increases and the model fails. In this case, however, even the 2D approximation for the density of states has no sense.

As an example, we have considered a structure of two 5 nm undoped barriers of $Ga_{0.67}Al_{0.33}As$, an undoped GaAs well of 5 nm, and two external lightly doped layers ($N_D=2\times10^{16}$ cm^{-3}) which play the role of the spacers. In Fig. 1 we show the self-consistent potential and the ground quasi-bound state for two values of applied voltage near to the main resonant peak of its $I-V$ characteristic (Fig. 2). Prior to the resonance [Fig. 1(a)], the ground state has maximum presence probability in the EQW, while beyond it [Fig. 1(b)], the maximum occurs in the QW. Their diverse spatial distributions determine a radically different occupation probability, and also demand different normalization procedures. The wave function of EQW states spatially overlaps with 3D emitter states so that inelastic interactions are very probable. Hence, we will consider them to be occupied according to an emitter pseudo-Fermi level. On the contrary, QW states can only become occupied by electrons being scattered in the QW region, where the 3D wave-function moduli are several orders of magnitude smaller. So, we will consider them occupied according to the collector pseudo-Fermi level, although this could be used for the parametric modeling of inelastic scattering effects in the valley region. The current for a 3D or a quasi-2D state is then given by

$$J=\frac{q\hbar}{j2m_x^*}\left(\psi^*\frac{\partial\psi}{\partial x}-\psi\frac{\partial\psi^*}{\partial x}\right). \tag{2}$$

As expected, the current associated with 2D states is not position independent except in the collector asymptotic region, where $\psi_i(x)$ is roughly a plane wave. Consequently, J_i should be calculated at any point beyond $x=L$. Overall current continuity should be preserved by introducing self-consistent interaction between the 3D and 2D subsystems. The contribution to the current of the whole 2D system is given by

$$J_{2D}=\sum_i \frac{q(m_y^*m_z^*)^{1/2}}{\pi\hbar^2}KT\sqrt{\frac{2(E_i-E_{cc})}{m_x^*}}\,|\psi_i(L)|^2 \times\log\left[1+\exp\left(\frac{E_{qf}-E_i}{KT}\right)\right], \tag{3}$$

where E_{cc} is the position of the conduction band in the collector asymptotic region, E_{qf} the quasi-Fermi level, and $E_i\equiv E_{i1}\approx E_{i2}$. A correct normalization of the quasi-2D states is crucial because charge and current are proportional to the wave-function modulus. Although the quasi-2D states are extended by construction, a local normalization is justified on the basis of the finite coherence length of electrons. We pro-

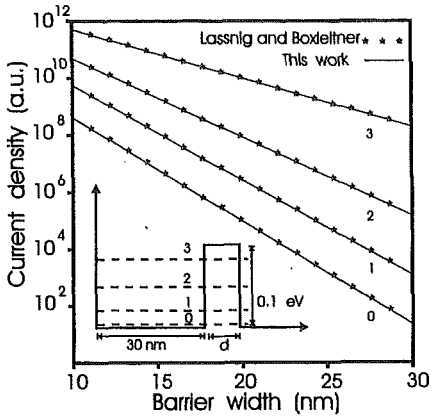

FIG. 3. Current from the four quasi-bound levels of the ideal potential structure shown in the inset. The charge in the well is assumed to be maintained stationary (i.e., electrons are supplied to substitute those which escape to the collector), and this models the effects of inelastic scattering in actual structures as far as the occupation of quasi-2D states is concerned. The solid lines correspond to the results obtained with our method. The marks have been calculated following the method proposed by Lassnig and Boxleitner for one-side bound systems (see Ref. 9).

pose normalizing the EQW states in the emitter (including the first barrier) and the QW states in a box which contains the QW and the two barriers. These normalization criteria can be shown to be consistent with our simple model for the occupation statistics and lead to an emitter charge which, as for stationary 3D states, is roughly equal on and off resonance. In Fig. 2, we show the self-consistent $I-V$ characteristic, together with the position of the eigenenergies as a function of bias. The first and wider current peak is related to the resonance from 3D states, and has the typical triangular shape. The other three sharper peaks are resonances due to the "anticrossing" of quasi-2D sub-bands, as shown in the figure by the evolution of the first five eigenvalues. In the most vertical (and noisier) segments of these curves the state presence probability peaks in the QW, while in the flatter regions it corresponds to the EQW. Both E_{i1} and E_{i2} are depicted for each state and both curves almost perfectly superpose even for QW states, whose lifetimes are certainly much smaller. Our results qualitatively confirm the experimental data obtained from structures with lightly doped spacers.[3–5] Peak currents of the order of kA/cm^2 simulated with standard values of conduction-band discontinuities[15] are also compatible with that obtained in actual devices. It is also important to notice that the experimental 2D resonant peaks are not so sharp[3] because the valley current is much larger due to inelastic scattering assisted tunneling (not considered in this work).

Finally, we compare the results of our model with those of Lassnig and Boxleitner,[9] using their idealized potential diagram. They define a local density of states to locate the quasi-2D eigenenergies and to calculate the tunneling escape lifetime (equivalent to the standard modeling of unstable states through complex energy eigenvalues[16]). After that they also assume a local normalization and a 2D approximation for the electron system. In Fig. 3 we show that the models are fully equivalent because the current from each sub-band and the position of the 2D eigenenergies are exactly coincident. However, our method is much simpler because we do not have to obtain the local density of states to locate the eigenenergies and to calculate the tunneling time. The main advantage of our approach is that the stationary eigenfunctions themselves contain all possible information about the 2D system: the self-consistent charge is directly obtained from the wave-function moduli and their contribution to the current by applying the standard current quantum operator. Another strength of our approach is that 2D and 3D states are treated on equal terms, being a natural and consistent generalization of the widely used stationary scattering picture.

[1] B. Riccò and M. Y. Azbel, Phys. Rev. B **29**, 1970 (1984).
[2] V. K. Reddy, A. J. Tsao, and D. P. Neikirk, Electron. Lett. **26**, 1742 (1990).
[3] J. S. Wu, C. Y. Chang, C. P. Lee, K. H. Chang, D. G. Liu, and D. C. Liou, Appl. Phys. Lett. **57**, 2311 (1990).
[4] H. M. Yoo, S. M. Goodnick, and J. R. Arthur, Appl. Phys. Lett. **56**, 84 (1990).
[5] E. T. Koenig, C. I. Huang, and B. Jogai, J. Appl. Phys. **68**, 5905 (1990).
[6] J. H. Smet, T. P. E. Broekart, and C. G. Fonstad, J. Appl. Phys. **71**, 2475 (1992).
[7] Y. W. Choi and C. R. Wie, J. Appl. Phys. **71**, 1853 (1992).
[8] L. Burgnies, O. Vanbesien, V. Sadaune, D. Lippens, J. Nagle, and B. Vinter, J. Appl. Phys. **75**, 4527 (1994).
[9] R. Lassnig and W. Boxleitner, Solid State Commun. **64**, 979 (1987).
[10] M. O. Vassell, J. Lee, and H. F. Lockwood, J. Appl. Phys. **54**, 5206 (1983).
[11] A. M. Kriman, N. C. Kluksdahl, and D. K. Ferry, Phys. Rev. B **36**, 5953 (1987).
[12] R. E. Salvino and F. A. Buot, J. Appl. Phys. **72**, 5975 (1992).
[13] W. R. Frensley, Rev. Mod. Phys. **62**, 745 (1990).
[14] F. Chevoir and B. Vinter, Phys. Rev. B **47**, 7260 (1993).
[15] R. C. Miller, D. A. Kleinman, and A. C. Gossard, Phys. Rev. B **29**, 7065 (1984).
[16] C. Cohen-Tanoudji, B. Diu, and F. Laloë, *Quantum Mechanics* (Wiley, New York, 1977), p. 337.

ELSEVIER

Applied Surface Science 102 (1996) 255–258

applied surface science

Bohm trajectories and their potential use for the Monte Carlo simulation of resonant tunnelling diodes

J. Suñé *, X. Oriols, F. Martín, X. Aymerich

Departament d'Enginyeria Electrònica, Universitat Autònoma de Barcelona, 08193 Bellaterra, Spain

Abstract

The tunnelling of electrons in resonant tunnelling diodes is studied within the framework of Bohm's interpretation of quantum mechanics. Bohm trajectories are studied in detail to determine whether they can be used for the Monte Carlo simulation of tunnelling devices. In agreement with the intuitive picture of the resonances, oscillatory Bohm trajectories are found, but only in some cases. The oscillatory behaviour is related to the relation between the transmission time and the local density of states in the quantum well of the device. Finally, we present the general guidelines for the implementation of a Monte Carlo simulator which uses Bohm trajectories to model quantum-mechanical tunnelling.

1. Introduction

The simulation of resonant tunnelling diodes has usually been based on the effective-mass Schrödinger equation (SE) [1], or on the Liouville equation which is used to obtain the Wigner distribution function (WDF) [2]. The first approach assumes full wave-coherence (extended scattering states), and has the severe limitation of using the equilibrium distributions of the contacts for the whole device. The second approach is in principle free of this drawback because it only uses the contact equilibrium distributions as boundary conditions for the WDF. However, its computation requirements impose serious limitations to the size of the simulation box, and the equilibrium distributions cannot be adequate boundary conditions in some cases. On the other hand, although resonant tunnelling devices are mainly based on quantum-mechanical coherence effects, scattering processes are also of extreme importance: (i) in the active device region (the quantum window), because of scattering-assisted tunnelling; and (ii) in the adjacent layers, because they determine the energy distribution of the carriers injected into the quantum window. As a consequence, a reliable simulation of these devices should simultaneously consider quantum-coherence effects and stochastic scattering interactions. For this purpose, the extension of the Monte Carlo (MC) simulation technique has already been pointed out as a promising alternative [3,4], but this requires the consideration of electron trajectories in the quantum window of the device. While in the standard interpretation of quantum mechanics (QM), the concept of particle trajectory is meaningless, there are alternative formulations (that give the same results for all measurables) where trajectories are fundamental. Associated to the Weyl–Wigner representation of QM, for example, it is possible to

* Corresponding author. Tel.: +34-3-5811829; fax: 34-3-5811350; e-mail: ifell@cc.uab.es.

PII S0169-4332(96)00060-8

formally define Wigner phase-space trajectories, which have been proposed for quantum MC simulations [5]. However, it has been recently shown that these trajectories only satisfy the Liouville's theorem locally (for restricted phase-space and time domains), so that they can be created or destroyed at singularities of the 'quantum force' [6]. In our opinion, this fact could limit their application to device simulators, and it is worth considering other alternatives such as Bohm trajectories [7]. In this paper, we present a detailed analysis of Bohm trajectories in resonant tunnelling structures, and a simple scheme for their use in a quantum MC simulator.

2. Numerical procedure

According to Bohm's representation, an electron is a particle which is guided by the wavefunction $\Psi(x, t)$, so that at each instant of time it has a well defined position $x(x_0, t)$ and velocity $v(x_0, t)$ which depend on the initial position x_0. This formulation requires the use of an arbitrary initial wavefunction as a boundary condition. If one makes the choice of a scattering energy eigenstate, as it is usual in the SE approach, unphysical results are found [8]. The reason is not a failure of Bohm's theory but rather a consequence of the actual nature of these states, which are not square-integrable. Thus, the Bohm's approach requires the selection of time-dependent wavefunctions, and the most usual choice is a minimum uncertainty Gaussian packet.

Since we are interested in time independent potential profiles (this is the situation between time steps in a MC simulation), we proceed by numerically integrating the stationary SE with scattering waves as boundary conditions in the potential asymptotic regions [1] (using Chow's integration procedure [9]). Then we project the initial Gaussian wavepacket onto the calculated eigenstates, and we can readily calculate the wavefunction at any grid point and instant of time:

$$\Psi(x, t) = \int_0^\infty a(k)\exp\left(\frac{-\mathrm{i}E_k t}{\hbar}\right)\Psi_k(x)\,\mathrm{d}k, \qquad (1)$$

where $\Psi_k(x)$ represents an energy eigenstate and $a(k)$ the projection of $\Psi(x, 0)$ onto this state. The main advantage of this method is that it avoids unphysical reflections at the walls of the integration box. Of course, the integral is discretized, and the number of k-points is chosen to be equal to the number of spatial grid points (this is similar to a fast Fourier transform procedure). Since the imaginary and real parts of the wavefunction are separately obtained, the wavefunction phase, $S(x, t)$, and the velocity of the Bohm's particles, $v(x, t) = \nabla S(x, t)/m$, can be easily calculated. Finally, the ensemble of trajectories is obtained by numerical integration of the velocity with the different initial positions within the wavepacket as boundary conditions. Although the trajectories are determined by a potential which is modified by the wavefunction, they are classical in the sense that the position and momentum are considered to be both determined. This fact allows the calculation of some quantities which are controversial within the standard interpretation of QM, such as the transmission and reflection dwell times [10].

3. Results and discussion

In this paper we are concerned with Bohm trajectories in double barrier resonant tunnelling diodes (DBRTD). Let us consider the tunnelling of electrons through a double barrier structure with the following parameters: barrier height of 0.3 eV, barrier thickness of 2 nm, well width of 7 nm, and uniform effective mass of $0.067m_0$ (that of AsGa in the lowest valley), m_0 being the free electron mass. We consider that the electrons are prepared in a Gaussian wavepacket of spatial standard deviation $\sigma_x = 10$ nm, located in the emitter, and centered around the energy E_c. In Fig. 1 we show the trajectories corresponding to a transmission resonance ($E_c = 0.22$ eV coincides with the second resonance of the structure). Consistently with previous results of other authors, the trajectories of the front of the packet are transmitted and those of the rear are reflected (most of them without ever reaching the barrier). Due to the fact that Bohm trajectories cannot intersect, one can find a trajectory (which correspond to an initial position x_c) which separates the packet in two parts at all times: that to be transmitted, and that to be reflected. The trajectories which begin in positions in the vicinity of x_c are those that remain at longest in the well region before being finally transmitted or

reflected (see Fig. 1). Notice, however, that no trajectories are seen to bounce between the barriers as in the usual intuitive picture of the transmission resonances. From an analysis of stationary states (supplemented by an example of a wavepacket as such of Fig. 1), Leavens and Aers concluded that resonant Bohm trajectories do not oscillate [10]. However, this is not exclusively related to the Bohm trajectories, but to the evolution of the wavefunction itself (Bohm trajectories perfectly reproduce the probability presence distribution at any instant of time). In other words, Bohm trajectories will only be found to oscillate in the well of a double barrier structure, if the corresponding wavepacket is seen to bounce in the well. Since the time scale of evolution of the wavefunction is related to its energy uncertainty, we expect to find oscillations when the effective energy spectrum in the well is wide enough for the oscillation period to be small as compared with the transmission times. Since the local density of states is quasi-2D in the double-barrier well, if the wavepacket spectrum overlaps only one resonant peak, oscillations are not found. However, if the wavepacket overlaps two or more peaks, we expect to find oscillations. To avoid wavepackets too wide in k-space, we have considered a structure with a

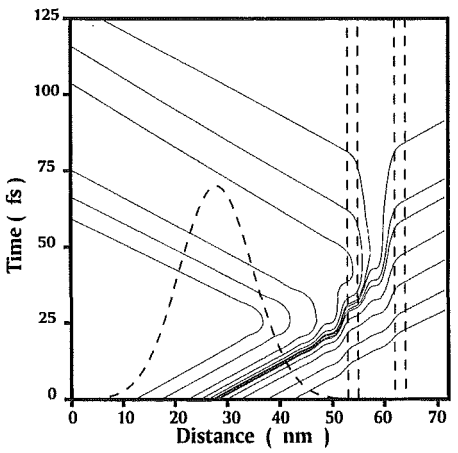

Fig. 1. Representative Bohm trajectories associated to an initial Gaussian wave-packet ($E_c = 0.22$ eV and $\sigma_x = 10$ nm) impinging upon a typical $AsGa/AsGa_{1-x}Al_x$ DBRTD with 2 nm barriers of 0.3 eV separated by a 7 nm well. The position of the barriers and the initial Gaussian wave-packet are also shown with dashed lines.

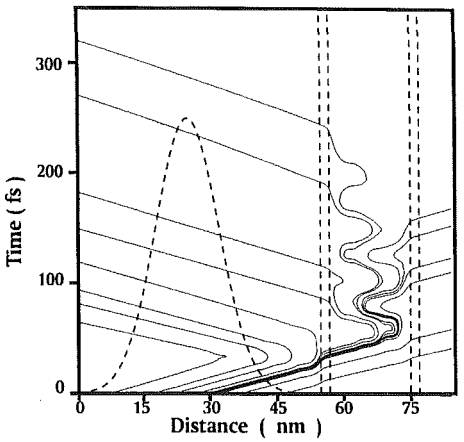

Fig. 2. Representative Bohm trajectories for an initial Gaussian wave-packet ($E_c = 0.16$ eV and $\sigma_x = 10$ nm) transversing a DBRTD similar to Fig. 1, but with a well of 18 nm. The position of the barriers and the initial Gaussian wave-packet are indicated by dashed lines.

wider well (18 nm), and the results are shown in Fig. 2. As expected, well defined oscillations are found in the Bohm trajectories starting in the vicinity of x_c. The period of oscillation $T \approx 50$ fs is found to be in good agreement with the value predicted by the energy-time uncertainty relation: $T_E = h/(E_1 - E_2)$, E_1 and E_2 being the resonant energies, which in this case is $T_E = 57$ fs. These results are supplemented by the transmission time distributions corresponding to the cases shown in Figs. 1 and 2. These distributions are shown together in Fig. 3. Notice that the oscillations of the trajectories are also apparent in the time distribution when they exist. In the case of Fig. 3(a), which corresponds to that of Fig. 1, oscillations cannot be observed because the corresponding value of T_E is larger than the transmission time of all Bohm particles. In other words, no particles remain long enough in the well to show oscillatory behavior.

All the results obtained from Bohm trajectories have been found to be consistent with those obtained directly from the solution of the Schrödinger equation. In this regard, for example, the transmission coefficient calculated by counting the transmitted/reflected trajectories from a total ensemble of 10^4 (or by searching x_c through a binary procedure) coincides with the value calculated for

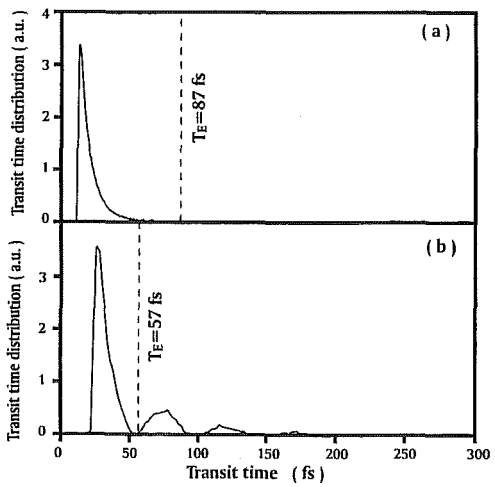

Fig. 3. Transit time distributions: (a) for the wave-packet and structure of Fig. 1, and (b) for the wave-packet and structure of Fig. 2.

the corresponding wavepacket within an error smaller than 1%. The obtained results indicate that Bohm trajectories are adequate for the extension of the MC technique to quantum-based devices. The guidelines for the implementation of such a quantum MC simulator, could be as follows. The device should be considered as being divided in two regions: (i) the quantum window, where electrons are quantum-mechanical entities which follow Bohm trajectories; and (ii) the classical region, where the standard MC technique should be used. When an electron reaches one boundary of the quantum window, it must be described by a gaussian wavepacket whose temporal evolution is needed to calculate the electron trajectory. The previously described procedure for the calculation of the evolution of the wavepacket is very convenient because it only requires the solution of the stationary SE in the quantum window after each actualization of the potential profile. Only one trajectory, randomly chosen according to the initial probability distribution $|\Psi(x_0, 0)|^2$, is calculated per each electron. Scattering events would also be considered within the quantum window as sudden changes of the wavepacket associated to the electron. Work is in progress towards the implementation of this procedure. To our knowledge, this is one of the very first attempts to consistently consider a quantum-mechanical effect as such of tunnelling within a MC simulator. This can be of importance not only to simulate quantum-based devices, but also to consider the tunnelling of carriers in conventional devices such as MOSFETs (hot-carrier effects) or EEPROMs.

Acknowledgements

The authors are grateful to the Direccion General de Investigación Científica y Técnica for supporting this work under the project PB94-0720.

References

[1] M.O. Vasell, J. Lee and H.F. Lockwood, J. Appl. Phys. 54 (1983) 5206.
[2] W.R. Frensley, Rev. Mod. Phys. 62 (1990) 745.
[3] K. Gallipulli, D.R. Miller and D.P. Neikirk, IEEE Int. Electron Device Meeting Tech. Dig. (1991) 511.
[4] R.E. Salvino and F.A. Buot, J. Appl. Phys. 72 (1992) 5975.
[5] K.L. Jensen and F.A. Buot, IEEE Trans. Electron Devices ED-38 (1991) 2337.
[6] R. Sala, S. Brouard and J.G. Muga, J. Chem. Phys. 99 (1993) 2708.
[7] D. Bohm, Phys. Rev. 85 (1952) 166.
[8] M.J. Hagmann, Solid State Commun. 86 (1993) 305.
[9] P.C. Chow, Am. J. Phys. 40 (1972) 730.
[10] C.R. Leavens and G.C. Aers, in: Scanning Tunnelling Microscopy III, Eds. R. Wiesendanger and H.-J. Güntherodt (Springer, Berlin, 1993) p. 105.

Pergamon

Solid State Communications, Vol. 99, No. 2, pp. 123–128, 1996

0038–1098/96 $12.00+.00

PII S0038-1098(96)00140-8

OSCILLATORY BOHM TRAJECTORIES IN RESONANT TUNNELING STRUCTURES

X. Oriols, F. Martín and J. Suñé

Departament de Física, Universitat Autònoma de Barcelona, 08193-Bellaterra, Spain

(*Received* 10 *August* 1995; *in final form* 16 *January* 1996 *by F. Yndurain*)

Tunneling of electrons in double-barrier resonant tunneling diodes (DBRTDs) is studied within the Bohm's formulation of quantum mechanics. As previously done by other authors, stationary scattering states and time-dependent wavepackets are considered. The scattering eigenstates are shown to provide unphysical results, but this is attributed to their actual nature rather than to the failure of Bohm's interpretation. Using time-dependent wavepackets, the behavior of Bohm trajectories at the resonances of DBRTDs is thoroughly examined. The oscillating nature of the resonant trajectories is discussed in terms of the wavefunction energy spectrum and the local density of states in the barrier region. The energy–time uncertainty relationship is shown to provide a necessary condition for the observation of the oscillations which reproduce the intuitive picture of resonances. The case of oscillating trajectories in single potential barriers is also considered as a test of generality. Copyright © 1996 Published by Elsevier Science Ltd.

Keywords: Bohm's interpretation, resonant tunneling, quantum devices.

THE DESCRIPTION of the dynamic evolution of quantum-mechanical systems in terms of particle trajectories provides an interesting visualization of quantum phenomena, and is also a useful tool to acquire a better intuitive understanding. In particular, quantum trajectories are being considered with renewed interest because they are expected to provide a natural way for the coupling of semi-classical and quantum-mechanical approaches to carrier transport in nanometric electron devices, via the Monte Carlo simulation technique [1, 2]. In this regard, Bohm trajectories are particularly promising for they have been demonstrated to exactly reproduce the results of the standard interpretation of Quantum Mechanics (QM) in many interesting situations (interaction of wavepackets with potential profiles [3], two-slit experiment [4], etc.), and also because they can enlighten some aspects (such as tunneling times) which are controversial within the standard formulation. To our knowledge, Dewdney and Hiley were the first to use the Bohm's interpretation for the study of the time-dependent scattering of wavepackets by square potential barriers [3]. They reported Bohm trajectories which spent much time inside the barrier, and which occasionally exhibited oscillations between its edges. This oscillating behavior inside single potential barriers was also reported by Leavens and Aers [5–7], who also analyzed the phenomenology of Bohm trajectories at the resonances of Double Barrier Resonant Tunneling Diodes (DBRTDs). In this regard, they analyzed the case of perfect transmission [$T(K) = 1$] in terms of energy eigenstates and demonstrated that the associated "stationary" trajectories do not oscillate, also showing that superluminal velocities would otherwise be reached. They also considered time-dependent wavepackets narrow enough around the resonant energy to be almost perfectly transmitted, and they did not find oscillating trajectories either. In this communication we present new results regarding the oscillatory behavior of Bohm trajectories in tunneling structures. We emphasize that these trajectories exactly reproduce the dynamics of the wavefunction, and we discuss which conditions are required for them to oscillate in a limited spatial region. We complete our results with the calculation of the transmission time distribution, which is shown

to reproduce the oscillations of the Bohm trajectories when these occur. Our analysis is focused on DBRTDs, but the case of single potential barriers is also considered as a test of generality.

Let us begin by briefly reviewing the basics of Bohm's interpretation of QM for non-relativistic particles [8–10]. If the wavefunction is expressed as

$$\Psi(x,t) = R(x,t)\exp\left(i\frac{S(x,t)}{\hbar}\right), \tag{1}$$

$R(x,t)$ and $S(x,t)$ being real functions, the complex Time-Dependent Schrödinger Equation (TDSE) is found to be equivalent to two real equations: a continuity equation for the presence probability density $P(x,t) \equiv R^2(x,t)$; and another one which can be interpreted as a modified classical Hamilton–Jacobi equation. In this scheme, the particle velocity is given by $v(x,t) = 1/m\cdot(\partial S(x,t)/\partial x)$, and the classical potential energy $V(x,t)$ is augmented by a new term, $Q(x,t)$, which is interpreted as a quantum potential [8]

$$Q(x,t) = -\frac{\hbar^2}{2m}\frac{1}{R(x,t)}\frac{\partial^2 R(x,t)}{\partial x^2}. \tag{2}$$

The quantum potential introduces non-local features and modifies the trajectories so that the measurable results of the standard interpretation of QM are perfectly reproduced. The most convenient way to calculate the trajectories is usually to solve TDSE for the wavefunction, so that $S(x,t)$ and $R(x,t)$ are obtained. From them, one can evaluate the velocity and determine the trajectories by integration. For any initial position x_0 within the initial wavepacket, the particle trajectory is uniquely determined but, because of the limitations imposed by the uncertainty principle, the physical quantities must be obtained by averaging over all the possible trajectories weighted by $P(x_0,0)$. Regarding to the initial wavefunction, two alternatives have been considered in the literature: (i) time-independent eigenfunctions of the hamiltonian (scattering states) [7, 11, 12]; and (ii) localized time-dependent wavepackets [3, 5–7].

A particle with energy E_K and momentum $\hbar K$ can be associated to a stationary scattering state $\Psi_K(x)$. In this case, since the particle energy is perfectly defined, one can adopt the energy conservation law

$$E_K = V(x) + Q(x) + \tfrac{1}{2}m\cdot v^2(x,t) \tag{3}$$

as the simplest procedure to calculate Bohm trajectories. Since E_K and $V(x)$ are known, and $Q(x)$ can be directly computed from $\Psi_K(x)$ using equation (2), the particle velocity, $v(x,t)$, is determined. In this paper, the eigenfunctions of the hamiltonian are calculated following the procedure of Vasell *et al.* [13], but using the Numerov integration method [14] to improve the numerical efficiency [15]. It can easily be proved that $v(x,t)$ is always positive and time-independent at every point x of the Bohm trajectories associated with scattering states [6]. This means that there is a unique phase–space trajectory and that all the space–time trajectories of the ensemble are identical, except for the time delay derived from the difference in the initial positions x_0 [11]. In Fig. 1(a), we have represented a Bohm trajectory for a scattering state with energy $E_k = 0.05$ eV, which corresponds to the first resonant level of a $AsGa/AsGa_{1-x}Al_x$ structure with 2 nm barriers of 0.3 eV separated by a 7 nm well. In this particular case, the results obtained within the Bohm's formulation are compatible with those of the standard interpretation of QM because $T(K) = 1$. However, even if $T(K)$ is smaller than unity, all Bohm "stationary" trajectories cross the barrier region because the velocity is always positive, and this is unphysical and inconsistent. In Fig. 1(b), we have represented a Bohm trajectory associated to a non resonant scattering state. The quantum potential tends to diverge at the quasi-nodes of the wavefunction modulus, so that the particle velocity becomes very large at these points. These velocity divergences, which were considered unphysical by Hagmann [12], are a direct consequence of the quasi-nodes of the wavefunction, which are

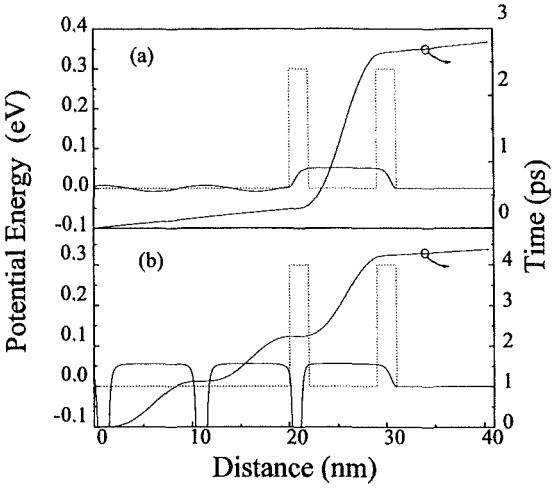

Fig. 1. Bohm trajectories associated with stationary scattering states impinging on a typical AsGa/$AsGa_{1-x}Al_x$ DBRTD with 2 nm barriers of 0.3 eV separated by a 7 nm well. The electron mass is considered to be the effective mass in the Γ point of AsGa. The classical potential (dashed line) and the total potential (solid line) are also depicted. (a) Resonant eigenstate, $E_K = 0.05$ eV; (b) Non-resonant eigenstate, $E_K = 0.06$ eV.

caused by the interference of the incident and reflected beams. To be fair, if the velocity divergences are considered unphysical, the same should be said about the behavior of the wavefunction. Although stationary scattering states are useful in many instances, they can not provide a fully satisfactory description of the quantum state of a particle because they are not square-integrable. On the contrary, the Bohm's formulation works properly for all normalizable wavefunctions (including bound stationary states). For this reason, we conclude that the failure for stationary states does not reveal weaknesses of the theory, but rather intrinsic limitations of these states themselves.

In the unavoidable time-dependent approach, a reasonable choice for the initial wavefunction is a minimum-uncertainty gaussian wavepacket

$$\Psi(x,0) = \frac{1}{(\pi\sigma_x^2)^{1/4}} \exp\left(-\frac{(x-x_c)^2}{2\sigma_x^2} + ik_c x\right) \tag{4}$$

σ_x being the spatial dispersion, x_c the spatial centroid at $t = 0$, and k_c the centroid of momentum distribution which is related to a central energy E_c. To calculate the evolution of the wavefunction without discretizing the TDSE, the wavepacket has been numerically projected onto the previously calculated basis of stationary scattering states

$$\Psi(x,0) = \int_0^\infty a(E)\Psi_k(x)\mathrm{d}K \tag{5}$$

with

$$a(E) \equiv \int_{-\infty}^{\infty} 0\Psi_K^*(x)\Psi(x,0)\mathrm{d}x, \tag{6}$$

E being related to K via the dispersion relationship considered in the effective-mass Schrödinger equation. In this way, $\Psi(x,t)$ can be obtained at any instant of time as a linear combination of stationary wavefunctions $\Psi_K(x)$

$$\Psi(x,t) = \int_0^\infty a(E)\exp\left(-i\frac{E\cdot t}{\hbar}\right)\Psi_K(x)\mathrm{d}K. \tag{7}$$

Using this method, we have obtained the evolution of a gaussian wavepacket with resonant energy and $\sigma_x = 10\,\mathrm{nm}$ incident upon the potential profile of Fig. 1. In accordance with Leavens and Aers results [7], although some trajectories remain for quite a long time in the potential well, they are not found to oscillate at all. Nevertheless, this behaviour cannot be taken as a general result, but rather as a particular consequence of the considered structure and wavepacket. At this point, it is convenient to remember that Bohm trajectories perfectly reproduce all the measurable information contained in the wavefunction. In particular, the probability of finding the particle located at a position x at time t can be calculated by weighting the trajectories $x(x_0, t)$

$$P(x,t) = |\Psi(x,t)|^2 = \int_{-\infty}^{\infty} |\Psi(x_0,0)|^2 \delta[x - x(x_0,t)]\mathrm{d}x_0 \tag{8}$$

On the other hand, since Bohm trajectories do not cross [7], they will oscillate if (and only if) there is a portion of the wavepacket spatially oscillating between the barriers. The temporal scale for the evolution of the wavefunction within a limited spatial region ($x_1 < x < x_2$), such as the quantum well (QW) of the DBRTD, can be determined by the energy uncertainty relationship. In particular, a rough estimation of the time required for the wavepacket to evolve between the barriers (which is also an estimation of the period of the eventual oscillations) is given by

$$t_E \simeq \frac{h}{\Delta E}, \tag{9}$$

ΔE being the width of the effective energy spectrum in the quantum well, $D_\Psi(E)$:

$$D_\Psi(E) = |a(E)|^2 D(E) \tag{10}$$

which depends on the wavepacket energy spectrum, $|a(E)|^2$, and on the local density of states in the considered region, defined as [16]

$$D(E) = \int_{x_1}^{x_2} |\Psi_K(x)|^2 \mathrm{d}x. \tag{11}$$

An estimation of the energy uncertainty required in equation (9) can be obtained from the Full Width at Half Maximum (FWHM) of $D_\Psi(E)$. From this ΔE we obtain a value of t_E, which is interpreted as a measure of the time required for a significative change in the presence probability $P_W(t)$ in the considered region

$$P_W(t) = \int_{x_1}^{x_2} |\Psi(x,t)|^2 \mathrm{d}x. \tag{12}$$

If any kind of evolution is expected (oscillations, for example), it is mandatory that a significative number of particles (of the quantum ensemble) should remain in the considered spatial region during a time interval longer than t_E. In other words, a necessary condition for the observation of oscillations of the wavepacket (and also of the Bohm trajectories) is that $P_w(t)$ must be significant during a time interval longer than t_E.

In Fig. 2, we consider a wavepacket with $\sigma_x = 10\,\mathrm{nm}$ incident with resonant energy $E_c = 0.22\,\mathrm{eV}$) upon a

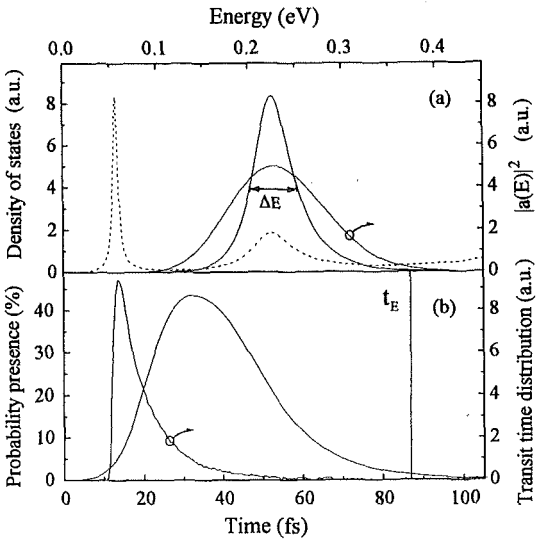

Fig. 2. Dynamic study of a gaussian wave-packet with $E_c = 0.22\,\text{eV}$ and $\sigma_x = 10\,\text{nm}$ impinging upon the potential profile of Fig. 1. (a) Density of states [$D(E)$ in dashed line and $D_\Psi(E)$ in solid line] and wavepacket spectra ($|a(E)|^2$). (b) Probability presence in the well [$P_W(t)$] and transmission time distribution. The vertical line indicates the evolution time $t_E = 87\,\text{fs}$ calculated from the FWHM of $D_\Psi(E)$.

AsGa/AsGa$_{1-x}$Al$_x$ DBRTD with 2 nm barriers of 0.3 eV and a 7 nm well, whose associated Bohm trajectories have not been found to oscillate. In Fig. 2(a) we show $|a(E)|^2$, $D(E)$ and the product of these two magnitudes which gives $D_\Psi(E)$ with a $\Delta E = 0.047\,\text{eV}$ and, according to equation (9), $t_E \approx 87$ fs. In Fig. 2(b), $P_W(t)$ is shown to be negligible at times of the order of t_E. This indicates that the transmission (reflection) process is much faster than the possible oscillations, so that these can not actually occur. Although, it is generally difficult to reduce t_E without simultaneously reducing the temporal width of $P_W(t)$ because the tunneling times are also dependent on the energy spectrum, if this spectrum shows resonance peaks, it is relatively easy to find situations in which oscillatory Bohm trajectories are observed. As an example, in Fig. 3 we show Bohm trajectories corresponding to a gaussian wavepacket ($\sigma_x = 10\,\text{nm}$, $E_c = 0.16\,\text{eV}$) impinging upon a DBRTD with 0.3 eV barrier height, 2 nm barrier thickness, and 18 nm well (the strategy is considering a wider well to bring closer the resonances so that the wavepacket spectrum overlaps two or more resonant peaks). The behaviour of the trajectories is very similar to that found in the previously analyzed examples and by other authors [3–7]. What is new is the oscillation of some trajectories in the QW. In Fig. 4(a) $|a(E)|^2$, $D(E)$ and $D_\Psi(E)$ are shown, and we notice that the energy spectrum $D_\Psi(E)$ has two peaks related to the resonances of $D(E)$. The 0.072 eV difference between these two energy components can be taken as a measure of ΔE which gives $t_E \approx 57$ fs. In Fig. 4(b), we show $P_W(t)$ and compare it with t_E. The fact that t_E is smaller than the width of $P_W(t)$, allows the oscillatory behavior observed in Fig. 3. The period of the trajectory oscillations (see Fig. 3 again) is nearly constant ($\tau \approx 50$ fs) and, as expected, roughly equal to t_E. Moreover, within Bohm's interpretation, one can evaluate the time that the transmitted particles take to cross the well region and obtain a transmission (transit) time probability distribution [7]. As shown in Fig. 4(b), this distribution presents periodic bumps related to the number of oscillations that the particles experience before finally escaping from the well. Notice that the temporal separation of successive extrema is roughly equal to the oscillation period τ. The oscillations are much better appreciated in the transmission time distribution than in $P_W(t)$ because the time spent by the Bohm particles in the pre-barrier region does not mask the information.

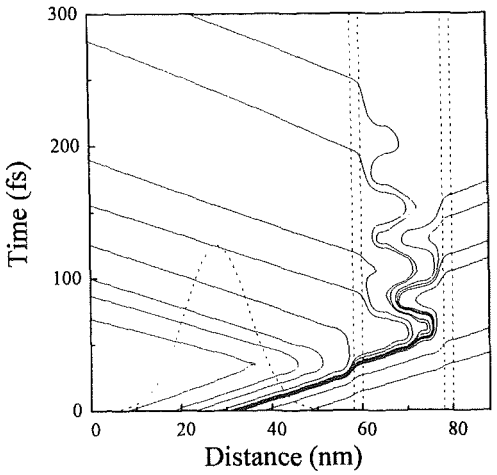

Fig. 3. Representative Bohm trajectories for an initial gaussian wave-packet ($E_c - 0.16\,\text{eV}$ and $\sigma_x = 10\,\text{nm}$) incident upon an AsGa/AsGa$_{1-x}$Al$_x$ DBRTD with 2 nm barriers of 0.3 eV and a 18 nm well. The position of the barriers and the initial gaussian wavepacket are indicated by dashed lines.

As a test of generality, we examine whether the previous physical analysis can be applied to the case of a single potential barrier. In this regard, Leavens [6] considered a 1 nm rectangular barrier of 10 eV and two impinging electron wavepackets both centered around $E_c = 5\,\text{eV}$, but with different dispersions in K-space: (**A**) $\Delta K = 0.4\,\text{nm}^{-1}$ and (**B**) $\Delta K = 0.8\,\text{nm}^{-1}$ (see [6] for the exact definition of ΔK). Oscillations

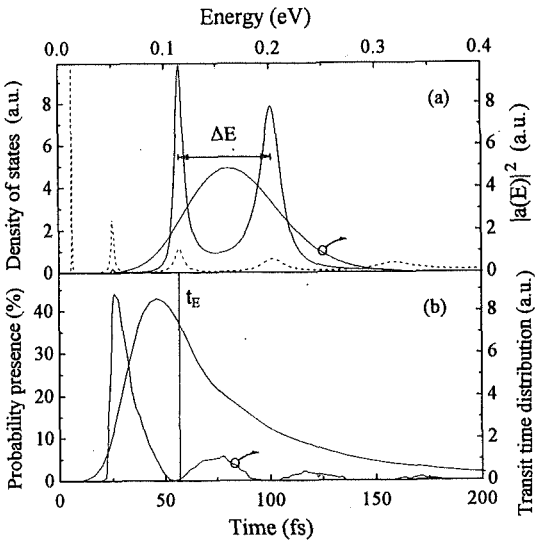

Fig. 4. Dynamic study of the scattering process of Fig. 3. (a) Density of states [$D(E)$ in dashed line and $D_\Psi(E)$ in solid line] and wavepacket spectra ($|a(E)|^2$). (b) Probability presence in the well [$P_W(t)$] and transmission time distribution. The vertical line corresponds to $t_E = 57$ fs, which is calculated from the effective energy spectrum width of Fig. 4(a), $\Delta E = 0.072$.

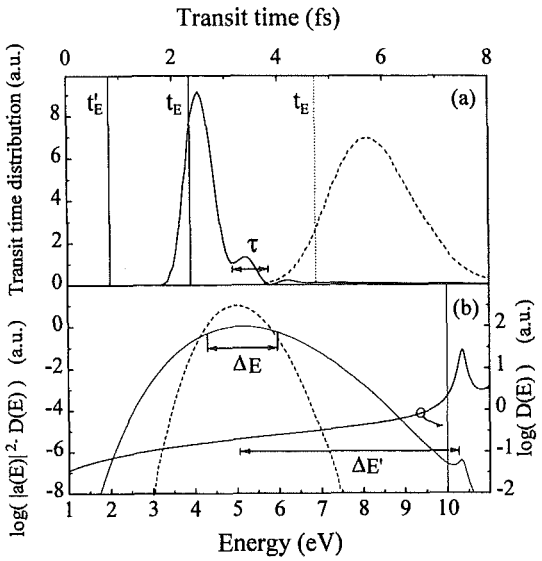

Fig. 5. Dynamic study of two gaussian free electron wavepackets impinging upon a single square potential barrier of 10 eV and 1 nm thickness. Wavepacket **A** has $\Delta K = 0.04\,\text{nm}^{-1}$ and wavepacket **B** has $\Delta K = 0.08\,\text{nm}^{-1}$. (a) Transmission time distribution (dashed lines corresponds to wavepacket **A** and solid lines to wavepacket **B**). The corresponding evolution times $t_E(A) = 4.7$ fs and $t_E(B) = 2.3$ fs, calculated from the FWHM of $D_\Psi(E)$ are also indicated. The value $t'_E = 0.79$ fs [calculated from the $\Delta E' = 5.2$ eV shown in Fig. 5(b)] corresponds to wavepacket **B**. (b) Effective energy spectrum, $D_\Psi(E)$, associated to wavepacket **A** (dashed line) and wavepacket **B** (solid line). The density of states, $D(E)$, shows an overbarrier resonant peak (the vertical line indicates the barrier energy height).

were only observed in some trajectories corresponding to wavepacket **B**, i.e. the widest in the energy domain. In Fig. 5(a), we show the transit time distributions and the values of t_E calculated from the FWHM of the corresponding $D_\Psi(E)$ spectra. First of all, notice that the transit time distribution is strongly affected by the width of the wavepacket's energy spectrum. In this regard, we find that the wider the energy spectrum, the shorter the average transmission time, so that t_E and the transmission time distribution move together towards smaller values when ΔK changes from $0.4\,\text{nm}^{-1}$ to $0.8\,\text{nm}^{-1}$. For both wavepackets, the calculated t_E are shorter than the transmission time of most of the particles, so that one could expect oscillations in both bases. However, as shown in [6], oscillatory trajectories are only found in case **B** which are also evident in the corresponding transmission time distribution. In any case, there is not a contradiction with our phenomenological oscillation criterium since, as discussed above, it provides a necessary but not sufficient condition for the occurrence of oscillations. In spite of this, a closer look to $D_\Psi(E)$ can justify the differences between the two cases. In Fig. 5(b), the $D_\Psi(E)$ spectra corresponding to both wavepackets are represented together with $D(E)$. In case **B**, the effective density of states has two relative maxima: one due to the wavepacket spectrum, and a much smaller one which is related to the first above-barrier resonance. On the contrary, wavepacket **A** is much narrower and does not have significant components on the above-barrier resonant states. If the energy uncertainty of wavepacket **B** is calculated from the FWHM, we find $\Delta E = 1.76$ eV and $t_E \approx 2.3$ fs. If on the contrary, it is defined as the difference between the two relative maxima, it gives $\Delta E' = 5.2$ eV and $t_E' \approx 0.79$ fs. This value of t_E' roughly coincides with the period of the oscillations, $\tau \approx 0.75$ fs. From this, we conclude that a peaked energy spectrum (a structure with transmission resonances) is also required for oscillations to occur. This is a plausible result, since only at transmission resonances the stationary states are quasi-bound, i.e. tend to maintain the electron partially confined in the QW by "constructive multiple reflections". However, the presence of a transmission resonance does not guarantee the occurrence of oscillations since t_E must also be smaller than the time interval during

which a non-negligible percent of particles remain in the considered spatial region. The picture of multiple reflections and oscillations is not adequate for narrow resonances. These situations are closer to a stationary state, which is strongly confined in the barrier region, and which hardly evolves with time.

In this paper, the tunneling of electrons in one dimensional structures has been analyzed within the Bohm's interpretation of QM. Scattering energy eigenstates have been shown to be inadequate for this formulation because these wavefunctions are non square-integrable. On the other hand, we have considered this problem using time-dependent wave-packets, and we have discussed the evolution of the wavefunction in terms of the energy–time uncertainty relationship. We have shown that the effective energy spectrum of the wavefunction in a limited region helps to understand the behavior of Bohm trajectories. In particular, we have shown that oscillations can only appear if the evolution time (inversely proportional to the energy width) is shorter than the time required for full transmission and reflection. This criterium has been shown to be a necessary but non sufficient condition for the observation of oscillations. The analysis of tunneling through a single square barrier has confirmed the validity of our oscillation criterium, but has shown that the presence of transmission resonances is also required. Our results have been supplemented with the calculation of the transmission time distribution, which also shows a periodic structure whenever oscillating Bohm trajectories appear. Finally, we have emphasized that Bohm trajectories are fully determined by the wavefunction, and that their behavior reproduces its evolution, which is given by the TDSE. Whether the intuitive picture of the transmission resonances in DBRTDs (or of other quantum effects) is correct or not, is uniquely determined by the TDSE. In this regard, the Bohm's approach can be considered as a useful tool to enlighten quantum-mechanical phenomena.

Acknowledgements—The authors are grateful to the Dirección General de Investigación Científica y Técnica for supporting this work under project number PB94-0720.

REFERENCES

1. K.L. Jensen & A.K. Ganguly, *J. Appl. Phys.* **73,** 4409 (1993).
2. R. E. Salvino & F. D. Buot, *J. Appl. Phys.* **72,** 5981 (1992).
3. C. Dewdney & B.J. Hiley, *Foundations of Physics* **12,** 27 (1982).
4. C. Philippidis, C. Dewdney & B.J. Hiley, *Il Nuovo Cimento* **52,** 15 (1979).
5. C.R. Leavens, *Solid State Commun.* **74,** 923 (1990).
6. C.R. Leavens, *Solid State Commun.* **76,** 253 (1990).
7. C.R. Leavens & G.C. Aers, *Scanning Tunneling Microscopy III*, p. 105. Springer (1993).
8. D. Bohm, *Phys. Rev.* **85,** 166 (1952).
9. D. Bohm & B.J. Hiley, *The Undivided Universe: An Ontological Interpretation of Quantum Mechanics.* Routledge, London (1993).
10. P.R. Holland, *The Quantum Theory of Motion.* Cambridge University Press, Cambridge (1993).
11. T.P. Spiller, T.D. Clark, R.J. Prance & H. Prance, *Europhys. Lett.* **12,** 1 (1990).
12. M.J. Hagmann, *Solid State Commun.* **86,** 305 (1993).
13. M.O. Vasell, J. Lee & H.F. Lockwood, *J. Appl. Phys.* **54,** 5206 (1983).
14. P.C. Chow, *Am. J. Phys.* **40,** 730 (1972).
15. X. Oriols, J. Suñé, F. Martín & X. Aymerich, *J. Appl. Phys.* **78,** 2135 (1995).
16. R. Lassnig & W. Boxleitner, *Solid State Commun.* **68,** 979 (1987).

Implications of the noncrossing property of Bohm trajectories in one-dimensional tunneling configurations

X. Oriols, F. Martín, and J. Suñé
Department d'Enginyeria Electrònica, Universitat Autònoma de Barcelona, 08193-Bellaterra, Spain
(Received 2 January 1996)

Several practical implications of the noncrossing property of one-dimensional Bohm trajectories are examined. It is shown that the position of a Bohm particle, the average transmission, reflection and dwell times, and the probability distribution of these tunneling times, can all be obtained without actually calculating trajectories. On the other hand, the intuitive interpretation of the scattering of wave packets by potential barriers is discussed within the framework of Bohm's interpretation of quantum mechanics. In this regard, claims that Bohm's approach leads to counterintuitive results are shown to be subjective. [S1050-2947(96)02209-3]

PACS number(s): 03.65.−w, 73.40.Gk, 85.30.Mn, 02.70.Lq

I. INTRODUCTION

In the context of one-dimensional tunneling configurations, the dwell time is defined as the average (ensemble) time spent by the incoming particles in the potential barrier region ($a<x<b$):

$$\tau_D=\int_0^\infty dt\int_a^b dx|\Psi(x,t)|^2. \tag{1}$$

This time was first postulated by Büttiker [1], and more recently rigorous derivations have been obtained within Feynman's [2] and Bohm's [3–5] formulations of quantum mechanics (QM). Although there are some divergences regarding its physical interpretation [6,7], this is widely recognized as a meaningful concept [8,9]. On the other hand, much more controversy exists about the transmission (τ_T) and reflection (τ_R) times, which are sometimes loosely defined as the *average times spent in the barrier region by the particles that are ultimately transmitted or reflected*, respectively. In the same way, the relation

$$\tau_D=|T|^2\tau_T+|R|^2\tau_R \tag{2}$$

($|T|^2$ and $|R|^2$ being the transmission and reflection probabilities associated with the wave packet) is also controversial. Some authors have claimed that this is a necessary requirement for any meaningful τ_T and τ_R, arguing that transmission and reflection are mutually exclusive events that exhaust all the possibilities [8]. However, it has also been pointed out that the questions, "*Will the particle be transmitted*" and "*Is the particle in the potential barrier region?*" correspond to noncommuting observables [9–11]. As a consequence, an additional interference term appears in the right-hand side of Eq. (2) [11]. In our opinion, however, if the definition of the tunneling times given just prior to Eq. (2) is to be interpreted literally, there should be no doubt about the validity of relation (2). Nevertheless, the problem is that this definition is not meaningful within the conventional interpretation of QM because *the time spent in the barrier region by one particle* cannot actually be measured. To determine this time, two successive measurements of position would be required, but this procedure leads to meaningless results due to the collapse of the wave function after the first measurement. For this reason, there is no contradiction if some of the diverse quantities proposed to represent the tunneling times within conventional QM do not satisfy Eq. (2). On the contrary, tunneling times are unambiguously defined within Bohm's interpretation of QM [12–14], which is a causal theory of quantum-mechanical processes in space and time, and not just a theory about experimental results [15]. Since, on the other hand, the Bohm tunneling times perfectly fit the previous general definition, they indeed satisfy Eq. (2), as required [3–5].

According to Bohm's interpretation, an electron is a particle that is guided by a pilot field related to the wave function $\Psi(x,t)$, and follows a well-defined trajectory $x(x_0,t)$, which only depends on its starting position x_0 within the initial wave packet $\Psi(x,0)$. A complete description of any quantum-mechanical problem, however, requires the consideration of a (classical) ensemble of trajectories. All measurable quantities, which are obtained by averaging the values of the single trajectories weighted according to $|\Psi(x_0,0)|^2$, exactly reproduce the results of the standard interpretation of QM. Furthermore, since the particle trajectories are perfectly defined, some quantities that are controversial within the standard interpretation (such as tunneling times) are unambiguous within Bohm's framework. Mainly for this reason, the tunneling of electrons through potential barriers has been recently analyzed by Leavens and Aers within Bohm's interpretation [3–5]. These authors presented the theory in detail, worked out several examples of transmission of wave packets through one-dimensional barriers, obtained the distributions of transmission and reflection times (in addition to their average values), and compared their results with those of other conventional approaches to the tunneling time problem [5]. They also emphasized that one-dimensional Bohm trajectories never intersect at any space-time point, and discussed one of its consequences. There is a bifurcation trajectory (starting at x_{c0}) that separates the wave packet in two parts: that to be transmitted ($x_0>x_{c0}$), and that to be reflected ($x_0<x_{c0}$). This means that, within Bohm's approach, all the transmission comes from the spatial front of the wave packet, and that all the rear part of it is reflected. This had been previously observed by Dewdney and Hiley [16], and motivated the somehow skeptical comments of Landauer and

Martin [9], who stressed apparent contradictions between these results and the common intuitive interpretation of the scattering of wave packets by potential barriers. In a very recent paper, the noncrossing property of Bohm trajectories was also used by McKinnon and Leavens [17] to obtain the distribution of transmission times without calculating trajectories. Their method is very interesting and significantly reduces the time required to compute this distribution. However, further discussion is required because, as we will show, their procedure cannot be applied to all possible cases.

It is the purpose of this paper to discuss several practical implications of the noncrossing property of Bohm trajectories. In particular, it is shown that the average transmission and reflection times can be obtained without actually calculating a single trajectory, and that the position of a Bohm particle can be directly obtained from the wave function, i.e., without following its trajectory. On the other hand, the method of McKinnon and Leavens [17] is reformulated so that it can be used to obtain the distributions of transmission, reflection, and dwell times corresponding to *arbitrary* wave packets and potential barriers, without calculating trajectories. Finally, subjective implications of the fact that Bohm trajectories never intersect are also discussed. In this regard, we try to reconcile the results obtained within Bohm's approach with the common sense interpretation of the scattering processes in one-dimensional tunneling configurations. We center our discussions in double-barrier resonant tunneling structures (DBRTS) because the phenomenology is richer than in the simpler case of single barriers. In all the numerical examples, physical parameters (effective mass, barrier heights and thicknesses, etc.) typical of the GaAs/AlGaAs system are considered.

II. NONCROSSING PROPERTY OF BOHM TRAJECTORIES

In Bohm's interpretation of nonrelativistic QM [12–14], an electron is a particle the motion of which is completely determined by an objectively real field related to the wave function $\Psi(x,t)$, so that it has a well-determined position and velocity at each instant of time, i.e., a well-defined trajectory. In this casual interpretation, $\Psi(x,t)$ is a solution of the time-dependent Schrödinger equation (TDSE), the velocity at any space-time point is uniquely given by $v(x,t)=\partial S(x,t)/\partial x$ [$S(x,t)$ being the phase of the complex wave function], and $|\Psi(x,t)|^2dx$ is the probability of the electron being between x and $x+dx$ at time t even in the absence of a position measurement. The description of any scattering problem requires the choice of an initial wave function $\Psi(x,0)$ adequate to the particular situation, and the analysis of its subsequent time evolution. A description in terms of scattering energy eigenstates is not convenient because these are stationary states and time evolution is inherent to the concept of trajectory. Moreover, if stationary states are used, unphysical and inconsistent results come out within Bohm's framework [18,19]. In any case, this is not a limitation of Bohm's interpretation but rather a consequence of the nature of these states themselves which, not being normalized, cannot be a perfect description of the quantum system. For these reasons, localized time-dependent wave packets have to be used to analyze scattering processes within Bohm's approach. Assuming a particular $\Psi(x,0)$, and given the position x_0 of an electron within the wave packet, its subsequent trajectory $x(x_0,t)$ is uniquely determined by simultaneous integration of the TDSE and the guidance equation $dx/dt=v(x,t)$. However, due to the uncertainty principle, the position of the electron at $t=0$ cannot be precisely known and, as a consequence, one must deal with an ensemble of trajectories that can be labeled by x_0. To determine the expectation value of any function (observable or not) one has to average the results of all the possible trajectories according to a weight given by $|\Psi(x_0,0)|^2dx$.

The Bohm trajectories can also be viewed as the solutions of a modified Hamilton-Jacobi equation [12] and, as such, they cannot cross each other in the configuration space. Moreover, since the velocity of the Bohm particles is uniquely determined by $\partial S(x,t)/\partial x$, it immediately follows that the trajectories do not cross in space-time either. In fact, if two trajectories should cross at a point (x,t), the corresponding velocities would also be identical, and the trajectories would cross in the configuration space. In one-dimensional systems, the fact that Bohm trajectories do not intersect each other means that any pair of particles starting at initial points $x_{02}>x_{01}$ will maintain their relative positions all the time, i.e., $x(x_{02},t)>x(x_{01},t)$. Since, on the other hand, the probability density $|\Psi(x,t)|^2$ is directly related to the positions of the Bohm particles,

$$|\Psi(x,t)|^2=\int_{-\infty}^{\infty}dx_0|\Psi(x_0,0)|^2\delta(x-x(x_0,t)), \tag{3}$$

it follows that the total probability presence at the right (or left) of any trajectory is constant for all the times. Thus, if we define $Q(x,t)$ as the probability presence to the right of point x at time t:

$$Q(x,t)\equiv\int_x^{\infty}|\Psi(x',t)|^2dx'=\int_0^t J(x,t')dt', \tag{4}$$

we can also label each trajectory by $Q(x_0)\equiv Q(x_0,0)$ and the probability presence to the right of $x(x_0,t)$ is always $Q(x_0)$:

$$Q(x_0)\equiv\int_{x_0}^{\infty}dx|\Psi(x,0)|^2=\int_{x(x_0,t)}^{\infty}dx|\Psi(x,t)|^2. \tag{5}$$

The first consequence of the noncrossing property of Bohm trajectories, already pointed out by Leavens and Aers [5], is that there is a bifurcation trajectory $x_c(t)=x(x_{c0},t)$ implicitly given by

$$|T|^2=\int_{x_c(t)}^{\infty}dx|\Psi(x,t)|^2, \tag{6}$$

which divides the wave packet in two spatially separated parts, $|\Psi_T(x,t)|^2$ and $|\Psi_R(x,t)|^2$, which are to be transmitted and reflected, respectively:

$$|\Psi_T(x,t)|^2=|\Psi(x,t)|^2\Theta[x-x_c(t)],$$
$$|\Psi_R(x,t)|^2=|\Psi(x,t)|^2\Theta[x_c(t)-x], \tag{7}$$

$\Theta[x]$ being the unit step Heaviside function. This is particle-like decomposition [20], which allows the calculation of the

average transmission and reflection times directly from the wave function without weighting trajectories [5]:

$$\tau_T=\frac{1}{|T|^2}\int_0^\infty dt\int_a^b dx|\Psi_T(x,t)|^2,$$

$$\tau_R=\frac{1}{|R|^2}\int_0^\infty dt\int_a^b dx|\Psi_R(x,t)|^2. \tag{8}$$

Notice that only the bifurcation trajectory $x_c(t)$ is needed to obtain $|\Psi_T(x,t)|^2$ and $|\Psi_R(x,t)|^2$, and that this directly allows the calculation of τ_T and τ_R. However, the explicit calculation of $x_c(t)$ is not required to obtained these tunneling times, as it will be shown below.

The noncrossing property of Bohm trajectories has other interesting practical consequences that were not discussed in [5]: (1) the position of any Bohm particle can be obtained at any arbitrary time without calculating the corresponding trajectory; and (2) the causal distributions of transmission, reflection, and dwell times can also be directly determined from the time-evolved wave function. Section III is entirely dedicated to show how these distributions can be obtained without evaluating trajectories, and the rest of this section is devoted to the discussion of how to assess the position of any Bohm particle from $\Psi(x,t)$, and to some practical implications of this property. From Eq. (5), it immediately follows that we can determine the position of a Bohm particle at any time by integrating the presence probability. In other words, for a particle starting at x_0, we can compute its position $x(x_0,t_0)$ at any arbitrary instant of time t_0 without wondering about its trajectory between $t=0$ and $t=t_0$. In fact, having calculated $Q(x_0)$ from the initial wave packet, we can determine $x(x_0,t_0)$ by spatial integration of the time-evolved wave function $\Psi(x,t_0)$. This is quite a trivial result, but it may have very interesting practical consequences. If, for example, Bohm trajectories were used for the extension of the Monte Carlo (MC) simulation technique to quantum-based electron devices such as resonant tunneling diodes [21], the direct calculation of the position of the Bohm particles would significantly reduce the computation times. In a MC scheme, the time of flight is chosen through the generation of a random number according to the total scattering rate. Using Eq. (5), we would be able to obtain the position of the electrons after their free flight without computing their entire trajectory. This would largely improve the numerical efficiency because of the huge number of trajectories that should otherwise be calculated. Let us finally indicate that the convenience of this procedure to assess the position of the Bohm particles can be enhanced by the use of an appropriate method to solve the TDSE. In this regard, instead of time-discretizing this equation, as it is usually done [22], it is more convenient to begin by numerically solving the stationary Schrödinger equation (see, for example, [23,24]), and then project the initial wave packet onto the basis of Hamiltonian scattering eigenstates $\Psi_E(x)$. In this way, the time-dependent wave function can be directly obtained by superposition, i.e., without calculating it at intermediate times:

$$\Psi(x,t_0)=\int_0^\infty a(E)e^{-i(Et_0)/\hbar}\Psi_E(x)dE \tag{9}$$

with $a(E)=\int_0^\infty\Psi_E^*(x)\Psi(x,0)dx$. Thus, to obtain the position of any Bohm particle at time t_0, we do not need to evaluate the associated wave function nor its trajectory at intermediate times between $t=0$ and $t=t_0$. This method, which is the one used in this paper to integrate the TDSE is only valid for time-independent potential profiles (this is the case between successive actualizations of the potential in a MC simulation), and has the additional advantage of avoiding spurious reflections at the boundaries of the integration box [22].

III. DISTRIBUTION OF TUNNELING TIMES

As we have advanced in Sec. II, another important consequence of the noncrossing property of Bohm trajectories is that the distributions of transmission, reflection, and dwell times can also be be obtained without calculating trajectories. As for the transmission time distribution, McKinnon and Leavens have recently discussed how to evaluate it by connecting the arrival time distributions at the two boundaries of the barrier ($x=a$ and $x=b$) with the help of Eq. (5) [17]. Although we agree with their basic idea of connecting arrival time distributions, we want to point out that their method is not completely general. In particular, they implicitly assumed that different Bohm particles must have different transmission times and, although this is the case in the most common situations, this is not true in general. This is discussed in detail below, and a reformulation of McKinnon and Leavens's method is presented to overcome its limitations.

Recently, Muga, Brouard, and Macías have rigorously justified the use of the current density as an arrival time distribution within the conventional interpretation of QM [25]. If $J(x,t)$ is the probability current density at point x and time t, the quantum-mechanical particles cross (arrive at) this point distributed according to

$$P_x(t)=\frac{|J(x,t)|}{\int_{-\infty}^{\infty}|J(x,t)|dt}. \tag{10}$$

The absolute value is required to take into account that the current density can take negative values, and the normalization is needed because it is neither guaranteed that all the particles arrive at point x, nor that they do not cross the x interface several times from left to right and vice versa. Equation (10) is quite intuitive, and had already been previously proposed by other authors [10,26,27]. Following McKinnon and Leavens [17], we consider $Q(x,t)$ [see Eq. (4)] at the boundaries of the barrier, i.e., $Q(a,t)$ and $Q(b,t)$. For the typical problem of a Gaussian wave packet impinging upon a DBRTS (see diagram in Fig. 1) from left to right, $Q(a,t)$ and $Q(b,t)$ appear as shown in Fig. 2. Notice that $Q(b,t)$ increases monotonously towards $|T|^2$ (though oscillating for reasons that will be discussed below), and that this means that $J(b,t)>0$ at all times. In this regard, we have to point out that although the positivity of the current density has been recently demonstrated for the asymptotic region sufficiently far from the barrier [25], it can be shown that the current density can eventually take negative values at $x=b$ in extreme situations (capricious wave packets). However, in the rest of the paper we will assume that $J(b,t_b)>0$ or, in other words, we will neglect the possibility of reentrant

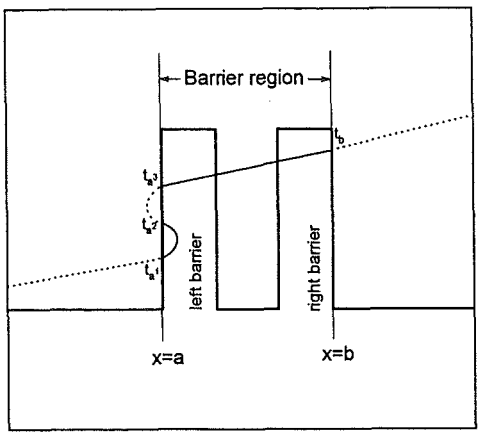

FIG. 1. Schematic diagram of the considered symmetric double-barrier heteroestructures. A hypothetical trajectory is used to define t_a (t_a^i) and t_b as the times the trajectory crosses the $x=a$ and the $x=b$ interface, respectively.

Bohm trajectories at the $x=b$ interface. In this sense, our numerical results of this and previous works have always confirmed this assumption [19,28], in spite of the fact that in QM the probability current can take negative values even for states having only positive momentum components [29]. This is in agreement wiht Leavens and Aers's results [5], who never found Bohm trajectories crossing the $x=b$ boundary from right to left. In Leavens's words, "a flag in the author's computer codes to monitor reentrant trajectories at $x=b$ has yet to be triggered" [27]. This is not the case, of course, at the $x=a$ boundary. In particular, all the reflected particles that cross this interface from left to right cross it again from right to left. For the case shown in Fig. 2, $Q(a,t)$ increases monotonously [though oscillating as $Q(b,t)$] before reaching its maximum and then it decreases towards $|T|^2$. However, this behavior is not the most general one (as it will be shown below) because, depending on the shape of the initial wave packet, $Q(a,t)$ can present several relative maxima, which correspond to particles that cross the $x=a$ boundary more than once before being finally reflected or transmitted.

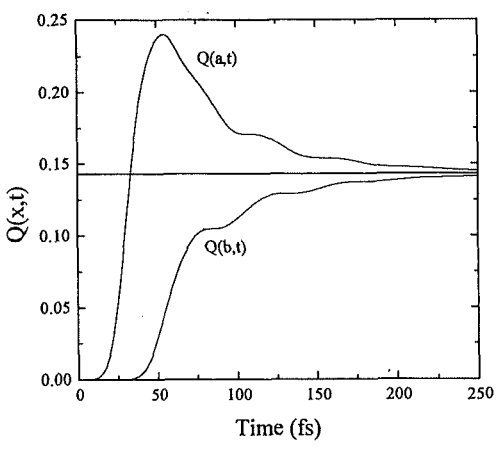

FIG. 2. Probability presence at the right of the extreme double-barrier points $Q(a,t)$ and $Q(b,t)$ as a function of time. These results correspond to the resonant transmission of a Gaussian electron wave packet (with the effective mass of point Γ in GaAs, i.e., 0.067 times the free-electron mass) incident upon a double-barrier potential typical of the GaAs/AlGaAs system: barrier height of 0.3 eV, barrier thickness 2 nm, and well width of 18 nm. The well is wide so as to observe the oscillations in the Bohm trajectories. The horizontal line corresponds to $Q(t)=|T|^2$, or in other words, to the $x_c(t)$ trajectory.

A. Average tunneling times

Before discussing the method to calculate the tunneling time distributions, let us show how τ_D, τ_T, and τ_R can all be obtained from $Q(a,t)$ and $Q(b,t)$, i.e., without evaluating a single trajectory. For the sake of simplicity, we begin by considering cases as that of Fig. 2, i.e., with $Q(a,t)$ showing a single maximum. First of all, notice that the probability presence in the barrier region, $D(t)=\int_a^b|\Psi(x,t)|^2dx$, is equal to $Q(a,t)-Q(b,t)$. Thus, according to Eq. (1), the dwell time is

$$\tau_D=\int_0^\infty[Q(a,t)-Q(b,t)]dt \tag{11}$$

and this corresponds to the area enclosed by the two curves of Fig. 2. It can also be shown that this area is divided by the horizontal line $Q(t)=|T|^2$ in two subareas that are proportional to τ_T and τ_R, respectively. Effectively, since Bohm trajectories do not cross, all the particles that have entered the barrier are to be finally transmitted if $Q(a,t)<|T|^2$. Thus, for $t<t_1$ [with t_1 implicitly defined by $Q(a,t_1)=|T|^2$], the probability presence of *to be transmitted* particles in the barrier region, $D_T(t)=\int_a^b|\Psi(x,t)|^2dx$, is equal to $Q(a,t)-Q(b,t)$, and coincides with $D(t)$. For $t>t_1$, only those particles located at the right of $x_c(t)$ (which for $t>t_1$ is located within the barrier or at the right side of it) are to be transmitted, and hence $D_T(t)=|T|^2-Q(b,t)$. As a consequence, the average transmission time is given by

$$\tau_T=\frac{1}{|T|^2}\int_0^{t_1}[Q(a,t)-Q(b,t)]dt + \frac{1}{|T|^2}\int_{t_1}^\infty[|T|^2-Q(b,t)]dt. \tag{12}$$

This demonstrates that the area enclosed by the two curves of Fig. 2, $Q(a,t)$, $Q(b,t)$, and by the horizontal line $Q(t)=|T|^2$, is equal to $|T|^2\tau_T$. On the other hand, from Eq. (2) it follows that the rest of the area enclosed by $Q(a,t)$ and $Q(b,t)$, i.e., the area over $Q(t)=|T|^2$ and below $Q(a,t)$, is equal to $|R|^2\tau_R$. This can also be formulated as

$$\tau_R=\frac{1}{|R|^2}\int_{t_1}^\infty[Q(a,t)-|T|^2]dt. \tag{13}$$

In the most general case when the wave packet is such that the corresponding $Q(a,t)$ has several maxima and crosses

he $Q(t)=|T|^2$ line several times before decreasing towards $T|^2$, the procedure to evaluate the average tunneling times is analogous. The case of the dwell time is trivial because τ_D is always given by Eq. (11), independently of the shape of $Q(a,t)$. The other two times can also be obtained from $Q(a,t)$ and $Q(b,t)$, but this requires a straightforward generalization of Eqs. (12) and (13). In the most general case, it can be easily demonstrated that the transmission time is given by

$$\tau_T=\frac{1}{|T|^2}\int_0^\infty \{\min[Q(a,t),|T|^2]-Q(b,t)\}dt \qquad (14)$$

and the reflection time by

$$\tau_R=\frac{1}{|R|^2}\int_0^\infty \{\max[Q(a,t),|T|^2]-|T|^2\}dt, \qquad (15)$$

Eqs. (12) and (13) being particular cases of Eqs. (14) and (15), respectively. This demonstrates that the calculation of trajectories is not needed to obtain the average tunneling times. In particular, the calculation of $x_c(t)$ is also not required, since the decomposition of the wave packet into *to be transmitted* and *to be reflected* components is implicitly done when the area between $Q(a,t)$ and $Q(b,t)$ is divided by the horizontal line $Q(t)=|T|^2$. In this regard, notice that in a $Q=Q(t)$ plot, the Bohm trajectories fall on horizontal lines because of their noncrossing property, and that $Q(t)=|T|^2$ actually corresponds to the bifurcation trajectory $x_c(t)$.

B. Transmission time distribution

As discussed by McKinnon and Leavens [17], the problem of calculating the transmission time distribution can be reduced to matching points of the arrival distribution at $x=a$ with points of the arrival distribution at $x=b$. In the standard interpretation of QM, this matching is not possible because the actual concept of a particle sequentially arriving at two points is meaningless. On the contrary, within Bohm's approach, there is a well-defined procedure that consists in identifying which particle arrives at these boundaries at each instant of time. In this regard, we have seen that a Bohm particle (trajectory) can be labeled by its starting position x_0. However, the noncrossing property of the trajectories provides an alternative identification method, which consists in labeling the particles by their corresponding value of $Q(x_0)$, as defined in Eq. (5). In this way, the particle that arrives at the $x=b$ boundary at $t=t_b$ is determined by $Q[x_0(t_b)]=Q(b,t_b)$, and one can readily calculate the instant of time t_a at which the same particle crossed $x=a$ by requiring $Q(a,t_a)=Q[x_0(t_b)]$. This latter equation can have more than one solution because the particles can cross the $x=a$ interface several times. However, and for the sake of simplicity, we will first consider that (as in Fig. 2) the transmitted particles only cross this boundary once. In this simplest case, the transmission time of the particle which starts at $x_0(t_b)$ is just $t_{ab}=t_b-t_a$.

Provided that there are no reentrant trajectories at $x=b$, the distribution of arrival times at this interface can be calculated from $Q(b,t)$ as

$$P_b(t_b)=\frac{1}{|T|^2}\left.\frac{\partial Q(b,t)}{\partial t}\right|_{t=t_b}. \qquad (16)$$

For this reason, McKinnon and Leavens [17] identified $Q(b,t_b)$ as $|T|^2$ times the cumulative arrival time distribution function associated with $P_b(t_b)$. After that, they considered that the cumulative transmission time distribution $Q_T(t_{ab})$ could be calculated by inverting the relation

$$t_{ab}(Q(x_0))=t_b(Q(x_0))-t_a(Q(x_0)), \qquad (17)$$

i.e., by determining the value of $Q(x_0)$ that corresponds to each transmission time t_{ab}, and assuming that $Q_T(t_{ab})=Q(x_0)$. Finally, they evaluated the transmission time distribution $P_T(t_{ab})$ by differentiating $Q_T(t_{ab})$ with respect to t_{ab} and normalizing by $|T|^2$. However, this procedure is correct only if all the transmitted particles have different transmitted times, i.e., if the relation between t_{ab} and $Q(x_0)$ is single valued. This condition is satisfied for all the cases worked out in [17] but, in the most general case, several particles can have the same transmission time and, as a consequence, Eq. (17) cannot be inverted. This will be explicitly shown by means of an example but, for the moment, let us reformulate the method so that it can be applied to all possible cases.

To calculate the transmission time distribution, we propose to proceed as follows: first that the transmission time t_{ab} is calculated for each value of t_b, i.e., for all the Bohm particles that arrive at $x=b$. In this way, a function $t_{ab}=t_{ab}(t_b)$ is obtained. If the transmission time is different for all the trajectories, i.e., if the function $t_{ab}(t_b)$ is monotonic, the transmission time distribution $P_T(t_{ab})$ is directly given by

$$P_T(t_{ab})=P_b(t_b)\left[\frac{dt_{ab}(t_b)}{dt_b}\right]^{-1}=\frac{1}{|T|^2}J(b,t_b)\left[\frac{dt_{ab}(t_b)}{dt_b}\right]^{-1}. \qquad (18)$$

This expression is exactly equivalent to the inversion of Eq. (17) proposed by McKinnon and Leavens [17], and it reveals that the transmission distribution is obtained from a local renormalization of the arrival time distribution. For the particular case of Fig. 2, which corresponds to a Gaussian wave packet impinging upon a DBRTS, the function $t_{ab}(t_b)$ is shown in Fig. 3(a). After a certain time delay, the relation between t_{ab} and t_b becomes linear and with unity slope, and this occurs when all the *to be transmitted* particles have crossed the $x=a$ interface. Since t_{ab} increases monotonously with t_b, Eq. (18) can be used to calculate $P_T(t_{ab})$, as it is explicitly demonstrated in Fig. 3(b), where the obtained distribution is compared to that evaluated by integration of 2.5×10^4 Bohm trajectories. The periodic bumps of the obtained distribution are due to the presence of Bohm trajectories that oscillate in the well of the DBRTS before being finally transmitted, and which are also the cause for the oscillatory structure in $Q(a,t)$ and $Q(b,t)$ of Fig. 2. Equation (18) is valid for a monotonic $t_{ab}(t_b)$ but, as previously said, this function can be nonmonotonic under some circumstances. In these situations, several discrete values $N(t_{ab})$ of arrival times, t_b^i [with $1<i<N(t_{ab})$], give exactly the same transmission time t_{ab}. The dependence of N on t_{ab} is explic-

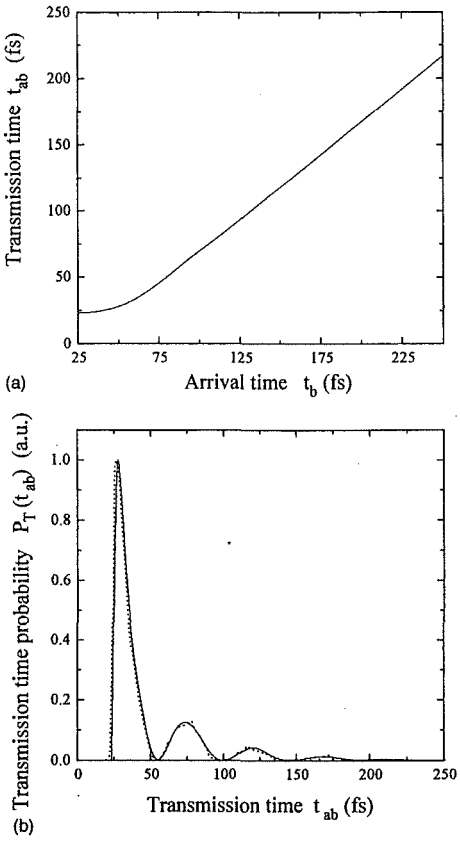

FIG. 3. (a) Transmission time as a function of time of arrival at the $x=b$ interface for the scattering process of Fig. 2. (b) Transmission time distribution obtained by calculating 2.5×10^4 trajectories (dotted line) compared with that obtained using the procedure presented in the text (continuous line).

itly indicated to emphasize that the number of Bohm particles that have identical transmission times can be different for the different t_{ab} values. In any case, since $t_{ab}(t_b)$ is not single valued, Eq. (17) cannot be inverted to obtain $P_T(t_{ab})$ as proposed by McKinnon and Leavens [17]. However, the generalization of Eq. (18) is straightforward, as it only requires to sum up the contribution of all the $N(t_{ab})$ particles. In this way, the transmission time distribution can be calculated as

$$P_T(t_{ab})=\sum_{i=1}^{N(t_{ab})}\frac{1}{|T|^2}J(b,t_b^i)\left[\left.\frac{dt_{ab}(t_b)}{dt_b}\right|_{t_b=t_b^i}\right]^{-1}. \quad (19)$$

Before considering a particular example of this situation, let us remove the assumption that the left boundary of the barrier is only crossed once by each transmitted trajectory. Even in this case, however, if the particle is to be transmitted, we know that the $x=a$ boundary has to be crossed an odd number of times, $N'(t_{ab})$. These multiple crossings affect the calculation of t_{ab} since the equation $Q(a,t_a)=Q[x_0(t_b)]$ has $N'(t_{ab})$ solutions t_a^i that correspond to the sequential arrival of the $x_0(t_b)$ particle to the point $x=a$ from left to right and vice versa. When a particle crosses $x=a$ from left to right, it enters the barrier region, and when the crossing takes place in the opposite sense, the particle abandons the barrier. Only those time intervals with the particle within the barrier have to be counted up to calculate the transmission time to be consistent with the definition of τ_T as the average time spent by the transmitted particles in the barrier region. In other words, we have to determine the time elapsed from the very first crossing of $x=a$ (i.e., t_a^1) to the time when it finally crosses $x=b$ (i.e., t_b), but we have to subtract the time intervals between right-to-left and left-to-right crossings. Thus, the transmission time is given by

$$t_{ab}=t_b-t_a^1-\sum_{n=1}^{[N'(t_{ab})-1]/2}(t_a^{2n+1}-t_a^{2n}) \quad (20)$$

when the $x=a$ boundary is crossed $N'(t_{ab})$ times by the same particle. The rest of the procedure to calculate the transmission time distribution is identical to that corresponding to a monotonic $Q(a,t)$. As an example of the need of Eqs. (20) and (19) to calculate the transmission time and the transmission time distribution, respectively, we consider a wave function composed of two spatially separated Gaussian wave packets impinging upon a DBRTS. A similar example, initially studied by Leavens and Aers [5], was subsequently used by Landauer and Martin to comment on the *counterintuitive* consequences of the noncrossing property of Bohm trajectories [9]. Section IV is entirely devoted to the intuitive interpretation of scattering events within Bohm's approach, and this example will be further examined. However, let us now concentrate on how the transmission time distribution can be calculated in this case. The electrons are considered to be prepared at $t=0$ in the wave function:

$$\Psi(x,0)=\frac{1}{\Omega(\pi\sigma_1^2)^{1/4}}\exp(ik_1x)\exp\left[-\frac{(x-x_1)^2}{2\sigma_1^2}\right]+\frac{1}{\Omega(\pi\sigma_2^2)^{1/4}}\exp(ik_2x)\exp\left[-\frac{(x-x_2)^2}{2\sigma_2^2}\right], \quad (21)$$

which is composed of two packets centered at the coordinate points x_1 and x_2 (with $x_1<x_2$), and at wave numbers k_1 and k_2 (with $k_1<k_2$), and which evolves towards a DBRTS that has a transmission resonance at k_1. The constant Ω is for normalization, and σ_1 and σ_2 are the standard deviations of two successive packets. The actual parameters that define the barrier and the wave function are those specified in the caption of Fig. 4. This figure shows the corresponding cumulative arrival time distributions at $x=a$ and $x=b$, i.e., $Q(a,t)$ and $Q(b,t)$, respectively. The asymptotic behavior at $t\to\infty$ is identical to that shown in Fig. 2, i.e., both $Q(a,t)$ and $Q(b,t)$ converge towards $|T|^2$ because the probability presence at the right side of the barrier is equal to $|T|^2$ when the scattering event is finished. As expected, $Q(b,t)$ increases monotonously because of the positivity of $J(b,t)$. On the other hand, however, the behavior of $Q(a,t)$ is different from that shown in Fig. 2 in several respects. First of all,

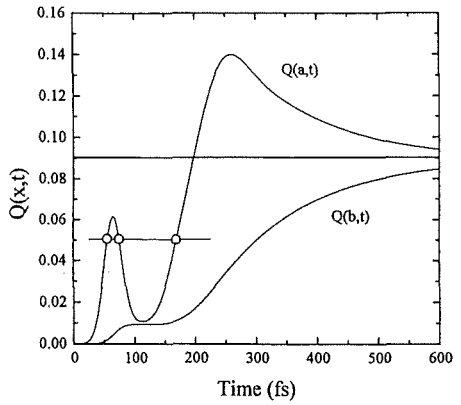

FIG. 4. Probability presence at the right of the extreme barrier points $Q(a,t)$ and $Q(b,t)$ as a function of time. These results correspond to the double Gaussian wave packet ($m^*=0.067m_0$) described in the text [Eq. (21)] impinging upon a double-barrier potential with 0.3-eV-barrier height, 3-nm-thick barriers, and 5-nm-wide well. The horizontal corresponds to $Q(t)=|T|^2$, i.e., it separates transmitted and reflected particles. The horizontal line (whose crossing are marked with open circles) corresponds to one of the Bohm particles that cross the $x=a$ interface three times before being finally transmitted.

notice that $Q(a,t)$ shows two relative maxima before finally decreasing towards $|T|^2$. These maxima are related to the arrival and reflection of the two successive packets but, as we will later show explicitly, only particles from the first one enter into the barrier region in the two successive attempts to cross it. When $Q(a,t)$ decreases after the first relative maximum, some of the particles that have entered the barrier are provisionally reflected (i.e., they cross the $x=a$ interface from right to left) before being thrown again towards the barrier after a collision with the second wave packet. Since the magnitude of the first maximum is smaller than $|T|^2$, all the particles contributing to it are to be finally transmitted. As a consequence, some of the transmitted particles cross the $x=a$ interface three times (see the horizontal line and the circles in Fig. 4). For these particles, Eq. (20) is required to calculate their transmission time because during the interval between the second and the third crossings they are outside the barrier region. On the other hand, if we look in Fig. 5(a) at the relation $t_{ab}(t_b)$ obtained using this equation, we perceive that it contains negative slope regions. These negative slopes are related to the extrema of $Q(a,t)$ and, in particular, to the first minimum and the first maximum, respectively. It must be said that several crossings of the $x=a$ interface are a necessary (though not sufficient) condition for having a nonmonotonic relation between t_{ab} and t_b. On the other hand, this nonmonotonic behavior means that several Bohm particles cross the barrier in exactly the same transmission time. In particular, as shown in the inset of Fig. 5(a), in the particular example that we are analyzing, there are groups of three particles with identical transmission times. In cases as this one, Eq. (17) cannot be inverted, and the calculation of $P_T(t_{ab})$ requires the use of our reformulated procedure that is explicitly represented by Eq. (19). Using this procedure,

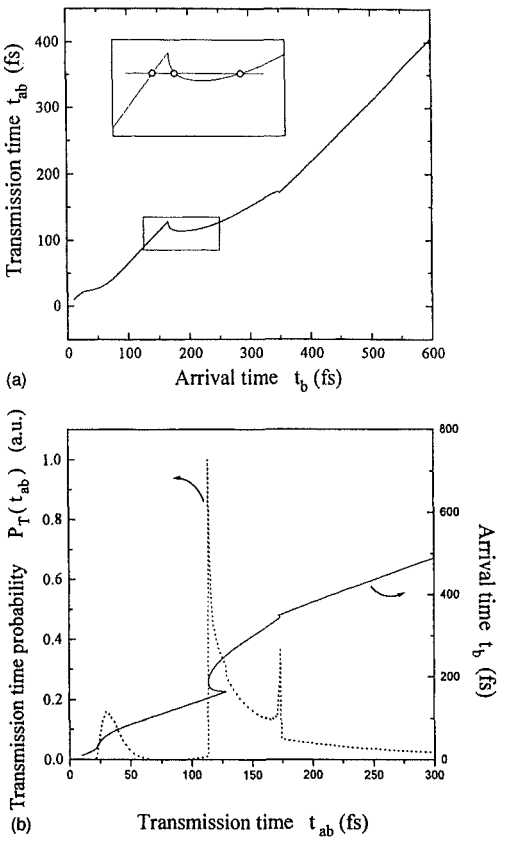

FIG. 5. (a) Transmission time versus arrival time at the $x=b$ interface for the scattering process of Fig. 4. The inset highlights a region with negative slope and the fact that some groups of three Bohm particles (indicated by open circles) that arrive at $x=b$ at different times have exactly the same transmission time. (b) Transmission time distribution associated with the scattering of the double-packet wave function. The $t_{ab}(t_b)$ curve of (a) is repeated here to explain the origin of the two sharp peaks of the transmission distribution.

the transmission time distribution shown in Fig. 5(b) has been obtained without calculating a single trajectory. The curve $t_{ab}(t_b)$ of Fig. 5(a) has also been repeated in Fig. 5(b) to enlighten some relevant features of the transmission time distribution. The first broad bump of this distribution is related to the particles that are transmitted during the first interaction of the front wave packet with the barrier. This can be appreciated in Fig. 4, where $Q(b,t)$ is seen to increase and saturate for $t_b<100$ fs, showing a flat terrace that extends up to $t_b>150$ fs, and which corresponds to the time interval elapsed between the two successive interactions of the front wave packet with the barrier (these sequential interactions and the fact that all the transmission comes from the front packet will become more evident in Sec. IV). Returning back to the description of the transmission distribution of Fig. 5(b), we appreciate a second broad peak that corresponds to the second interaction of the packet with the

barrier. This second bump, however, is limited by two sharp peaks that can be understood by looking at the superposed $t_{ab}(t_b)$ function. In this regard, we must notice that eventual flat regions in the $t_{ab}(t_b)$ characteristic are an indication of particles that arrive at different instants of time to $x=b$ and that spend exactly the same time in the barrier region. These flat regions would consequently lead to δ functions in the transmission time distribution. In the same way, the extrema of $t_{ab}(t_b)$ are locally flat regions which lead to sharp peaks [as those of Fig. 5(b)] in the transmission time distribution because $dt_{ab}/dt_b=0$.

C. Distribution of dwell and reflection times

Although we have used the arrival time distribution at $x=b$ as the starting point to calculate $P_T(t_{ab})$, an analogous procedure can be followed using the arrival distribution at $x=a$. In this regard, it is straightforward to demonstrate that the transmission time distribution can also be calculated as

$$P_T(t_{ab})=\sum_{i=1}^{N(t_a)} \frac{1}{|T|^2} J(a,t_a^i)\left[\left.\frac{dt_{ab}(t_a)}{dt_a}\right|_{t_a=t_a^i}\right]^{-1}, \quad (22)$$

where t_a^i represents the time of first crossing of the $x=a$ interface of the $N(t_{ab})$ particles that have exactly the same transmission time t_{ab}. Moreover, this procedure can be easily extended to calculate the reflection and dwell time distributions. Until now, we have only considered transmitted particles which, as discussed above, are those with $Q(x_0)<|T|^2$, i.e., those that arrive at $x=a$ before t_1. Now, we can also consider those particles which are reflected, i.e., those that arrive at the $x=a$ interface later than t_1. According to the assumption that $J(b,t_b)$ is always positive, the reflected particles never cross the $x=b$ interface, and they remain within the barrier during time intervals enclosed by their first and last crossings of the $x=a$ interface. Contrary to the transmitted particles, the reflected ones cross this interface an even number of times, but the procedure to calculate their residence time in the barrier region t_{aa} is analogous to that used to evaluate t_{ab} [see Eq. (20)]. As for the calculation of the reflection time distribution, although the procedure is very similar, a relevant difference arises from the fact that not all the reflected particles enter into the barrier region, many of them being reflected without ever reaching $x=a$. The fraction of particles that enter the barrier and are ultimately reflected, $|R_1|^2$, can be directly obtained from $Q(a,t)$, since its absolute maximum is precisely $|T|^2+|R_1|^2$. The rest of the reflected particles, i.e., a fraction of the total equal to $|R|^2-|R_1|^2$, never enter the barrier and, as a consequence, have zero reflection time. Thus, the reflection time distribution must always include a term $[|R|^2-|R_1|^2]\delta(t)$ to preserve the normalization. The distribution of reflection times of those particles that actually enter the barrier region is obtained following a procedure analogous to that of Eq. (22) for transmitted particles, but now for those particles arrive at $x=a$ later than t_1. In this way, the reflection time distribution $P_R(t_{aa})$ is obtained:

$$P_R(t_{aa})=\frac{|R|^2-|R_1|^2}{|R|^2}\delta(t) + \frac{1}{|R|^2}\sum_{i=1}^{N(t_{aa})} J(a,t_a^i)\left[\left.\frac{dt_{aa}(t_a)}{dt_a}\right|_{t_a=t_a^i}\right]^{-1}, \quad (23)$$

where the t_a^i represent the first time of arrival to $x=a$ of the $N(t_{aa})$ reflected particles that have exactly the same residence time in the barrier. Finally, consistently weighting $P_T(t_{ab})$ and $P_R(t_{aa})$ by $|T|^2$ and $|R|^2$, respectively, we can directly obtain the dwell time distribution $P_D(t)$:

$$P_D(t)=[|R|^2-|R_1|^2]\delta(t)+\sum_{i=1}^{N(t_{ab})} J(a,t_a^i)\left[\left.\frac{dt_{ab}(t_a)}{dt_a}\right|_{t_a=t_a^i}\right]^{-1} + \sum_{i=1}^{N(t_{aa})} J(a,t_a^i)\left[\left.\frac{dt_{aa}(t_a)}{dt_a}\right|_{t_a=t_a^i}\right]^{-1}, \quad (24)$$

t being equal to t_{ab} or t_{aa} for transmitted and reflected particles, respectively.

Notice that in all the considered cases, the distributions of tunneling times have been obtained without calculating trajectories. All that is needed is the time-evolved wave function, which is used to calculate the current probability density at the boundaries, and to link the corresponding times of arrival. Again, this represents a very important improvement in the efficiency of the numerical procedures because a very large number (10^4–10^5) of trajectories is usually needed to obtain reliable distributions. Finally, it is worth remarking again that although the arrival time distributions are perfectly defined within the standard interpretation of QM, the distributions of transmission and reflection times only make sense in Bohm's framework because a causal connection between the crossings of the two boundaries of the barrier is needed to calculate t_{ab} and t_{aa}.

IV. INTUITIVE INTERPRETATION OF THE SCATTERING OF WAVE PACKETS

Let us now consider the implications of the noncrossing property of Bohm trajectories on the intuitive interpretation of the scattering of wave packets by one-dimensional potential barriers. In this regard, Landauer and Martin [9] have made skeptical comments concerning two limit cases: (i) a wave function composed of two spatially separated packets incident on an opaque barrier; and (ii) a very long wave packet (a day in duration) incident on a very short but high barrier. In the first case they wrote "*wave packets in succession, separated by a long time interval . . . all the transmitted paths still come from the very first tip of the first packet,*" and in the second, "*all the transmitted packet will come from about the first microsecond of the incident packet . . . a day is long compared to any of the kinetic times associated with such a short barrier.*" The second example is difficult to analyze numerically for obvious reasons, but we will use an enriched version of the first one to show that Bohm's results are fully compatible with an intuitive interpretation of both cases. In particular, we consider the double-packet wave function, defined in Sec. III B [Eq. (21)], which evolves towards a double-barrier structure that has a resonance around k_1. Since k_1 is the center of the rear packet spectrum, this

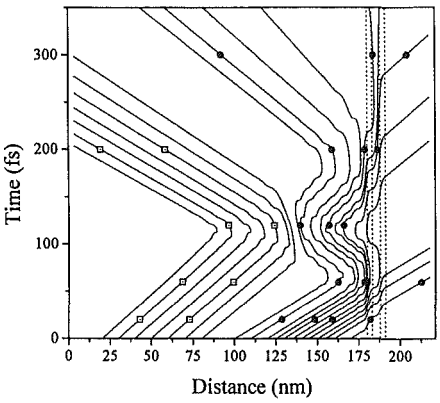

FIG. 6. Representative Bohm trajectories associated with double-packet scattering of Fig. 4. The position of the barriers is indicated by vertical dashed lines. The marks (squares for the rear packet and circles for the front one) are a visual aid to relate the trajectories with the evolution of the wave function shown in Fig. 7. Notice that the five horizontal lines (constant time) defined by the marks correspond to the five "snapshots" of the picture motion of the wave function shown in Fig. 7.

second packet is expected to practically control the whole transmission probability (this emphasizes the unexpected features of the first case considered by Landauer and Martin). Figure 6 shows selected Bohm trajectories and Fig. 7 is a picture motion of the traveling wave packet as obtained by numerical integration of the TDSE. At the beginning, the front packet travels faster towards the barrier and arrives to it

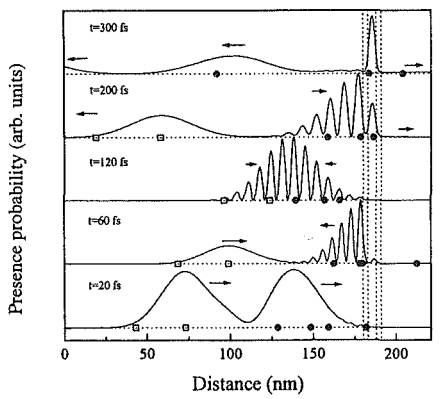

FIG. 7. Picture motion of the same double-packet wave function considered in Fig. 6, calculated by numerical integration of the time-dependent Schrödinger equation. Five representative "snapshots" obtained at different times are shown with the vertical scale arbitrarily changed in each case for clarity (although the norm of the wave function is always unity, it does not seem so because of the scale changes). The marks are visual aids that indicate the position of some related Bohm trajectories shown in Fig. 2. The double-barrier position is indicated by the vertical dashed lines, and the arrows indicate the sense of motion of the two packets.

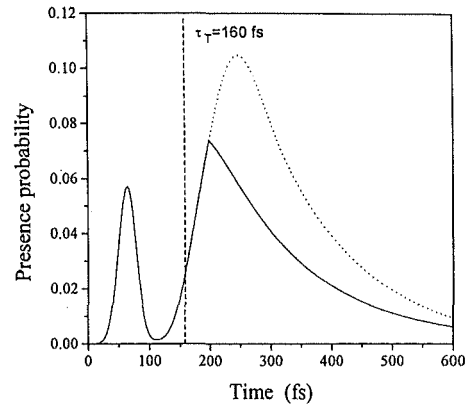

FIG. 8. Ensemble probability of finding the particles described by the double-packet wave function of Figs. 6 and 7 as a function of time during the scattering with the double-barrier potential. The dotted line corresponds to $D(t)$, which represents the probability of finding the particles in the barrier region, independently of the scattering channel (transmission or reflection). The continuous line corresponds to $D_T(t)$, which is the probability of finding *to be transmitted* particles in the barrier region. The vertical line indicates the average transmission dwell time as defined in expression (8), which in this case is 160 fs.

in first position. Only a small portion of this first packet is transmitted, and the rest of it is reflected with roughly the same momentum (k_2). At times of the order of 120 fs strong interference effects take place between the two packets, which in Fig. 6 appear as a collision between Bohm trajectories. Momentum is interchanged, and the front packet travels again towards the barrier, but now with roughly k_1. This change of momentum can be noticed in Fig. 6 by a change of the slope of the trajectories, but could also be appreciated in the spatial oscillations of the real (or the imaginary) part of the wave function [30]. This second attempt to cross the barrier is more successful because now the front packet reaches the double barrier under resonance (accumulation of particles in the well is also apparent in both figures). In the Schrödinger picture, there is not an unambiguous criterion to decide whether the observed self-interference effects correspond to the scattering or to the crossing of wave packets. However, although both interpretations are equally acceptable, only the first one is compatible with Bohm's picture. The intuitive idea that the second wave packet, being resonant, controls most of the transmission continues to be valid. What Bohm's formulation tells us is that the second packet does its job by *pushing* the first one with the appropriate momentum towards the barrier, instead of being transmitted itself. A similar point of view, and the same example analyzed in Figs. 6 and 7, is also suitable to enlighten the case of the one-day-long wave packet impinging upon a very short and opaque barrier.

To establish a clear distinction between the transmission time [as defined in expression (8)] and the duration of the whole scattering process, we have plotted in Fig. 8 the probability of finding a particle in the barrier region $D(t)$, and that of finding a particle *to be transmitted* in the same spatial

interval, $D_T(t)$. Two different peaks are perceived that correspond to the sequential interaction of the first wave packet with the barrier. In the first interaction event, $D_T(t)$ coincides with $D(t)$, and this means that all the particles that enter the barrier region are ultimately transmitted. The duration of the whole scattering process, which in this case is longer than 400 fs, can be appreciated to be much different from the average transmission time ($\tau_T \sim 160$ fs). The period of time between the successive interactions of the front packet with the barrier (separation of peaks in the figure) does not contribute to the transmission time, while it is certainly a relevant portion of the whole scattering process. This indirectly explains why the scattering of the one-day-long packet can be roughly interpreted as a steady-state situation (the common sense view according to Ref. [9]). What Bohm's formulation tells us is that most of the packet is reflected by self-interference effects and not by direct interaction with the barrier (it is reflected by the quantum potential in regions where the classical potential is zero). As a consequence, although the average transmission time can be of the order of picoseconds, the transmission of the small tip of the front packet can take much more time, i.e., as much as the interference time of the finally reflected packet (of the order of a day).

To finish with the intuitive interpretation of the wave-packet scattering, let us take another look at Fig. 6. In this figure we see that Bohm trajectories can be reflected for two different reasons: (i) interaction with the classical potential (i.e., the particles collide with the barrier) and (ii) collision with other trajectories traveling in the opposite direction. The second process is responsible for the reflection of those particles of the first packet, which never reach the barrier, and for the reflection of the entire second packet. These collisions between Bohm particles are related to the quantum potential in regions where the classical potential is zero but, for them to occur, there should be particles coming from right to left. In this regard, if the initial wave packet is prepared as a superposition of eigenstates incident from left to right (as is always assumed in scattering thought experiments), and the classical potential is zero for $x > b$, then finding particles coming from the right-hand side in this region will be at least very uncommon. This observation provides further intuitive support to the assumption of a positive current $J(b,t_b)$ or, equivalently, of the absence of reentrant trajectories at the $x=b$ boundary. From the above discussion, we conclude that the noncrossing property of Bohm trajectories does indeed allow an intuitive interpretation of the scattering of wave packets by potential barriers, and this means that claims that Bohm's approach provides counterintuitive results are only subjective appreciations.

V. CONCLUSIONS

Several aspects of the tunneling of electrons through potential barriers have been examined within the framework of Bohm's interpretation of quantum mechanics. In particular, we have focused our attention on the noncrossing property of the electron's trajectories. Although this property is also valid for three-dimensional problems, we have only considered the particular case of one-dimensional potentials and wave functions.

It has been shown that, due to the noncrossing property, the average tunneling times and the position of the Bohm particles can both be calculated without integrating and weighting trajectories. The consequences of this fact for the possible use of these trajectories for the extension of the Monte Carlo simulation technique to quantum-based devices have also been emphasized. On the other hand, a method to obtain the distributions of dwell, transmission, and reflection times without calculating trajectories has been presented. This method generalizes that of McKinnon and Leavens [17], which has been shown to have some limitations, but preserves the fundamental idea of connecting arrival time distributions. The presented method (hundreds of times faster than explicitly calculated 10^4 Bohm trajectories), not only largely improves the numerical efficiency in the calculation of distribution of tunneling times, but also allows the assessment of sharp features as those of Fig. 5(b), which would be very difficult to appreciate by calculating trajectories.

Finally, the intuitive physical interpretation of the scattering of wave packets by potential barriers has been considered within Bohm's picture. The obtained results show that not only are the Bohm trajectories fully compatible with the common interpretation of scattering processes, but that they can enlighten some aspects that are less clear in the standard interpretation of QM. In any case, it must be highlighted that the Bohm trajectories exactly reproduce the time-dependent behavior of the wave function so that all the dynamical information is contained in the solution of the time-dependent Schrödinger equation. In other words, one cannot consider that the behavior of $\Psi(x,t)$ is intuitive, and that of the Bohm trajectories counterintuitive because both lead to the same observable results. Claims that Bohm trajectories lead to counterintuitive results are subjective.

ACKNOWLEDGMENTS

The authors are grateful to the Dirección General de Investigación Científica y Técnica for supporting this work under Project No. PB94-0720.

[1] M. Büttiker, Phys. Rev. B **27**, 6178 (1983).
[2] D. Sokolovski and L. M. Baskin, Phys. Rev. A **36**, 4604 (1987).
[3] C. R. Leavens, Solid State Commun. **74**, 923 (1990).
[4] C. R. Leavens, Solid State Commun. **76**, 253 (1990).
[5] C. R. Leavens and G. C. Aers, in *Scanning Tunneling Microscopy III*, edited by R. Wiesendanger and H.-J. Güntherrodt (Springer, New York, 1993), p. 105.
[6] D. Sokolovski and J. N. L. Connor, Phys. Rev. A **47**, 4677 (1993).
[7] V. S. Olkhovski and E. Recami, Phys. Rep. **214**, 339 (1992).
[8] E. H. Hauge and J. A. Stóvneng, Rev. Mod. Phys. **61**, 917 (1989).
[9] R. Landauer and Th. Martin, Rev. Mod. Phys. **66**, 217 (1994).

[10] R. S. Dumont and T. L. Marchioro II, Phys. Rev. A **47**, 85 (1993).
[11] S. Brouard, R. Sala, and J. G. Muga, Europhys. Lett. **22**, 159 (1993).
[12] D. Bohm, Phys. Rev. **85**, 166 (1952).
[13] P. R. Holland, *The Quantum Theory of Motion* (Cambridge University Press, Cambridge, 1993).
[14] D. Bohm and B. J. Hiley, *The Undivided Universe: An Ontological Interpretation of Quantum Mechanics* (Routledge, London, 1993).
[15] C. Pagonis, Nature **364**, 398 (1993).
[16] C. Dewdney and B. J. Hiley, Found. Phys. **12**, 27 (1982).
[17] W. R. McKinnon and C. R. Leavens, Phys. Rev. A **51**, 2748 (1995).
[18] M. Hagmann, Solid State Commun. **86**, 305 (1993).
[19] X. Oriols, F. Martín, and J. Suñé, Solid State Commun. **99**, 123 (1996).
[20] C. R. Leavens, Found. Phys. **25**, 229 (1995).
[21] R. E. Salvino and F. A. Buot, J. Appl. Phys. **72**, 5975 (1992).
[22] A. Goldberg, H. M. Schey, and J. L. Schwartz, Am. J. Phys. **35**, 177 (1967).
[23] M. O. Vasell, J. Lee, and H. F. Lockwood, J. Appl. Phys. **54**, 5206 (1983).
[24] X. Oriols, J. Suñé, F. Martín, and X. Aymerich, J. Appl. Phys. **78**, 2135 (1995).
[25] J. G. Muga, S. Brouard, and D. Macías, Ann. Phys. (N.Y.) **240**, 351 (1995).
[26] J. G. Muga, S. Brouard, and R. Sala, Phys. Lett. A **167**, 24 (1992).
[27] C. R. Leavens, Phys. Lett. A **178**, 27 (1993).
[28] J. Suñé, X. Oriols, F. Martín, and X. Aymerich, Appl. Surf. Sci. (to be published).
[29] G. R. Allcock, Ann. Phys. (N.Y.) **53**, 311 (1969).
[30] R. Landauer and Th. Martin, Solid State Commun. **84**, 115 (1992).

ELSEVIER

Microelectronic Engineering 36 (1997) 125–128

MICROELECTRONIC ENGINEERING

Bohm trajectories for the modeling of tunneling devices

J. Suñé, X. Oriols, J.J. García-García, and F. Martín
Departament d'Enginyeria Electrònica. Universitat Autònoma de Barcelona. 08193-Bellaterra.
Tel. 34-3-581 18 29. Fax. 34-3-581 13 50. e-mail: jsune@cc.uab.es

T. González, J. Mateos, and D. Pardo
Dep. de Física Aplicada. Universidad de Salamanca. 37008-Salamanca. SPAIN.

It is shown that quantum phenomena in electron devices, such as tunneling of electrons, can be modeled using Bohm trajectories. Fowler-Nordheim tunneling in thin-oxide MOS structures and resonant tunneling in double barrier diodes are considered.

1.INTRODUCTION

The tunneling of electrons is of increasing interest in silicon devices. Leakage currents, oxide degradation, dielectric breakdown, hot electron effects, are examples of phenomena which are related to tunneling in MOSFETs. This quantum-mechanical (QM) phenomenon is basic to the operation of devices such as floating gate EEPROMs. Also, new tunneling-based silicon devices are being proposed as alternatives to agressively scaled down MOS transistors [1].

In conventional MOS devices, tunneling has usually been modeled using the WKB approximation. In very thin insulator structures numerical solution of the stationary Schrödinger equation has also been undertaken to reveal aspects which cannot be considered within the former approximation. In general, the results are in quantitative agreement with experiments if one considers the limitations derived from the exponential dependences of the tunneling probability on barrier height and barrier thickness. In the case of tunneling devices such as the resonant tunneling diode (RTD) more accurate simulations have been performed and two main approaches have been considered: the solution of the effective-mass (Schrödinger) equation [2], and the integration of the Liouville equation to obtain the Wigner distribution function [3]. In both cases, self-consistency with the Poisson equation has been accounted for with different degrees of approximation. The first approach assumes full wave-coherence (extended scattering states), and has the severe limitation of using the equilibrium distributions of carriers at the contacts when considering the occupation of these states. The second approach is in principle free of this limitation because scattering interactions can be introduced into the Liouville equation, and the contact distributions are only assumed as boundary conditions. However, the extensive computation burden required by this approach considerably limits the size of the simulation box so that these boundary conditions can be far from being realistic.

A reliable approach for the introduction of tunneling into multidimensional device simulators is still missing. In this regard, the coupling of a QM treatment of tunneling with the semi-classical Monte Carlo (MC) simulation technique would be very convenient because it would allow the simultaneous consideration of scattering and QM coherence effects. For this purpose we are considering two alternatives, i.e. Wigner trajectories [4] and Bohm QM trajectories [5]. In this work we deal with Bohm trajectories in two cases which are interesting for device applications: (1) Fowler-Nordheim (FN) injection in $Si/SiO_2/Si$ structure; and (2) resonant tunneling in double-barrier diodes.

2. BOHM'S INTERPRETATION.

Let us briefly review the basics of Bohm's interpretation for non-relativistic particles [6]. The wavefunction associated to a particle can always be expressed as

$$\psi(x,t) = R(x,t)\exp\left(i\frac{S(x,t)}{\hbar}\right) \qquad (1)$$

with $R(x,t)$ and $S(x,t)$ being real functions. Thus the complex time-dependent Schrödinger equation

PII: S0167-9317(97)00031-2

(TDSE) is found to be equivalent to two real equations: the continuity equation for the presence probability density $P(x,t) = R^2(x,t)$; and another equation which can be interpreted as a modified Hamilton-Jacobi equation. In this scheme, the particle velocity is directly given by $v(x,t) = (1/m)(\partial S(x,t)/\partial x)$, and the classical potential energy $V(x,t)$ is augmented by a new term, $Q(x,t)$, which is interpreted as a quantum potential:

$$Q(x,t) = -\frac{\hbar^2}{2m}\frac{1}{R(x,t)}\frac{\partial^2 R(x,t)}{\partial x^2} \qquad (2)$$

This quantum potential introduces non-local features and modifies the trajectories so that the measurable results of the standard interpretation of Quantum Mechanics are perfectly reproduced. Assuming an initial wavepacket $\Psi(x,0)$, the particle trajectory is causally determined at all instants of time, provided that the initial position x_0 is known. However, because of the limitations of the uncertainty principle, the initial position is not perfectly determined within the initial wavepacket, and the physical quantities must be obtained by averaging over all the possible trajectories weighted by $P(x_0,0)$.

3. NUMERICAL PROCEDURE.

Regarding to the choice of the initial wavefunction, two alternatives have been considered in the literature: stationary scattering states, and localized time-dependent wavepackets. However, since Bohm trajectories associated to the scattering eigenstates of the effective-mass hamiltonian give non-consistent results (this failure is not due to Bohm's interpretation but to the nature of the scattering states themselves), time-dependent wavepackets are required. Our procedure is as follows: (i) we define a gaussian wavepacket located at t=0 in the emitter electrode, far enough from the barriers so that the potential is flat and the probability presence in the barrier region negligible; (ii) we integrate the hamiltonian eigenstates following the method of Vasell et al. [2]; (iii) we project the initial wavefunction onto the obtained basis to calculate $\Psi(x,t)$ by superposition; and (iv) finally we integrate Bohm trajectories. In step (iv), we first calculate R(x,t) and S(x,t) from the wavefunction, we calculate the velocity by dereivation of S(x,t), and we spatially integrate it to obtain the trajectory.

4. RESULTS.

4.1 Fowler-Nordheim tunneling through a thin MOS capacitor.

Consider first a silicon MOS structure with a 4 nm oxide and highly doped electrodes (no band bending effects).

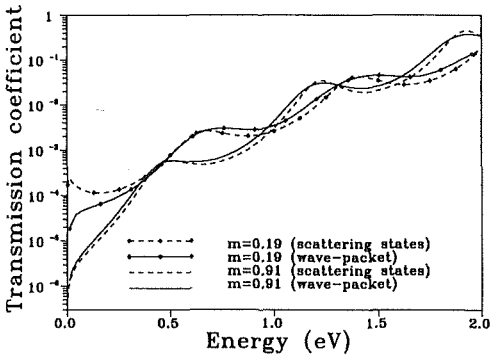

Figure 1. Transmission coefficient for a typical MOS structure with an applied bias of 9 V and oxide thickness of 4 nm in a (100) interface.

In Fig. 1 we show the transmission coefficient as a function of energy for the two sets of silicon valleys ($m^*=0.19m_0$, and $m^*=0.91m_0$) in a (100) interface. We show the results for energy eigenstates and gaussian wavepackets with spatial standard deviation of s_x=7 nm. The results justify this selection of s_x because the transmission coefficient is very similar to that of the scattering eigenstates (spatially more localized packets are too de-localized in energy so that the relevant energy dependences are washed-out). The oscillations are due to reflections at the oxide/anode interface [7] and, as expected, are also apparent in the simulated FN plot (Fig. 2). Since the injection is controlled by the $m^*=0.19m_0$ valley, the following results correspond to this case.

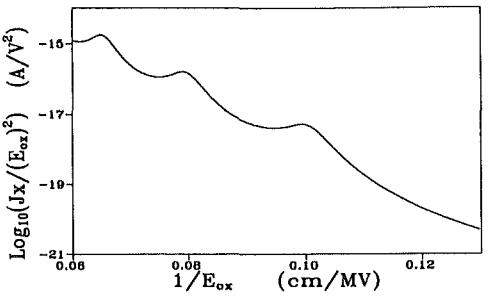

Figure 2. Simulated Fowler-Nordheim plot associated to the structure of fig 1.

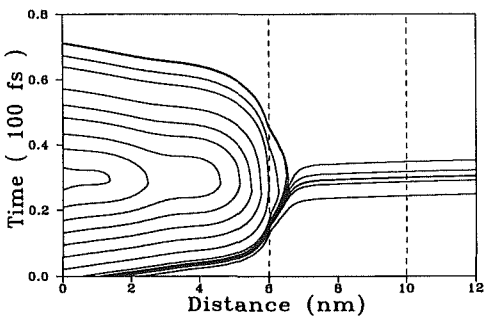

Figure 3. Bohm trajectories for an initial gaussian wave-packet with a central energy of 0.25 eV and a saptial dispersion of 7 nm impinging on the MOS structure (dashed lines) of fig 1.

Fig. 3 shows selected Bohm trajectories for one of the transmission maxima. Most of the trajectories are reflected (without ever reaching the barrier) and only those of the very front of the packet (Bohm trajectories do not cross) are transmitted [8]. No qualitative differences are observed in the trajectories of the transmission minima. The results are consistent because the ensemble of Bohm trajectories perfectly reproduce the evolution of the wavefunction obtained by integration of the time-dependent Schrödinger equation (TDSE). In particular, the transmission coefficient has been calculated by averaging Bohm trajectories with a precision better than 1% in both cases.

4.2 Double barrier resonant tunneling diodes.

RTDs are most adequate to show the strengths of the Bohm's approach because the tunneling phenomenoly is richer than in single barrier structures. Fig. 4 shows Bohm trajectories corresponding to the ground resonance of a double barrier structure typical of AsGa/AsGaAl system. No oscillations are observed and this seems to contradict the usual intuitive interpretation of resonances.

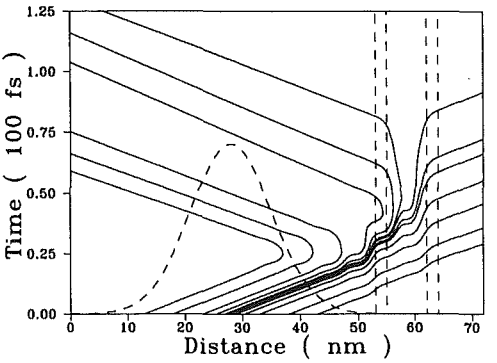

Figure 4. Bohm trajectories associated to an initial gaussian wave-packet (central energy of 0.22 eV and spatial dispersion of 10 nm) incident on a double barrier (dashed lines).

However, the wavefunction solution of the TDSE does not show any oscillation either. This is due to the fact that the local density of states in the well is very narrow. If the well width is increased, the peaks of the density of states become more closely spaced, and the wavefunction shows oscillations.

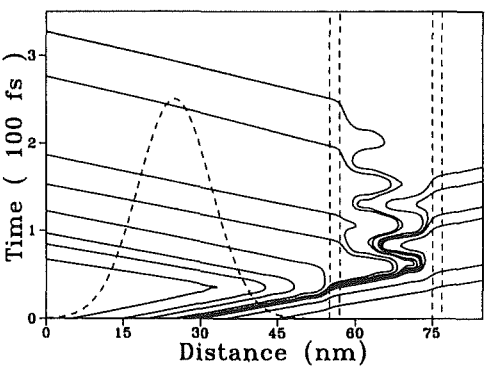

Figure 5. Bohm trajectories associated to an initial gaussian wave-packet (central energy of 0.16 eV and spatial dispersion of 10 nm) impinging on a double barrier (dashed lines) with a wider well.

As expected, Bohm trajectories also bounce between the barriers as shown in Fig. 5 for a 2nm/18nm/2nm structure. The distribution of tunneling times (this quantity is perfectly defined within Bohm's interpretation) also shows periodic bumps according to the sequential attemps to cross the second barrier (Fig. 6) [9].

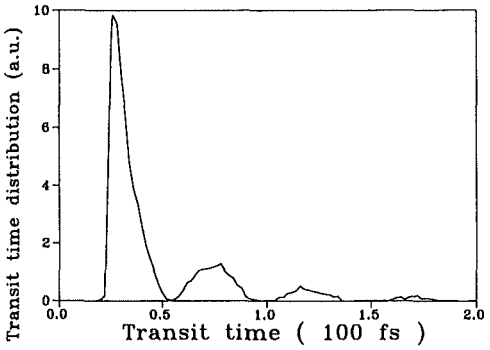

Figure 6. Transit time distribution obtained from 25000 Bohm trajectories for the wave-paket an potential profile of fig 5.

5. Discussion.

We have shown that the tunneling of wavepackets can be described by Bohm trajectories and that, as expected, the obtained results are fully equivalent to those obtained from the wavefunction solution of the TDSE. However, in our opinion, the main interest of this approach is the possibility of using Bohm trajectories for the extension of the MC technique to tunneling devices.

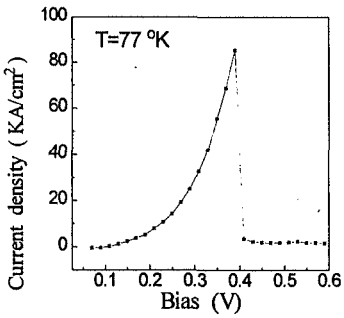

Figure 7. Simulated I-V characteristic of a RTD.

In this regard, we have already developed a preliminary MC simulator (without scattering in the QM region) based on the coupling of classical and Bohm trajectories. The simulator cannot be described here in detail, but we want to show the main results obtained with this tool, i.e. the self-consistent I-V characteristic (Fig. 7); and the position-momentum distribution function at the resonance which clearly shows the tunneling ridge (Fig. 8).

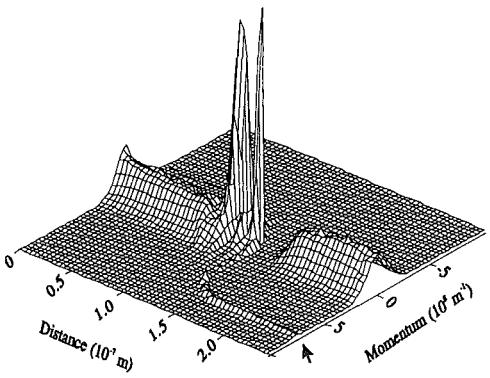

Figure 8. Particle position-distribution function at 0.29 V . Notice the tunneling ridge indicated by an arrow.

These results demonstrate that such simulations are possible and show their great potentiality for the accurate modeling of tunneling in electron devices.

References

1. W.E. Zhang, F.-C. Wang and C.H. Yang, IEEE Trans. Elect. Dev., 43, 1441 (1996).
2. M.O. Vasell, J. Lee, and H.F. Lockwood, J. Appl. Phys., 54, 5206 (1983).
3. W.R. Frensley, Rev. Mod. Phys., 62, 745 (1990).
4. K.L. Jensen and F.A. Buot, IEEE Trans. Elect. Dev., 38, 2337 (1991).
5. C.R. Leavens and G.C. Aers, in: *Scanning Tunneling Microscopy III*, ed. R. Wiesendanger and H.J. Güntherodt (Springer-Varleg, Berlin, 1993) p. 105.
6. D. Bohm, Phys. Rev 85, 166 (1952).
7. J. Maserjian and N. Zamani, J. Appl. Phys., 53, 559 (1982).
8. X. Oriols, F. Martín, and J. Suñé, Phys. Rev. A, 54, 4 (1996).
9. X. Oriols, F. Martín, and J. Suñé, Solid State Comm., 99, 123 (1996).

phys. stat. sol. (b) **204**, 404 (1997)

Subject classification: 73.23.Ps; 73.40.Gk; 73.50.Fq

Quantum Monte Carlo Simulation of Tunneling Devices Using Bohm Trajectories

X. ORIOLS (a), J. J. GARCÍA-GARCÍA (a), F. MARTÍN (a), J. SUÑÉ (a), T. GONZÁLEZ (b), J. MATEOS (b), and D. PARDO (b)

(a) Dep. d'Enginyeria Electrònica, Universitat Autónoma de Barcelona, 08193-Bellaterra, Spain
Tel.: 34-3-581 18 29; Fax: 34-3-581 13 50; e-mail: jsune@cc.uab.es

(b) Dep. de Física Aplicada, Universidad de Salamanca, 37008-Salamanca, Spain
Tel.: 34-3-29 44 36; Fax: 34-23-29 45 84; e-mail: tomasg@rs6000.usal.es

(Received August 1, 1997)

A generalization of the classical Monte Carlo (MC) device simulation technique is proposed to simultaneously deal with quantum-mechanical phase-coherence effects and scattering interactions in tunneling devices. The proposed method restricts the quantum treatment of transport to the regions of the device where the potential profile significantly changes in distances of the order of the de Broglie wavelength of the carriers (the quantum window). Bohm trajectories associated to time-dependent Gaussian wavepackets are used to simulate the electron transport in the quantum window. Outside this window, the classical ensemble simulation technique is used. Classical and quantum trajectories are smoothly matched at the boundaries of the quantum window according to a criterium of total energy conservation. A simple one-dimensional simulator for resonant tunneling diodes is presented to demonstrate the feasibility of our proposal.

For a reliable simulation of devices which are based on quantum-mechanical (QM) phenomena such as tunneling, the simultaneous consideration of phase coherence effects and of scattering interactions is required. One approach to deal with this problem consists in solving the Liouville equation to obtain the Wigner distribution function [1 to 3]. Another approach pursues the generalization of the semiclassical Monte Carlo (MC) device simulation technique through the use of QM trajectories. This is the path followed by Salvino and Buot [4], who used an ad-hoc model of quantum trajectories for double-barrier resonant tunneling diodes (RTD) which was based on the phase tunneling time. In this work we propose a quantum MC procedure based on Bohm trajectories, which provides a consistent description of the QM dynamics [5 to 8]. As a proof, we have developed a one-dimensional simulator and we have applied it successfully to describe the behavior of an RTD.

Among the various causal formulations of quantum mechanics, the most widely known is the one due to Bohm [5]. Within the Bohm's interpretation, all the particles of a quantum pure-state ensemble follow different and well-defined causal trajectories under the combined influence of the classical potential, $V(x, t)$, and a new term called the quantum potential, $Q(x, t)$, which is directly related to the wavefunction. The most important property of this approach is that the measurable results of standard quantum mechanics (those which would be directly obtained from the wavefunction) are perfectly reproduced by averaging the Bohm trajectories with adequate relative weights.

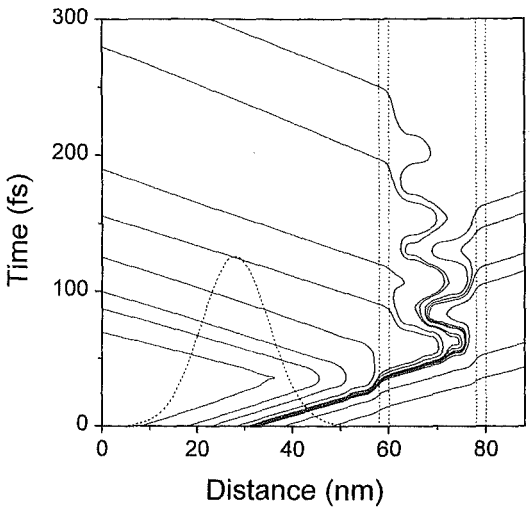

Fig. 1. Bohm trajectories associated to an initial Gaussian wavepacket with a central energy of 0.16 eV and a spatial dispersion of 10 nm, impinging upon a double barrier structure with 2 nm barriers of 0.3 eV and a 18 nm well. The barriers and the initial Gaussian wavepacket are indicated by dashed lines

The procedure that we use for the calculation of the Bohm trajectories has been published elsewhere [7,8]. Since stationary scattering eigenstates are not adequate for a dynamical description of transport, time-dependent wavefunctions are required. In Fig. 1 we show some representative trajectories in the particular case of a Gaussian wavepacket impinging upon a AlGaAs/GaAs double barrier structure. In particular, since Bohm trajectories cannot cross each other, those which are transmitted through the barrier come from the leading front of the wavepacket. Those from the rear are reflected, many of them without ever reaching the barrier. Oscillations between the barriers are also observed [7]. Since Bohm trajectories are causal, they naturally lead to magnitudes, such as tunneling times [6,8], which are not well defined within the standard framework of the quantum theory. Although these non-standard magnitudes can be regarded with diffidence, we must emphasize that the charge and current densities associated to the time-dependent wavefunction are perfectly reproduced by the Bohm trajectories. In this regard, our proposal is a simulation tool which obtains standard QM results using a methodology based on Bohm trajectories

Our simulator defines a QM window (QW) which includes the double-barrier of the RTD, and restricts the QM treatment to this window. Outside the QW, where the potential changes smoothly in the scale of the de Broglie wavelength of the carriers, the classical MC technique is used to simulate the electron transport. This allows to consider large integration boxes without excessive computational burden (this is the most important limitation found in the Wigner distribution approach). When an electron reaches the boundary of the QW, a Gaussian wavepacket is associated to it and a Bohm trajectory is randomly selected according to the appropriate distribution, given by the QM probability presence. The choice of the wavepackets requires the selection of values for two magnitudes, the central wavevector, and the spatial width. The former is selected using a coupling criterium based on the conservation of the total electron energy (the fact that part of the energy resides in the quantum potential is taken into account). On the other hand, the width of the wavepacket is chosen to be larger than 25 nm because the wavepacket transmission probability is almost width-independent above this

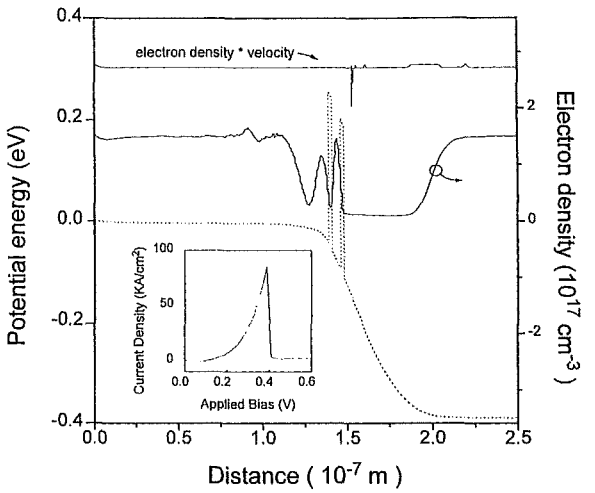

Fig. 2. Simulated electron concentration (solid line) and potential profile (dashed line) of the RTD at resonant bias ($V = 0.39$ V). The horizontal solid line above the electron density represents the current density (in arb. units) which has been computed as the local product of the average charge density per average velocity. The inset represents the simulated I–V curve

threshold and coincides (with negligible error) with that of the scattering eigenstate associated to the central wavevector.

In Fig. 2 and 3, we show the simulation results obtained for a typical RTD, which consists of an AlGaAs/GaAs/AlGaAs 3/5/3 nm double barrier structure at 77 K with an ionized impurity density of 1.5×10^{17} cm^{-3}. The self-consistent potential does not show spurious effects at the boundaries of the QW and current continuity is preserved in the whole device (Fig. 2). The obtained I-V characteristic shows the main features found in actual devices (inset of Fig. 2). A quantitative comparison with experiments in

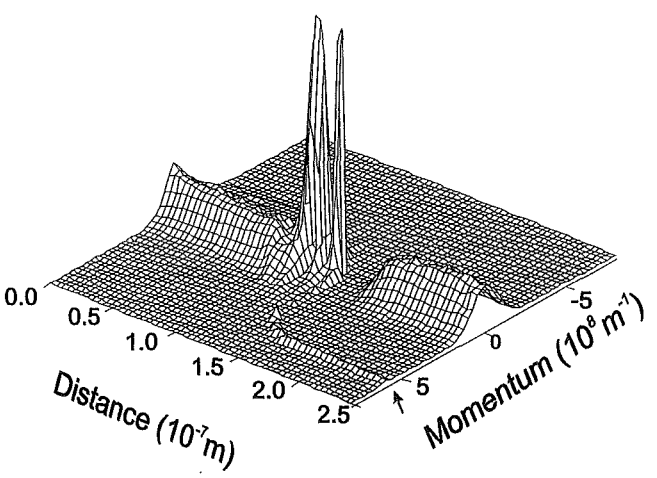

Fig. 3. Phase space distribution function along the whole device just before resonance ($V = 0.35$ V). Notice the tunneling ridge (indicated by an arrow), which is originated in the QW by resonant Bohm trajectories and progressively thermalized in the collector by scattering mechanism

important figures such as the peak-to-valley ratio is still premature because scattering in the QW has not been considered in this first version of the program. In this regard, we must stress that previous tools did not consider scattering either [4], and that they used ad-hoc models for the QM dynamics. As shown in Fig. 3, the MC simulator provides a positively defined phase-space distribution. The obtained results qualitatively resemble those obtained within the Wigner function approach [9], showing QM oscillations of the electron concentration in the pre-barrier region, accumulation of charge in the quantum well at the resonance bias (Fig. 2), and a tunneling ridge (also at resonance, Fig. 3) which progressively vanishes due to thermalization of carriers in the collector. Although the information contained in the phase-space distribution might be certainly useful to improve our understanding and design of QM devices, we must not forget that, in the QW, this distribution corresponds to hidden variables [6,10]. In this sense, we can completely trust all measurable results (charge densities, self-consistent potential profiles, current densities), but we must treat with caution all nonconventional results which arise from the causal structure of the Bohm's interpretation, and which do not have a counterpart within standard quantum mechanics (tunneling times, distribution of particle velocities, etc.).

In general, we can conclude that the obtained results demonstrate the feasibility of using Bohm trajectories to extend the classical MC technique to tunneling devices, and show once again the strengths of the MC particle technique in device simulation. Immediate future developments will include the consideration of scattering between Bohm trajectories in the QW, and the analysis of Bohm trajectories associated to one-side bound states in the emitter accumulation layer.

Acknowledgements. The authors are grateful to the Dirección General de Investigación General y Técnica and to the Consejería de Educación y Cultura de la Junta de Castilla y León for supporting this work under the project numbers PB94-0720 and SA11/96, respectively.

References

[1] W. R. FRENSLEY, Rev. Mod. Phys. **62**, 745 (1990).
[2] B. A. BIEGLE and J. D. PLUMMER, IEEE Trans. Elect. Dev. **44**, 733 (1997).
[3] F. ROSSI, P. POLI, and C. JACOBONI, Semicond. Sci. Technol. **7**, 1017 (1992).
[4] R. E. SALVINO and F. A. BUOT, J. Appl. Phys. **72**, 5975 (1992).
[5] D. BOHM and B. J. HILEY, The Undivided Universe: An Ontological Interpretation of Quantum Mechanics, Routledge, London 1993.
[6] C. R. LEAVENS and G. C. AERS, in: Scanning Tunneling Microscopy III, Eds. R. WIESENDANGER and H. J. GÜNTHERODT, Springer, Berlin 1993 (p. 105).
[7] X. ORIOLS, F. MARTÍN, and J. SUÑÉ, Phys. Rev. A **54**, 54 (1996).
[8] X. ORIOLS, F. MARTÍN, and J. SUÑÉ, Solid State Comm. **99**, 123 (1996).
[9] K. L. JENSEN and F. A. BUOT, IEEE Trans. Elect. Dev. **38**, 2337 (1991).
[10] J. R. BARKER, Semicond. Sci. Technol. **9**, 911 (1994).

Bohm trajectories for the Monte Carlo simulation of quantum-based devices

X. Oriols,[a] J. J. García-García, F. Martín, and J. Suñé
Departament d'Enginyeria Electrònica, Universitat Autònoma de Barcelona, 08193-Bellaterra, Spain

T. González, J. Mateos, and D. Pardo
Departamento de Física Aplicada, Universidad de Salamanca, 37008-Salamanca, Spain

(Received 24 October 1997; accepted for publication 13 December 1997)

A generalization of the classical ensemble Monte Carlo (MC) device simulation technique is proposed to simultaneously deal with quantum-mechanical phase-coherence effects and scattering interactions in quantum-based devices. The proposed method restricts the quantum treatment of transport to the regions of the device where the potential profile significantly changes in distances of the order of the de Broglie wavelength of the carriers (the quantum window). Bohm trajectories associated to time-dependent Gaussian wave packets are used to simulate the electron transport in the quantum window. Outside this window, the classical ensemble MC simulation technique is used. Classical and quantum trajectories are smoothly matched at the boundaries of the quantum window according to a criterium of total-energy conservation. A self-consistent one-dimensional simulator for resonant tunneling diodes has been developed to demonstrate the feasibility of our proposal.
 [S0003-6951(98)01007-9]

The reliable simulation of devices based on quantum-mechanical (QM) phenomena (such as tunneling) requires the simultaneous consideration of phase-coherence effects and of scattering interactions. Three main different approaches have been proposed to pursue this goal: (i) the solution of the Liouville equation to obtain the Wigner distribution function (WDF);[1–4] (ii) the nonequilibrium Green function theory recently reformulated by Lake *et al.*[5,6] to include band-structure and scattering effects; and (iii) the solution of the effective-mass Schrödinger equation combined with a Monte Carlo (MC) based introduction of scattering.[7–10] In our opinion, the latter approach would be very useful if an adequate description of tunneling in terms of particle trajectories were found. This is the path followed by Salvino and Buot,[9] who used an *ad hoc* model based on the phase tunneling time, and it is also our choice. In this letter, we propose a quantum-MC method based on Bohm trajectories, which provide a consistent description of the QM dynamics.[11,12] Although we have developed a one-dimensional quantum-MC simulator for a resonant tunneling diode (RTD), the proposed technique is appropriate for any vertical-transport-based QM device.

The most widely known causal interpretation of quantum mechanics is the one due to Bohm.[11] Within the Bohm's interpretation, all the particles of a quantum pure-state ensemble follow deterministic trajectories under the combined influence of the classical potential, $V(x,t)$, and a quantum potential, $Q(x,t)$, which is directly related to the wave-function $\Psi(x,t)$:

$$Q(x,t)=-\frac{\hbar}{2m^*}\frac{1}{|\Psi(x,t)|}\frac{\partial^2|\Psi(x,t)|}{\partial x^2}, \tag{1}$$

m^* being the particle's effective mass. From the point of view of device simulation, the most important property of the Bohm's interpretation is that all the measurable results of standard quantum mechanics are perfectly reproduced by averaging over the Bohm trajectories with correct relative weights.[11]

The tunneling of electrons through one-dimensional potential barriers has been carefully studied within the Bohm's framework.[12,13] Scattering eigenstates have been shown to be unsuitable and time-dependent wave packets are required. In this case, the most convenient procedure to calculate the trajectories is the following:[13] (i) numerical solution of the stationary Schrödinger equation; (ii) choice of the initial wave-packet $\Psi(x,0)$ and projection onto the basis of eigenstates; (iii) calculation of $\Psi(x,t)$ by superposition to obtain the current density $J(x,t)$ and the velocity of the Bohm's particles, $v(x,t)$, which is given by

$$v(x,t)=\frac{1}{q}\frac{J(x,t)}{|\Psi(x,t)|^2}, \tag{2}$$

q being the absolute value of the electron charge; and (iv) integration of $v(x,t)$ to calculate the trajectories $x=x(x_0,t)$ which are uniquely defined for each position x_0 within the initial wave packet. In Fig. 1 we show some representative trajectories in the particular case of a Gaussian wave packet impinging upon a double barrier structure. Since $v(x,t)$ is single valued, the trajectories do not cross each other either in phase space or in configuration space, and this has interesting consequences.[13] In particular, the trajectories which are transmitted through the barrier come from the leading front of the wave packet. Those from the rear are reflected, many of them without ever reaching the barrier. By weighting the transmitted trajectories according to the initial probability density $|\Psi(x_0,0)|^2dx_0$, the standard transmission coefficient is obtained.[12]

[a]Electronic mail: xoriols@cc.uab.es

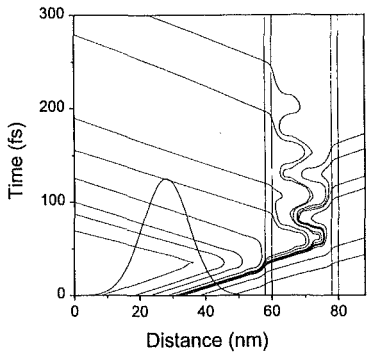

FIG. 1. Bohm trajectories associated to an initial Gaussian wave packet with a central energy of 0.16 eV and a spatial dispersion of 10 nm, impinging upon a GaAs/AlGaAs double barrier structure with 2 nm wide barriers of 0.3 eV and a 18 nm wide well. The position of the barriers and the initial Gaussian wave packet are also shown.

Since Bohm trajectories are causal, some magnitudes such as the tunneling times,[12,13] which are not well defined within the standard QM theory, are natural within the Bohm's picture. Although these nonstandard magnitudes should be regarded with diffidence, we must emphasize that the charge and current densities are perfectly reproduced by the Bohm trajectories:

$$|\Psi(x,t)|^2=\int_{-\infty}^{\infty} dx_0|\Psi(x_0,0)|^2\,\delta(x-x(x_0,t)), \tag{3}$$

$$J(x,t)=q\int_{-\infty}^{\infty} dx_0|\Psi(x_0,0)|^2 v(x,t)\,\delta(x-x(x_0,t)). \tag{4}$$

In this regard, our proposal is a simulation tool which obtains standard QM results, though by means of Bohm trajectories, i.e., the Bohm's theory is used as an equivalent mathematical reformulation of quantum mechanics, rather than as an alternative physical interpretation.

Our simulator defines a QM window (QW) and restricts the QM treatment to this window. Outside the QW, the classical MC technique is used taking into account impurity and phonon-scattering mechanisms. When an electron reaches the boundary of the QW, a Gaussian wave packet is associated to it:

$$\Psi_k(x,0)=\frac{1}{(\pi\sigma_x^2)^{1/4}}\exp\left(-\frac{(x-x_B)^2}{2\sigma_x^2}+ikx\right), \tag{5}$$

x_B being a fixed position centered in the emitter side of the QW, k the central momentum, and σ_x the spatial standard deviation. The selection of the wave-packet parameters is of critical importance. The central position x_B is chosen to be far enough into the emitter side of the diode, where the potential is flat enough to allow an analytical projection onto the eigenstates.[14] Since the transmission probability depends on the width of the wave packet, the selection of σ_x also requires a physical criterion. The narrower is the wave packet (small σ_x), the smoother and wider are the found transmission resonances and the smaller is the peak-to-valley current. A reasonable criterion is the choice of wide enough wave packets ($\sigma_x \geq 25$ nm) so that the corresponding transmission coefficient is roughly that of the eigenstate associated to the central momentum k (i.e., narrow in k space as compared with the features of the local density of states). In our MC simulator we have considered bias-independent wave-packet parameters and, in particular, $\sigma_x=25$ nm. Inside the QW, each electron follows a randomly selected Bohm trajectory and the charge and current densities inside the QW are computed using the methods of the classical MC technique. The coupling to classical trajectories and the selection of k are based on the conservation of the total electron energy. To implement these matching criteria, we require the following condition at both interfaces of the QW:

$$\frac{\hbar^2 k_c^2}{2m^*}+V(x)=\frac{1}{2}m^* v^2(x,t)+V(x)+Q(x,t), \tag{6}$$

where k_c is the x component of the momentum of the classical particle. This equation requires the previous choice of the trajectory, i.e, of the initial position x_0, which is selected by generating a random number distributed according to $|\Psi_k(x_0,0)|^2 dx_0$. Notice that this distribution does not depend on k. For a Gaussian wave packet such as of Eq. (5), the velocity and quantum potential at $t=0$ are given by

$$Q(x_0,0)=\frac{\hbar^2}{2m^*\sigma_x^2}\left(1-\frac{(x_0-x_B)^2}{\sigma_x^2}\right); \quad v(x_0,0)=\frac{\hbar k}{m^*}. \tag{7}$$

Substitution into Eq. (6) after having generated x_0, allows the determination of k. Discontinuity of the particle position is avoided by allowing the electron to travel classically from the boundary of the QW to the corresponding x_0. Electrons incident from the collector are classically reflected before entering in the QW (i.e., for the moment, only tunneling from emitter to collector is considered). Scattering has not been implemented in the QW and this is the main limitation of our approach in the present stage of development. In particular, this has forced us to consider a Thomas–Fermi approximation for the calculation of the electronic charge in the emitter accumulation layer to avoid unphysical depletion of charge in this region and nonrealistic self-consistent potential profiles.[15]

To show the feasibility of our proposal, we have simulated the current–voltage (I–V) characteristic of a typical GaAs/AlGaAs RTD (barrier width of 3 nm, barrier height of 0.3 eV, and well width of 5.1 nm) at 77 K. The ionized impurity density in the emitter and collector GaAs electrodes is 1.51×10^{17} cm^{-3} (i.e., a realistic doping of 5×10^{18} cm^{-3}). A one-valley model with a single effective mass (that of GaAs Γ point) has been considered for the whole structure. Figure 2 shows the self-consistent potential and the electron concentration profiles, together with the current calculated at each position of the RTD, for an applied bias of 0.39 V (near the resonant maximum of the I–V characteristic). The validity of our matching procedure is supported by the fact that the self-consistent potential does not show spurious effects at the boundaries of the QW and because current continuity is preserved in the whole device. The current is noisier in the collector because it is carried by a reduced number of high-energy electrons, while in the emitter the whole low-energy distribution is shifted towards small values of positive momenta. The largest current spike

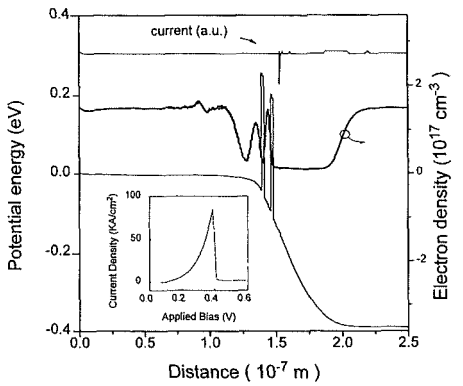

FIG. 2. Results obtained with our QM Monte Carlo simulator for a 3.0/5.1/3.0 nm GaAs/AlGaAs double barrier RTD (barrier height of 0.3 eV) at 77 K. Simulated electron concentration and self-consistent potential profile at a resonant bias near the peak of the $I-V$ curve ($V_{appl}=0.39$ V). The horizontal solid line represents the current density (in arbitrary units) along the whole device computed as the product of the average electron charge density per average velocity (i.e., current continuity is demonstrated). The inset represents the simulated $I-V$ curve.

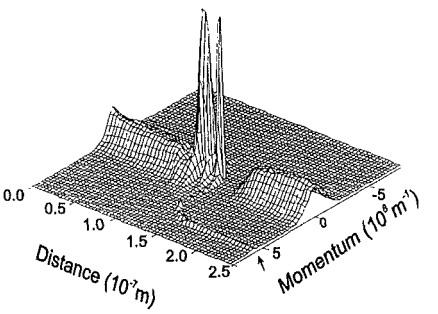

FIG. 3. Phase space distribution function along the device of Fig. 2 at the applied bias of 0.39 V. Notice the tunneling ridge (indicated by an arrow), which is originated in the QW by resonant Bohm trajectories and which becomes progressively thermalized in the collector by scattering mechanisms.

obtained at the boundary of the QW is not physically significant, being a spurious effect caused by the numerical calculation of $Q(x,t)$ as required by Eq. (6). The electron concentration profile shows an oscillatory behavior before the barriers and an accumulation in the quantum well. The obtained $I-V$ characteristic (inset of Fig. 2) shows the main qualitative features of those of actual devices. However, as in previous works,[7,9] the current almost vanishes after the resonant peak (it increases again at higher bias when electrons are injected through or over the top of the barrier) as a consequence of having ignored scattering in the QW (i.e., injection from the one-side bound states of the accumulation layer is neglected). In this regard, we must stress that previous tools did not consider scattering either and that they used *ad hoc* models for the QM dynamics.[7–9] As shown in Fig. 3, the MC simulator provides the momentum distribution of particles as a function of position along the device. These results qualitatively resemble those obtained within the WDF approach,[3] showing QM oscillations in the prebarrier region, accumulation of charge in the quantum well at the resonance bias, and a tunneling ridge (also at resonance) which progressively vanishes due to thermalization of carriers in the collector. However, contrarily to the WDF, our particle distribution is always positive by construction.

The presented results explicitly demonstrate the feasibility of using Bohm trajectories to extend the classical MC technique to tunneling devices. In addition to the potential profile and the current at the terminals of the device, the proposed quantum-MC technique provides local information of the momentum and energy distributions (the quantum potential must be accounted for, if the standard QM results are to be reproduced[12,16]), which can eventually contribute to improve the understanding and design of the devices. Our approach has the additional advantage of reaching the nanoelectronic range without abandoning the intuitive picture of carrier trajectories for the simulation of electron devices. Immediate future developments will include the consideration of scattering between Bohm trajectories inside the QW and the analysis of Bohm trajectories associated with one-side bound states in the emitter accumulation layer.

The authors are grateful to the Dirección General de Investigación General y Técnica (Project No. PB94-0720) and to the Consejería de Cultura de la Junta de Castilla y León (Project No. SA11/96) for supporting this work.

[1] W. R. Frensley, Rev. Mod. Phys. **62**, 745 (1990).
[2] B. A. Biegle and J. D. Plummer, IEEE Trans. Electron Devices **44**, 733 (1997).
[3] K. L. Jensen and F. A. Buot, IEEE Trans. Electron Devices **38**, 2337 (1991).
[4] F. Rossi, P. Poli, and C. Jacoboni, Semicond. Sci. Technol. **7**, 1017 (1992).
[5] R. Lake, G. Klimeck, R. C. Bowen, and D. Jovanovic, J. Appl. Phys. **81**, 7845 (1997).
[6] R. C. Bowen, G. Klimeck, R. Lake, W. R. Frensley, and T. Moise, J. Appl. Phys. **81**, 3207 (1997).
[7] T. Baba, M. Al-Mudares, and J. R. Barker, Jpn. J. Appl. Phys., Part 2 **28**, L1682 (1989).
[8] K. K. Gullapalli, D. R. Miller, and D. P. Neikirk, IEEE IEDM'91 Digest of Technical Papers, 511 (1991).
[9] R. E. Salvino and F. A. Buot, J. Appl. Phys. **72**, 5975 (1992).
[10] S. Ragazzi, A. Di Carlo, P. Lugli, and F. Rossi, Phys. Status Solidi B **204**, 339 (1997).
[11] P. R. Holland, *The Quantum Theory of Motion* (Cambridge University Press, Cambridge, 1993).
[12] C. R. Leaves and G. C. Aers, in *Scanning Tunneling Microscopy III*, edited by R. Wiesendanger and H. J. Güntherodt (Springer, Berlin, 1993), p. 105.
[13] X. Oriols, F. Martín, and J. Suñé, Phys. Rev. A **54**, 54 (1996).
[14] R. S. Dumont and T. L. Marchioro II, Phys. Rev. A **47**, 85 (1993).
[15] W. R. Frensley, Solid-State Electron. **32**, 1235 (1989).
[16] J. R. Barker, Semicond. Sci. Technol. **9**, 911 (1994).

Towards the Monte Carlo simulation of resonant tunneling diodes using time-dependent wavepackets and Bohm trajectories.

X. Oriols, J. J. García-García, F. Martín and J. Suñé.
Departament d'Enginyeria Electrònica, Universitat Autonoma de Barcelona, 08193-Bellaterra - Spain

J. Mateos, T. González and D. Pardo
Departamento de Física Aplicada. Universidad de Salamanca. 37008 - Salamanca - Spain

Abstract

Following the path of a previous letter [Appl. Phys. Lett. **72**, 806 (1998)], a generalization of the classical Monte Carlo (MC) device simulation technique is proposed with the final goal of simultaneously dealing with phase-coherence effects and scattering interactions in quantum-based devices. The proposed method is based on time-dependent wavepackets and Bohm trajectories, and restricts the quantum treatment of transport to the device regions where the potential profile significantly changes in distances of the order of the de Broglie wavelength of the carriers (the quantum window). Outside this region, electron transport is described in terms of the semiclassical Boltzmann equation, which is solved using the MC technique. In this paper, our proposed description for the electron ensemble inside the quantum window is rewritten in terms of the density matrix. It is shown that, neglecting scattering, the off-diagonal terms of the density matrix remain identically zero even if time-dependent wavepackets are used. Bohm trajectories in tunneling scenarios are reviewed to show their feasibility to extent the MC technique to mesoscopic devices. A self-consistent one-dimensional simulator for resonant tunneling diodes has been developed to technically validate our proposal. The obtained simulation results are promising and encourage further efforts to include Quantum effects into MC simulations.

1. Introduction

Extrapolations of the actual tendency of miniaturization of integrated circuits (IC) predict that the minimum dimensions of conventional semiconductor devices will enter into the sub-100 nm range by the beginning of the next century [1]. The wave character of the charge carriers will certainly influence any further scaling of conventional transistors, and novel devices based on quantum mechanical (QM) and/or single electron effects are expected to open a new path toward faster, lower consumption, and more compact semiconductor IC's. Among other QM phenomena, tunneling is one of the effects which are called to play an important role in future IC's. The well-known Resonant Tunneling Diode (RTD) is expected to play a relevant role in the improvement of both analog (microwave source[2]) and digital (high speed electronics [3]) circuits.

Although RTDs have been thoroughly studied during the past 25 years, it is only recently that a quantitative comparison with experiment has given reasonable results [4,5]. In addition to the inherent limitations for reaching agreement between theory and experiment whenever tunneling is involved (it depends exponentially on many parameters such as barriers height and thickness), the main difficulties for the accurate modelling of these devices are related to: (i) reasonable 'open system' boundary conditions [6,7], and (ii) the simultaneous consideration of phase coherence effects and of scattering interactions. Different approaches have been taken to face these difficult problems. Full quantum-kinetic treatments of electron transport, based on obtaining the Wigner distribution function [8-12] or using a Green function approach [4,5,13,14], are generally considered as necessary. However, although a recent reformulation of the nonequilibrium Green functions theory by Lake et al. [4] has given very good results, they need extremely high computational requirements. In this regard, efforts devoted to more phenomenological approaches can also enlighten our understanding of quantum-based devices. Several works follow this direction [15-19]. Among them, the work of Fischetti [17], which suggests the use of the Pauli master equation, is particularly interesting because it starts a discussion about the actual need of fully off-diagonal formulations of quantum transport to deal with the devices of interest. On the other hand, Rossi et al. [18] have developed a density matrix formulation to include scattering inside the dynamics of a single time-dependent wavepacket. In the present work, we follow the path initiated by Salvino and Buot [16] who proposed a semiclassical Monte Carlo (MC) simulator for RTD's considering quantum trajectories in the double barrier region. In this regard our main goal is to present a proposal to deal with electron transport in quantum devices which is simultaneously reliable and intuitive. In a previous letter [20], we have shown the technical viability of a quantum Monte Carlo simulator based on Bohm trajectories associated to time-dependent wavepackets. In the present paper, particular interest is devoted to give an alternative view of our model for electron transport in terms of the density matrix, to briefly review the phenomenology of tunneling with Bohm trajectories and to discuss several possibilities to include scattering.

The paper is organised as follows: In section 2, an introduction to our model is presented and it is reformulated in terms of the density matrix. Section 3 is devoted to analyse the properties of Bohm trajectories in tunneling devices, with emphasis on double-barrier structures. The general features of the quantum MC simulator for RTD are discussed in section 4. Several considerations about scattering are presented. Finally, section 5 presents the results obtained with this new technique and points out directions for future work.

2.- Time-dependent wavepackets

As previously indicated, the main goal of the present work is to explore the possibilities of extending the semiclassical MC technique to mesoscopic devices by means of wavepackets and Bohm trajectories. However, in order to consider large integration boxes without unnecessary computational burden, quantum-transport models are restricted to a small portion of the device that we call the quantum window (QW). Actually, we deal with vertical transport devices which can be modelled using a one

dimensional picture and we distinguish three regions in the device: the emitter region, the quantum window and the collector region.

The emitter and collector regions, close to the respective contacts, are treated as semiclassical regions. From an ensemble MC simulation of particles at these semiclassical regions one can deduce a semiclassical distribution function at the limits of the QW. Each electron that enters into the QW is associated to an initial Gaussian wavepacket whose energy is directly related to its classical counterpart. The dynamics of this electron inside the QW is directly related to the wavepacket evolution.

Let us notice that the electron dynamics are determined by ordinary classical forces at the semiclassical regions. However, these classical forces are rigorously deduced by considering the quantum-mechanical evolution of a wavepacket when the externally applied electric field varies slowly over the dimensions of such a wavepacket [21]. This semiclassical model recuperates the classical picture of an electron as a particle and forgets its original wavepacket description. However, within actual devices whose dimensions can be comparable to the electron De Broglie wave length, the quantum nature of electrons can not be longer neglected. In this regard, the electron description inside the QW by wavepackets seems the most natural extension of the classical MC technique to quantum devices.

In a previous work [20], we have explained our proposal for a quantum MC simulation based on the time-dependent Schrödinger equation (TDSE) in the effective mass framework. Now, a description in terms of the density matrix formalism will be presented, which provides a new point of view of our proposal which is closer to those most commonly used for the description of mesoscopic devices.

2.1.- Density operator representation for the wave-packet dynamics inside the QW

As we have already mentioned, we associate an initial Gaussian wavepacket to each electron that enters into the QW. In particular, we consider minimum-uncertainty Gaussian wavepackets:

$$\psi_{k_c,t_o}(x,t_o) = \frac{1}{(\pi\sigma_x^2)^{1/4}} \exp\left(-\frac{(x-x_c)^2}{2\sigma_x^2} + ik_c x\right) \tag{1}$$

σ_X being the spatial dispersion, x_C the spatial centre of the wavepacket at the initial time $t=t_O$, and k_C the central wavevector which is related to a central energy E_C. It is important to notice that σ_X and x_C are identical for all electrons, but t_O and k_C depend on each particular electron history. In order to avoid a time discretization of the TDSE which would not be convenient for a MC simulation, we have chosen to calculate $\psi_{k_c,t_o}(x,t)$ by superposition. Hence, we begin by integrating the stationary Schrödinger equation to obtain a basis of scattering eigenstates, $\{\Psi_k(x)\}$, and then we proceed to numerically project the initial wavepacket onto this basis:

$$\psi_{k_c,t_o}(x,t_o) = \int_{-\infty}^{\infty} a_{k_c}(k)\psi_k(x)dk \tag{2}$$

with:

$$a_{k_c}(k) = \int_{-\infty}^{\infty} \psi_k^*(x)\psi_{k_c,t_o}(x,t_o)dx \tag{3}$$

The Hamiltonian eigenfunctions $\Psi_k(x)$ are calculated following the procedure described in [22]. The main advantage of this method is that $\psi_{k_c,t_o}(x,t)$ can be computed by superposition at any arbitrary instant of time t:

$$< x|\psi_{k_c,t_0} >= \psi_{k_c,t_o}(x,t) = \int_{\infty}^{\infty} a_{k_c}(k)\exp\left(-i\frac{E(k)(t-t_o)}{\hbar}\right)\psi_k(x)dk \tag{4}$$

without having to calculate it at intermediate times. $E(k)$ is the energy associated to the scattering eigenstate $\Psi_k(x)$, related to the wavevector k via a parabolic dispersion relationship.

Moreover, since a single particle system can be equivalently described by the Schrödinger or Liouville equation, the density operator for this single electron system can be written as:

$$\rho(t) = |\psi_{k_c,t_0}(t) >< \psi_{k_c,t_0}(t)| \tag{5}$$

and the density matrix, represented in the Hamiltonian eigenstates basis $\{\Psi_k(x)\}$, can be easily expressed as:

$$\rho_{k'k}(t) = < \psi_{k'}|\psi_{k_c,t_0} >< \psi_{k_c,t_0}|\psi_k >= a_{k_c}(k')a^*_{k_c}(k)e^{i\frac{(E(k)-E(k'))(t-t_o)}{\hbar}} \tag{6}$$

However, as we have pointed out, our quantum system is not only composed of a single wavepacket, but from an ensemble of them. In particular, it contains a constant flux of wavepackets that corresponds to a constant flux of electrons entering inside the QW at different initial times and with different energies. This picture can be summarised as following: (i) each particle enters into the QW at a different initial time, t_O and (ii) there is a distribution of central wavevector $f(k_C, t_O)$ which can be obtained from the number of classical particles that arrive at the QW, from the emitter[23], at different times. Since we are dealing with a pure coherent system (scattering is neglected in this preliminary version), $f(k_C, t_O)$ is position-independent.

The density matrix representing the whole electron ensemble can be written taking into account the above two points. The first one implies sum over all possible entering times, t_O, and the second point, a statistical average in accordance with $f(k_C, t_O)$. If we suppose that the initial entering time is uniformly distributed from -∞ to +∞, the density operator can be written as:

$$\rho(t) = \int_0^{\infty} dk_c f(k_c,t_o) \int_{-\infty}^{+\infty} |\psi_{k_c,t_o}(t) >< \psi_{k_c,t_o}(t)|dt_o \tag{7}$$

Let us suppose that we are in a steady-state situation where $f(k_C, t_O)$ is time-independent, then expression (7) can be largely simplified. If we use the identity:

$$\frac{1}{2\pi}\int_{-\infty}^{\infty} e^{i\frac{(E(k)-E(k'))t_o}{\hbar}} dt_o = \frac{m^*}{\hbar}\frac{1}{k}\{\delta(k-k')\} \tag{8}$$

then, we find that each element of the density matrix can be rewritten as:

$$\rho_{k'k}(t) = \int_{o}^{\infty} f(k_c) a_{k_c}(k') a^*{}_{k_c}(k) e^{i\frac{(E(k)-E(k'))t}{\hbar}} \cdot 2\pi \frac{m^*}{\hbar}\frac{1}{k}\delta(k'-k)\cdot dk_c \tag{9}$$

At this point, let us notice that, even working with time-dependent wavepackets (rather than with Hamiltonian eigenstates), we have found a diagonal density matrix for our coherent system under steady-state conditions. In the next section, we will use this property to compute the probability presence and the current density.

2.2.- Time-dependent wave-packets versus hamiltonian eigenstates

Once an expression for the density matrix is obtained (equation 9), all observables can be determined. In this regard, we will compare the results for the probability presence and current densities obtained with our time-dependent wavepacket model and with a description based on the Hamiltonian eigenstates.

The probability presence density operator neglecting the spin in one dimensional scenarios for the position and for the momentum variables, can be represented in the $\{\Psi_k(x)\}$ basis by:

$$q_{kk'} = \psi^*{}_k(x)\psi_{k'}(x) \tag{10}$$

Hence, its related observable, $Q(x, t)$, is computed as:

$$Q(x,t) = \int_{-\infty-\infty}^{\infty\infty} q_{kk'}\rho_{k'k}(t)dkdk' \tag{11}$$

After using the delta function of expression (9), one obtains:

$$Q(x,t) = 2\pi\frac{m^*}{\hbar}\int_{0}^{\infty}\int_{-\infty}^{\infty} f(k_c)|\psi_k(x)|^2 \frac{|a_{k_c}(k)|^2}{k} dk_c dk \tag{12}$$

The charge computed at any position inside the QW is time-independent (a steady-state situation is considered) and depends on the modulus of $a_{k_c}(k)$. In particular, if the electron is described by a wavepacket with $a_{k_c}(k) = \delta(k-k_c)$ (i.e. a scattering state), then the standard expression for the probability presence density in coherent models based on stationary states is recovered:

$$Q(x,t) = 2\pi \frac{m^*}{\hbar} \int_o^\infty f(k,t) \frac{|\Psi_k(x)|^2}{k} dk \tag{13}$$

Now, let us proceed identically for the current density. The current density operator, $J_{kk'}$, in the $\{\Psi_k(x)\}$ basis is represented by [24]:

$$J_{kk'} = \frac{\hbar}{2m^* i}\left[\psi^*{}_k(x)\frac{\partial\psi_{k'}(x)}{\partial x}\psi_{k'}(x)\frac{\partial\psi^*{}_k(x)}{\partial x}\right] \tag{14}$$

and then, its related unidimensional observable $J(x, t)$, is:

$$J(x,t) = 2\pi\frac{-i}{2}\int_0^\infty\int_{-\infty}^\infty f(k_c)\left[\psi^*{}_k(x)\frac{\partial\psi_k(x)}{\partial x}\psi_k(x)\frac{\partial\psi^*{}_k(x)}{\partial x}\right]\frac{|a_{k_c}(k)|^2}{k}\cdot dk_c dk \tag{15}$$

The current carried by a Hamiltonian eigenstate is position-independent and related with its transmission coefficient, $T(k)$. Thus, we obtain:

$$J(x,t) = \frac{\hbar}{m^*}\int_0^\infty\int_{-\infty}^\infty f(k_c)|a_{k_c}(k)|^2\, T(k)dk_c dk \tag{16}$$

Hence, as defined for a steady-state situation, the current density is constant and uniform. Once again, by defining $a_{k_c}(k) = \delta(k - k_c)$, one recovers the standard expression for the current density in the scattering states picture:

$$J(x,t) = \frac{\hbar}{m^*}\int_{-\infty}^\infty f(k,t)T(k)dk \tag{17}$$

Looking at expressions (16) and (17), the transmission coefficient for a time-dependent wavepacket can be easily identified [25]:

$$T(k_c) = \int_o^\infty |a_{k_c}(k)|^2\, T(k)dk \tag{19}$$

As for the probability presence, the current density associated to a time-dependent wavepacket can be quite different from that associated to an eigenstate. In figure 1, we have represented the influence of the spatial dispersion, σ_x, in the I-V curve of a typical RTD (calculated non-selfconsistenly). In particular, we consider a symmetric double barrier structure with 3 nm barriers of $Al_xGa_{1-x}As$, a 5 nm well of GaAs, and highly doped (N_D=10^{18} cm^{-3}) GaAs electrodes. We remark that an important peak-to-valley ratio is obtained for narrow wavepackets without the consideration of inelastic scattering. This dispersion in the results obtained from equations (12) and (16) (related to the arbitrary choice of σ_x) has been used to criticise our proposal. However, in the author's opinion, this is an advantage rather than a drawback, since it introduces some flexibility regarding the modelling of the "size of an electron", in the sense described by Fischetti [17]. In this way, regardless of technical or numerical difficulties, our proposal

can *a priori* simulate classical particles by defining $\sigma_x \approx 0$ (i.e. $a_{k_c}(k) \approx cte$), and also scattering states $\sigma_x \approx \infty$ (i.e. $a_{k_c}(k) = \delta(k - k_c)$). Obviously, these two limiting situations drive to quite macroscopic different results, as we have seen in figure 1.

In conclusion, we have shown that, under steady-state conditions, the density matrix associated to the described quantum system is diagonal in the basis of the Hamiltonian eigenstates (equation 9). This result has to be compared with the density matrix associated to a single time-dependent wave-packet (equation 6) which is non-diagonal in the same representation. Moreover, the results obtained from expression (9) can be qualitatively different from the ones obtained with Hamiltonian eigenstates. Finally, let us notice that expressions (12) and (16) can be equivalently deduced without appealing to the density matrix formalism, but this allows to look at our picture from a different point of view and to compare it with other models. Moreover, and this is much more important, it reveals a possible path [18] for the introduction of scattering interactions within the QW.

3. Trajectories in the Bohm's interpretation of quantum mechanics

Electron trajectories have been used to understand electron devices during decades. The successful use of this trajectories in classical MC simulators, and the existence of trajectory formulations of the QM suggest the idea to extent their use to the simulation of quantum devices [16, 20]. Several advantages can be anticipated: (i) the matching between the classical and quantum regions (the electrons getting in and out of the QW) can be done in terms of individual trajectories, (ii) Bohm trajectories open the possibility to consider scattering as a local event and, (iii) this would allow us to go on studying quantum devices without losing our intuitive picture for electronic transport.

As mentioned, several attempts have been made to describe the quantum dynamics in terms of causal trajectories of hidden variables. Among them, Bohm trajectories perfectly fit with our final goal since they have already been successfully applied to analyse the problem of tunneling through potential barriers [26-28] and perfectly reproduce the charge and current densities.

3.1.- Bohm's interpretation

Classically, a particle is dynamically described as a point in phase space which evolves according to Newton's second law or, equivalently, to the corresponding Hamilton-Jacobi equation. Standard QM in the Schrödinger picture substitutes this description by the use of a wavefunction $\Psi(x,t)$, which evolves according to the TDSE, and the notion of trajectory disappears. Bohm's formulation of QM mixes both types of descriptions, since it retains the concept of wavefunction and postulates the existence of well-defined causal particle trajectories. The evolution of a particle initially located at a position x_0 is uniquely determined by a Hamilton-Jacobi-like equation directly derived from the TDSE. A particle has (at each instant of time) a well-defined position and velocity causally determined by an objectively real (complex-valued) field directly related to $\Psi(x,t)$ (see the original Bohm's paper for a detailed formulation [26]).

Consistently with the Bohm's interpretation, once the wavefunction is completely determined by solving the TDSE, the velocity can be easily computed as:

$$v(x,t) = \frac{1}{q}\frac{J(x,t)}{|\psi(x,t)|^2} \tag{20}$$

where q is the absolute value of the electron charge. Then, for any initial position x_O, the trajectory $x(x_O, t)$ is uniquely defined by integration. The relevant point is that, in the Bohm's picture, a unique causal trajectory is found for each initial position x_o.

At this point we will discuss how the standard QM results can be exactly reproduced in terms of individual trajectories. Following the Bohm's formulation, the initial position is uncertain and only the presence probability density $|\Psi(x_o,0)|^2$ is considered to be known at t=0. According to this weak version of the Heisenberg uncertainty principle, the physical observables must be computed by averaging the corresponding magnitude $A(x_O,t)$ over all possible Bohm trajectories:

$$< A >= \frac{\int_{-\infty}^{\infty} A(x_o,t)|\psi(x_o,0)|^2\, dx_o}{\int_{-\infty}^{\infty} |\psi(x_o,0)|^2\, dx_o} \tag{21}$$

The observables obtained from Bohm trajectories using equation (21) are identical to those calculated within the standard interpretation of QM. In particular, as a direct consequence of the continuity equation, the presence probability density at an arbitrary position x can be recovered by 'counting' all the particles:

$$|\psi(x,t)|^2 = \int_{-\infty}^{\infty} dx_o |\psi(x_o,0)|^2\, \delta\big(x - x(x_o,t)\big) \tag{22}$$

and the current density by weighting their velocities:

$$J(x,t) = q\int_{-\infty}^{\infty} dx_o |\psi(x_0,0)|^2\, v(x,t)\delta\big(x - x(x_o,t)\big) \tag{23}$$

From the above two expressions, the Bohm's approach can be considered as a mathematical tool which is able to reproduce the presence probability and current density associated to $\Psi(x,t)$ using well defined particle trajectories. Moreover, since the main goal of any device simulator is to obtain charge densities (i.e. self-consistent potential profiles) and current fluxes, the two previous equations demonstrate that we can obtain reliable results using Bohm trajectories and treat the classical and quantum regions equivalently.

3.2. Phenomenology of Bohm trajectories in double barrier structures.

Since Bohm trajectories are absolutely determined by the Schrödinger equation, the initial wavefunction is the only degree of freedom available to model the particle's behavior in different experimental situations. Two alternatives have been considered in the literature: time-independent eigenfunctions of the Hamiltonian (scattering states), and localised time-dependent wavepackets.

In particular, since the current density associated to scattering states is positive and position-independent, the Bohm's velocity is positive everywhere according to equation (20). This means that, although Bohm trajectories perfectly reproduce the presence probability and the current density of scattering states, they are all transmitted through the barrier. In this regard, these trajectories do not reproduce our particle-intuitive understanding of the tunneling phenomenon and, as a consequence, their possible application to time-dependent electron transport simulation is hindered. However, we cannot conclude that the Bohm's approach fails for scattering states, because it perfectly reproduces the results of standard QM also in this case. In other words, the apparent failure of the Bohm's formulation applied to scattering states is due to undesired features of these time-independent states themselves to describe particle time-dependent phenomena [22].

The other alternative choice for the initial wavefunction is a time-dependent wavepacket (as that of equation 1). Since these wavepackets are adequate to reproduce the electron dynamics, the associated Bohm trajectories will also provide a reliable description, even from the intuitive point of view. An example of trajectories associated to a time-dependent wavepacket will be shown.

Since we are interested in the simulation of RTDs, we have chosen the double-barrier structure to show the main features of Bohm trajectories in tunneling structures. Let us study the tunneling of electrons (described as Gaussian wavepackets of spatial dispersion σ_X=10 nm) through a double barrier structure with the following parameters: barrier height of 0.3 eV, barrier thickness of 2 nm, well width of 7 nm, and uniform effective mass of $0.067m_O$ (Γ point of GaAs). In fig. 2 we show the trajectories corresponding to the second transmission resonance (E_C=0.22 eV) of the structure. The trajectories coming from the front of the wavepacket are transmitted, while those from the rear are reflected (most of them without even reaching the barrier). This is caused by the fact that Bohm trajectories do not cross each other in configuration space [29]. If the barrier region is limited by $x_L<x<x_R$, we can calculate the wavepacket transmission coefficient $T(k_C)$ by computing the probability presence at the right of point x_R for $t\to\infty$. Moreover, since we know that Bohm trajectories do not cross, $T(k_C)$ can also be computed by counting all the transmitted particles:

$$T(k_c) = \int_{x_R}^{\infty} |\psi_{k_c}(x, t\to\infty)|^2\, dx = \int_{-\infty}^{\infty} \alpha_T(x_o)\, |\psi_{k_c}(x_o,0)|^2\, dx_o \qquad (24)$$

where $\alpha_T(x_O)$ is equal to unity if the particle is transmitted and zero otherwise. Let us remind that it was not possible to reproduce the transmission and reflection coefficient of stationary scattering states by counting transmitted Bohm trajectories (all stationary Bohm particles are transmitted). It is in this sense that we have argued that the stationary Bohm trajectories do not reproduce our intuitive picture of tunneling.

We have already discussed how the measurable results of standard QM can be obtained by averaging the involved magnitude over all Bohm trajectories. However, Bohm's interpretation also provides other results which do not have a counterpart within the standard framework. This is not surprising since the causal trajectories give a deeper structure to the quantum theory. Within the Bohm's interpretation, concepts such as the momentum of particles at a given position, the arrival time or the transit time between

two points are defined for individual particles in a natural way. The distribution of these magnitudes can also be obtained by taking into account all the trajectories with their corresponding probabilities. All these results have not an analogue within the standard interpretation of QM and should be regarded with caution until Bohm's hidden theory is confirmed or refuted by experiments. As an example of the nonconventional information provided by the Bohm's approach we can mention the controversial field of tunneling times [30, 31]. References [22, 28] summarise several important aspects of the tunneling times associated to Bohm trajectories.

4. A Quantum Monte Carlo simulator: preliminary results

4.1. General considerations

As previously indicated, in order to consider large integration boxes without unnecessary computational burden, we have distinguished three regions in the device: the emitter region, the quantum window and the collector region (see fig. 3). The emitter and collector regions, close to the respective contacts and characterised by smooth potential profiles, are treated as semiclassical regions. Here, the conventional MC technique is used to simulate the particle dynamics. The scattering mechanisms considered in these regions are: (i) Acoustic phonon scattering treated in the elastic approximation, (ii) polar optical phonon scattering and (iii) ionised impurity scattering, whose scattering rates are calculated using the usual parameters for GaAs. For simplicity, only the lower valley with a constant effective mass has been taken into account. On the other hand, we define the QW as the device region where the potential changes abruptly over distances shorter than the de Broglie wavelength. In this particular device, the QW includes the double barrier region and its surroundings. The simulation of the electron transport in the QW is accomplished via Bohm trajectories associated with initial Gaussian wavepackets with different central wavevectors, k_C. In this particular simulation, 100 different initial Gaussian wavepackets (i.e. 100 different values of k_C) and 400 different stationary eigenstates are considered. At each time step of the MC procedure, ΔT, a table of (100x400) complex values has to be refreshed (which is the most significant additional effort needed to incorporate Bohm trajectories in our quantum MC simulator).

The selection of the main wavepacket parameters [x_C, k_C, and σ_X as defined in equation (1)] requires the determination of a matching procedure. The whole wavepacket is included within the QW (i.e. the probability presence outside the QW is negligibly small) and the position x_C is chosen to be far enough from the first barrier (into the emitter) so that the potential profile is practically flat and the projection onto the basis of scattering eigenstates can be done analytically [32]. The selection of σ_X also requires a physical criterion since, as has been discussed, its value is related with the electron "size" [33]. Finally, the selection of k_C is based on the conservation of the particle's total energy [20]. A criterion based on momentum conservation has been discarded because the quantum potential introduces differences in the definition of the kinetic energy inside the QW with respect to the semiclassical approach [34]. Finally, let us notice the intrinsic difficulties associated to define such a matching criterion: we are actually trying to make a classical and a quantum picture for electrons simultaneously compatible.

In fig. 3 we have represented three different trajectories to explain how the position continuity is also guaranteed. The circles represent the positions where the classical to quantum trajectory conversion takes place. The trajectory labelled by number 1 corresponds to one which is incident from the emitter and is finally transmitted. After choosing the initial position, the electron travels classically inside the QW (without scattering) until it arrives at x_O. Then, it follows the corresponding Bohm trajectory $x(x_O,t)$ until it exits the QW through the collector boundary. Similarly, trajectory number 2 corresponds to a particle incident from the emitter side which is finally reflected. We have also depicted a trajectory incident from the collector (labelled by number 3) that it is classically reflected at the collector boundary of the QW because, in order to save computational time, we have only considered tunneling from emitter to collector in this first version of the simulator.

At the present stage of the simulator, the effects of scattering in the device are only considered in the emitter and collector regions. This is clearly the main limitation of our simulator in its present implementation. Although in this paper we do not present our final choice for the introduction of scattering in the QW, some discussion is certainly required. Let us first discuss the evolution of an initial Gaussian wavepacket (equation 1) in a flat potential. In particular, the group velocity can be found as: $V_g = \hbar k_c / m^*$ (a parabolic dispersion relation is assumed) [24]. This result enables one to retrieve the classical description of the free particle, if the momentum and spatial dispersions are negligible (in others words, the centre of mass of the wavepacket moves like a particle which obeys the laws of classical mechanics). On the other hand, it is already well-known that, while the momentum dispersion is a constant of motion, the spatial dispersion of the wavepacket varies with time and, for sufficiently long times, increases without limit (spreading of a wave packet). This phenomenon is not limited to the special initial Gaussian wavepacket studied here, but to any arbitrary free wavepacket [35]. In this regard, it can be easily demonstrated that the velocity of Bohm trajectories associated to an initial Gaussian wavepacket in a flat potential tends to zero as time tends to infinity. Hence, Bohm particles, although they exactly reproduce the probability presence and current densities at any time, can lead to inappropriate results because the actual description of the system in terms of fully coherent time-dependent wavepackets is unrealistic. This result points out that, apart from other physical reasons, the inclusion of scattering inside the QW is an unavoidable task in order to correctly simulate mesoscopic devices within our proposal. Nevertheless, as we will see in section 5, reasonable results can be obtained, even without scattering, if the QW length is small enough for the wavepacket spreading to remain within tolerable limits. Two quite different possibilities can be suggested for the introduction of scattering mechanisms inside the QW: (i) the definition of position-dependent scattering rates to model microscopic scattering between Bohm trajectories as a local event, and (ii) the inclusion of scattering in the time evolution of the density matrix of single wavepackets. Although the actual evaluation of these possibilities is still being investigated, let us now discuss some general ideas.

In classical MC simulators, the scattering events are local (i.e. the position of the particle is continuous), but the scattering rates are calculated according to the Fermi golden rule (i.e. considering the matrix elements between completely extended plane

waves). Having proposed an extension of the simulation based on real classical-like trajectories, it seems reasonable to look for a scattering model based on local transitions between trajectories. In this regard, two main aspects have to be considered: (i) position-dependent transition rates following the idea of Zimmerman *et al.* [36]. and (ii) a criterion for selecting the wavepacket (and the Bohm trajectory) after the collision event. However, although this proposal is intuitively clear, it hits the fundamentals of "orthodox" Copenhagen interpretation of QM. So, more conventional proposals can also be considered. Among them, we remark the recent proposal of Rossi et al. [18] which includes the scattering mechanisms in the evolution of the density matrix associated to single wave-packets. The development done in section 2, describing our model in terms of the density matrix, perfectly fits with this proposal.

4.2.- Charge, phase-space distribution and current density.

Provided that Bohm trajectories are calculated as explained in the previous sections (i.e. correctly selecting x_O, and taking the quantum potential into account), they can be treated as classical trajectories for all purposes. Therefore, the same method can be used to compute the charge and current densities in the QW and in the classical regions of the device. At every time step, of duration ΔT, the contribution of the i-th particle to the charge density of the n-th cell of width Δx_n ($x_n<x<x_n+\Delta x_n$) is computed by evaluating the fraction of the time step spent by the particle in this cell, $t_i(\Delta x_n)/\Delta T$. In particular, the charge contribution of the i-th particle can be equal to unity if the particle remains inside the considered cell during the whole time step, or zero if the particle has not been present at all. An overall sum over the total number of particles N gives the electronic charge density associated to the specific cell at each time step:

$$\rho_n = \frac{\sigma}{\Delta x_n}\sum_{i=1}^{N}\frac{t_i(\Delta x_n)}{\Delta T} \tag{25}$$

where σ is the charge per unit area represented by each simulated particle. The obtained profile of the electronic charge density is used to update the potential at each time step by solving the Poisson's equation (alternative methods for the assignment of the charge to the device mesh can be found in [37]) . An identical procedure can be used to obtain the momentum distribution of the particles at each cell by using an additional momentum grid at each spatial cell. Since the exact position and momentum of each particle (even in the QW) can be perfectly defined, we can compute the time spent by the i-th particle in the phase-space cell ($x_n<x<x_n+\Delta x_n$ and $k_m<k<k_m+\Delta k_m$) during the simulated time T, $t_i(\Delta x_n,\Delta k_m)$. In this way, a time-averaged phase-space distribution $P(n,m)$ can be computed as:

$$P(n,m) = \frac{1}{T\Delta x_n \Delta k_m}\sum_{i=1}^{N} t_i(\Delta x_n, \Delta k_m) \tag{26}$$

On the other hand, for a constant applied voltage, the instantaneous current density $J(t)$ can be computed as the sum of the instantaneous velocities $v_i(t)$ of all the $N(t)$ particles contained in the device:

$$J(t) = \frac{\sigma}{L}\sum_{i=1}^{N(t)} v_i(t) \tag{27}$$

where L is the total simulated length of the device [38]. By time averaging $J(t)$ one obtains the stationary current for a given applied voltage. The current density can also be computed as the time derivative of the net charge collected at the collector or emitter contacts, although in this way more noisy results are obtained. The ohmic model that we use for the emitter and collector contacts in our simulation is described in detail in Ref. [39]. Basically, if the cell adjacent to the contact is positively charged, carriers are injected from a velocity-weighted hemi-Maxwellian distribution at equilibrium until the cell is charge neutral. On the other hand, if the cell is neutral or negatively charged, then the number of particles in the cell is left unchanged. Finally, let us emphasise that although the charge and current densities are calculated from individual trajectories, these reproduce the standard QM results. In other words, the self-consistent I-V characteristic would be the same if we had calculated it directly from time-dependent wavepackets, i.e. without using Bohm trajectories. These trajectories are just an adequate tool that perfectly reproduces the dynamics of the wavepackets, providing a natural way to extend the classical MC technique to the QW.

5. Results

In this section we discuss the results obtained with our quantum MC simulator in order to demonstrate the feasibility of our proposal. The steady-state I-V characteristic of a typical GaAs/AlGaAs double-barrier structure with 3 nm barriers of 0.3 eV and a 5.1 nm well has been simulated at 77 K. For simplicity, only one valley with an isotropic effective mass of $0.067m_0$ has been taken into account to model the conduction band. The ionised impurity density in the GaAs electrodes is $1.51 \cdot 10^{17}$ cm^{-3}, which corresponds to a realistic doping of $N_D=5 \cdot 10^{18}$ cm^{-3} at 77 K. The AlGaAs barriers and the GaAs well have been considered to be undoped. The total simulation length is 0.25 μm divided in 366 cells. The classical emitter (68.5 nm) and collector (96.5 nm) regions are divided into a non-uniform mesh. On the other hand, the QW (84,9 nm) is divided into 283 cells of 0.3 nm each. Let us emphasise that the integration box is much larger than those typically used for solving the Liouville equation, since most of the device is simulated with classical MC technique (Ref. [40] provides a larger box within the Liouville equation). As shown in fig. 3, the QW extends asymmetrically at both sides of the double barrier because the emitter region of the QW has to be large enough to define the initial Gaussian wavepacket in a flat potential region.

Hereafter, in figs. 4, 5 and 6, we show several results obtained for the double barrier structure and the simulation parameters described above. First of all, we show self-consistent results obtained at a particular bias point of 0.39 V, corresponding to a position close to the peak of the I-V curve. The results shown in figs. 4 and 5 were obtained by averaging instantaneous results over 1000 iterations after reaching the steady-state particle distribution (2000 iterations are usually required to reach it; the time step between iterations being ΔT=5 fs). In fig. 4(a) we represent (solid line) the electron density, which exhibits pre-barrier oscillations and an accumulation in the well. No technical spurious discontinuities are detected at the boundaries of the QW, this being an indication of the smoothness of our classical-to-quantum matching model. In dashed line we represent the average velocity, which is inversely proportional to the charge density, since their product must be position-independent to assure current uniformity along the device. In this regard,

the behavior in the collector depletion region is illustrative. It can be observed that the electrons travel faster in the depletion region because of the high electric field and, as a consequence, the electron density decreases in adequate proportion to maintain an uniform current. As reported by other authors [41], a depletion is also obtained in the emitter pre-barrier region as a consequence of the fact that electrons travel ballistically inside the QW. In this regard, the fact that no scattering is considered inside the QW has important consequences on the self-consistent results. To obtain an accumulation layer in the emitter region adjacent to the first barrier, the charge associated to quasi-bound states should be taken into account. However, since scattering in the QW is not considered yet, these states are unreachable from Bohm trajectories. To avoid this unphysical result, a semi-classical Thomas-Fermi approximation [42] has been used to compute this additional charge [see fig. 4(b)]. This electron charge is added to the MC charge obtained from expression (22) before solving the Poisson's equation.

As we have previously discussed, in addition to results such as those obtained for charge and current densities, the use of causal trajectories allows one to obtain more information related to the hidden variables. In particular, the use of Bohm trajectories directly leads to the existence of a classical-like phase-space distribution (just as in the classical MC simulations). In fig. 5 we have represented the particle phase-space distribution at the resonance voltage, obtained from expression (23) averaging over the last 1000 iterations. This distribution is qualitatively quite similar to the Wigner Distribution Function (WDF) solution of the Liouville equation [7, 8, 9, 40,41], but it must be stressed that, contrarily to WDF, our phase space distribution is positive by construction. On the other hand, we notice the presence of a tunneling ridge in the collector which was also reported within the WDF framework [41]. Electrons in the collector depletion region mainly come from Bohm trajectories associated with resonant wavepackets. Since these resonant trajectories behave ballistically, a number of electrons with large momentum appear in the collector. The presence of these resonant hot-electrons, which are thermalized along the collector, is responsible for the net current density at the right boundary of the QW. On the contrary, the whole wavevector distribution is shifted towards positive momenta in the emitter, so as to give an uniform current density.

Finally, in fig. 6 we present the self-consistently simulated current-voltage characteristic of the RTD described above. At the initial bias of 0.07 V, an arbitrary particle distribution is defined, and it evolves during 3000 iterations until the steady-state is reached (lower voltages are not considered since no electron transport from collector to emitter is implemented). In order to reduce the transient time required to reach the steady-state, the particle distribution obtained for one bias point is used as the seed for the next one. The current density is determined by averaging expression (24) over the last 100 iterations. A sharp resonant peak is obtained in the I-V curve at an applied bias of 0.39 Volts. The whole I-V curve is very similar to that obtained from a fully coherent treatment based on the solution of the stationary effective-mass Schrödinger equation. This is an expected result since we are not considering scattering in the QW yet.

6. Conclusions

An extension of the MC device simulation technique has been presented to simultaneously deal with phase-coherence effects and inelastic scattering interactions in QM devices. Our proposal is based on the description of the QM dynamics via Bohm trajectories associated to time-dependent wavepackets.

The description of the constant flux of wavepackets, evolving coherently in the QW, is developed in terms of the density matrix. It is shown that, under steady-state situations and without considering scattering mechanisms, the non-diagonal terms of the density matrix remain zero in the basis of Hamiltonian eigenstates. This new formalism provides a new view for our proposal and allows to compare it with previous models. Moreover, this new point of view suggest one way to implement the scattering mechanisms based on recent works [18].

The basics of the Bohm's interpretation of QM have been reviewed, and the application of Bohm trajectories for the description of the tunneling effect has been considered. It has been shown that stationary scattering eigenstates are not adequate for the description of the tunneling dynamics and this has led us to the use of time-dependent wavepackets. Although the Bohm's interpretation is a non conventional QM theory based on a hidden causal structure, the results for charge and current densities are exactly the same that would directly be obtained by applying the methods of standard QM to the wavepackets. Since the final scope of a device simulator is the calculation of self-consistent current-voltage relationships at the external contacts, we can conclude that Bohm trajectories are an adequate tool for device simulation.

To illustrate the principles of our proposal, a self-consistent one-dimensional quantum MC simulator has been developed for RTDs. The proposed method restricts the QM treatment of electron transport to those regions of the device where the potential significantly changes in distances of the order of the de Broglie wavelength of the carriers (i.e. the quantum window). This has allowed us to consider large integration boxes (which reach the asymptotic contact regions where the potential profile is flat) without excessive computational burden. Inside the QW, Bohm trajectories associated to Gaussian wavepackets have been considered. Outside this region, the standard semiclassical MC technique has been implemented and, consequently, the electrons follow classical trajectories which allows a smooth matching of the individual classical and quantum trajectories. The use of a general and consistent QM description of transport is a substantial improvement over previous quantum MC approaches which considered ad-hoc models [16].

In conclusion, we have demonstrated the feasibility of using time-dependent wavepackets and Bohm trajectories for the extension of MC simulators to deal with quantum devices. This kind of generalization of the semiclassical MC technique has the additional advantage of reaching the nanoelectronic range without abandoning the intuitive picture of carrier trajectories for the simulation of electron devices. Work is in progress towards the development of a complete quantum MC simulator for RTDs.

Acknowledgements

The authors are grateful to the Dirección General de Enseñanza Superior e Investigación Científica for supporting this work under the project numbers PB97-0182 and PB97-1331.

References

[1] H. Lüth 1995 *Phys. Status solidi (b)* **192** 287
[2] M. Reddy, S. C. Martin, A. C. Molnar, R. E. Muller, R. P. Smith, P. H. Siegel, M. J. Mondry, M. J. W. Rodwell, and S.J. Allen. Jr. 1997 *IEEE Electron Device Lett.*. **18**, 218
[3] P. Mazumder, S. Kulkarni, M. Bhattacharya, J. P. Sun G. I. Haddad, 1998 *Proceedings of the IEEE* **86** 664
[4] R. Lake, G. Klimeck, R. C. Bowen, and D. Jovanovic 1997 *J. Appl. Phys.* **81** 7845
[5] R. C. Bowen, G. Klimeck, R. K. Lake, W. R. Frensley, and T. Moise, 1997 *J. Appl. Phys.* **81** 3207
[6] W. Pötz 1989 *J. Appl. Phys.* **66** 2458
[7] W. R. Frensley 1990 *Rev. Mod. Phys.* **62** 745
[8] N. C. Kluksdahl, A. M. Kriman, D. K. Ferry, and C. Ringhofer 1989 *Phys. Rev. B* **39** 7720
[9] K. L. Jensen and F. A. Buot 1989 *J. Appl .Phys.* **65** 5248
[10] B. A. Biegel and J. D. Plummer 1997 *IEEE Trans. Elect. Dev.* **44** 733
[11] J. García-García, X. Oriols, F. Martin and J. Suñé 1996 *Solid State Elect.* **39** 1795
[12] J. García-García, X. Oriols, F. Martin and J. Suñé 1998 *J. Appl. Phys.* **83** 8057
[13] A. P. Jauho and J. W. Wilkins 1984 *Phys. Rev. B.* **29** 1919
[14] S. Datta 1990 *J. Phys. Condens. matter* **2** 8023
[15] K. K. Gullapalli, D. R. Miller, and D. P. Neikirk 1991 *Techn. Dig. of IEDM* p 511
[16] R. E. Salvino and F. A. Buot 1992 *J. Appl. Phys.* **72** 5975
[17] M. V. Fischetti, 1998 *J. Appl. Phys.* **83** 270
[18] F. Rossi, A. Di Carlo, and P. Lugli, 1998 *Phys. Rev. Lett.* **80** 3348
[19] L.Burgnies, O.Vanbésien, V.Sadune, D.Lippens, J.Nagle and B.Vinter, 1994 *J.Appl. Phys.* **75 4527**
[20]X. Oriols, J.J. García, F. Martin, J. Suñé, T. González, J. Mateos and D. Pardo, 1998 *Appl. Phys. Lett.***72** 806
[21]N. W. Ashcroft, N. D., Mermin 1976 *Solid State Physics. Philadelphia* (Saunders. 1976)
[22]X. Oriols, F. Martín and J. Suñé 1996 *Solid State Communications.* **99** 123
[23]The model can be easily generalised to also consider injection from the collector side to the QW. However, for simplicity, all the development will be done assuming only electrons incidents from the emitter.
[24]C. Cohen-Tanoudji, B. Diu, and F. Laloë, 1977 *Quantum Mechanics* (Wiley, New York, 1977)
[25]See equation (6.26) in C. R. Leavens and C. G. Aers 1990 *Bohm trajectories and the Tunneling Time Problems* Scanning Tunneling Microscopy III. Eds: R. Wiesendanger H. J. Güntherodt (Springer-Verlag Berlin Heidelberg)
[26]D. Bohm 1952 *Phys. Rev.* **85** 166
[27]P. R. Holland 1993 *The Quantum Theory of Motion,* (Cambridge: Cambridge University Press)

[28]C. R. Leavens and G. C. Aers 1993 *Scanning Tunneling Microscopy III,* Eds. R. Wiesendanger and H.-J. Güntherodt (New York: Springer) pp 105-140
[29]X. Oriols, F. Martín and J. Suñé 1996 *Physical Review A* **54** 2594
[30] E. H. Hauge and J. A. Stovneng 1989 *Review of Modern Physics.* **61** 917
[31] R. Landauer and T. Martin 1994 *Review of Modern Physics* **66** 217
[32] R.S. Dumont and T.L. Marchioro II 1993 *Phys. Rev. A* **47** 85
[33] A practical and reasonable possibility is the choice of wavepackets wide enough in position ($\sigma_X \geq 25$ nm) so that the corresponding transmission coefficient is approximately that of the eigenstate associated to the central momentum, k_C. Equivalently, we could say that the wavepacket must be narrow in k-space as compared with the features of the local density of states [21].
[34] J. R. Baker 1994 *Semicond. Science and Technology* **9** 991
[35] This phenomenon (spreading of a wave-packet) is not taken in consideration in classical MC since it is implicitly assumed that collisions relocalise the particle.
[36] J. Zimmermann at W. Yen, 1987 *Revue Phys. Appl.***22** 99
[37] C.Jacoboni and P.Lugli 1989 *The Monte Carlo method for semiconductor device simulation* (Springer-Verlag Wien New York)
[38] V. Gruzinskis, S. Kersulis and A. Reklaitis 1991 *Semicond. Sci. Technol.* **6** 602
[39] T. González and D. Pardo 1996 *Solid State Electronics* **39** 555
[40] J. García-García, F. Martín, X. Oriols, and J. Suñé 1998 *Appl. Phys. Lett.* (in press)
[41] W. Frensley 1989 *Solid State Electronics* **32** 1235
[42] J. A. López-Villanueva, I. Melchor, F. Gámiz, J. Banqueri and J. A. Jiménez Tejada 1995 *Solid State Electronics* **38** 203

Figure

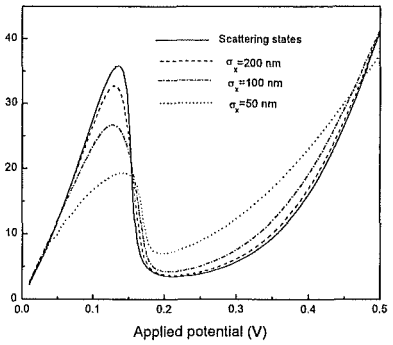

Figure 1:
Non-selfconsistent I-V curves for a typical RTD computed using scattering states or Gaussian wavepackets with different values of its spatial dispersion, σ_x.

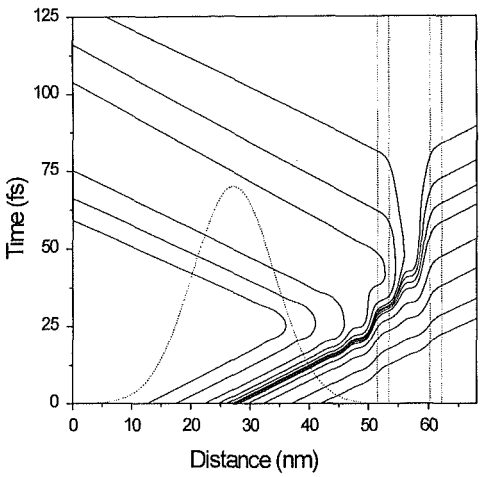

Figure 2:
Bohm trajectories associated to an initial Gaussian wavepacket with a central energy of 0.22 eV and a spatial dispersion of 10 nm, impinging upon a double barrier structure with 2 nm barriers of 0.3 eV and 7 nm well. The barriers and the initial Gaussian wavepacket are indicated by dashed lines.

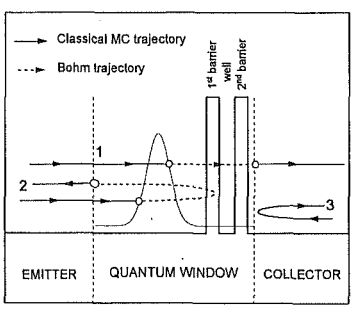

Figure 3:
Schematic diagram of the simulated RTD showing the location of the QW and the double barrier structure. Three different electron trajectories have been depicted to illustrate the classical-to-quantum matching model.

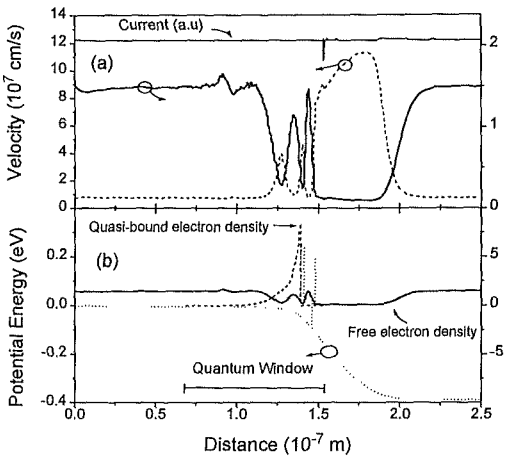

Figure 4:
Self-consistent results of 3.0/5.1/3.0 nm double barrier GaAs/AlGaAs RTD at 77 K with an impurity density of $5 \cdot 10^{18}$ cm^{-3} at a resonant bias of 0.39 eV: (a) Electron density (solid line) and average velocity (dashed line). The upper horizontal solid line represents the current density (in arbitrary units) computed as the product of the average charge density per average velocity. (b) Self-consistent potential profile (dotted line) and electron density: due to free electrons (solid line) and to quasi-bound electrons (dashed line).

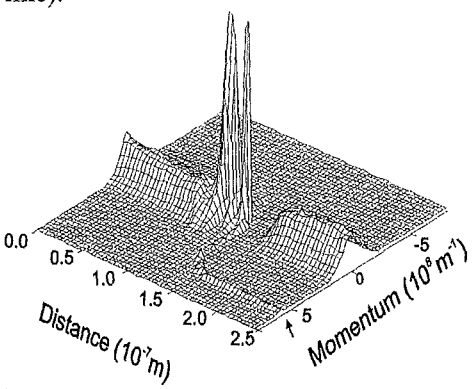

Figure 5:
Phase space distribution function along the whole device described in Fig. 4, just at the I-V peak current. Notice the tunneling ridge (indicated by an arrow), which is originated in the QW by resonant Bohm trajectories and progressively thermalized in the collector by the scattering mechanisms.

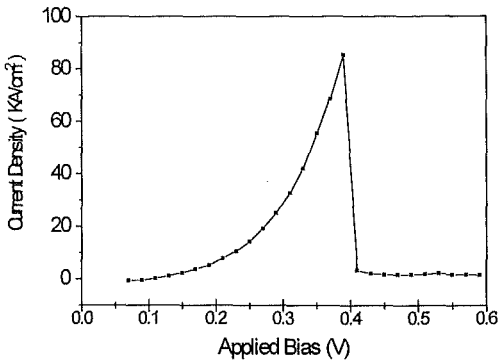

Figure 6:
I-V curve of the double barrier GaAs/AlGaAs RTD described in fig. 4(b).